Article:

von Lichtan, IJ, White, JDL, Manville, V et al. (1 more author) (2016) Giant rafted pumice blocks from the most recent eruption of Taupo volcano, New Zealand: Insights from palaeomagnetic and textural data. Journal of Volcanology and Geothermal Research, 318. pp. 73-88. ISSN 0377-0273

https://doi.org/10.1016/j.jvolgeores.2016.04.003

12950 total words
3 tables
9 figures
122 references

Giant rafted pumice blocks from the most recent eruption of Taupo volcano, New Zealand: insights from palaeomagnetic and textural data

I.J. von Lichtan[1], J.D.L. White[1*], V. Manville[2] and C. Ohneiser[1]

[1]*Geology Department, University of Otago, PO Box 56, Dunedin, New Zealand*
[2]*GNS Science, Wairakei Research Centre, Private Bag 2000, Taupo, New Zealand*
[*corresponding author: james.white@otago.ac.nz]

ABSTRACT

Giant blocks of pumice lie strewn along a former shoreline of intracaldera Lake Taupo, New Zealand, and are the sole subaerial evidence of the most recent volcanism at the Taupo supervolcano. Geochemically they are identical to material erupted during the complex and multiphase 1.8 ka Taupo eruption, which they post-date by one to two decades. The blocks, some of which are >10 m long, show complex jointing patterns indicative of both surface chilling and continued interior expansion, as well as heterogeneous vesicularity, with dense rims (mean density 917 kg/m^3) grading via an intervening transition zone (mean density 844 kg/m^3) into a more highly vesicular interior (mean density 815 kg/m^3). Analysis of thermal demagnetisation data indicates significant reorientation of the blocks as they cooled through a series of blocking temperatures. Some parts of block rims cooled to below 580°C well before emplacement on the shore, whereas other parts in the interior and transition zones, which cooled more slowly, acquired different orientations before stranding. Some block interiors cooled after blocks were finally deposited, and record the direction of the 1.8 ka field. The blocks are believed to be derived from one or both of a pair of rhyolitic lava domes that developed on the bed of Lake Taupo several decades after the climactic Taupo eruption over the inferred vent area.

These, and similar giant rafted pumice blocks in other marine and lacustrine settings raise a number of questions about how volatile-rich felsic magma can be erupted underwater with only limited thermal fragmentation. Furthermore, the prolonged flotation of out-sized fragments of vesiculated magma formed during subaqueous dome-growth contrasts with the rapid sinking of smaller pieces of hot plinian pumice under laboratory conditions. The genesis of pumice forming the blocks is not entirely clear. Most simply the blocks may represent part of a vesiculated carapace of a growing lava dome, broken loose as the dome grew and deformed then rising buoyantly to the surface. Parts of the carapace could also be released by local magma-water explosions. Some textures of the pumice, however, suggest fresher magma released from beneath the carapace. This may suggest that silicic dikes and pillows/pods intruded into a growing mound of silicic hyaloclastite, itself formed by quench fragmentation and thermal granulation of the dike margins. This fragmental cover would have inhibited cooling of a still-hot and actively vesiculating interior, which was then released to float to the surface by gravitational destabilisation and collapse of the growing pile. Following their formation, the large fragments of pumice floated to the lake's surface, where they were blown ashore to become embedded in accumulating transgressive shoreface sediments and continue cooling.

Keywords: giant rafted pumice, thermal remnant palaeomagnetism, vesicularity, subaqueous rhyolitic dome growth

1.0 INTRODUCTION

The ascent and degassing histories of magma influence processes of vesiculation, crystallization and fragmentation (Toramaru, 1989; Mangan et al., 1993; Klug and Cashman, 1996; Blower et al., 2001; Noguchi et al., 2006), and are critical factors in the style and magnitude of volcanic eruptions across a diversity of environments (Gilbert and Sparks, 1998). For subaqueous eruptions, there are further influences from the thermal, hydrostatic, viscous and phase-specific properties of water and their influences on fragmentation and dispersal (White et al., 2003). Subaqueous eruptions that produce highly vesicular silicic glass (pumice), are apparently common (Fiske, 1969; Kato, 1987; Kano et al., 1996; Allen and McPhie, 2000; Kano, 2003; Raos and McPhie, 2003; Bryan et al., 2004; Allen et al., 2008; Cantner et al., 2013; Rotella et al. 2013, 2014; Carey et al., 2014), and produce extensive pumice-rich aprons around submarine explosive calderas (Nishimura et al., 1991; Fiske et al., 2001; Wright et al., 2003). Rapid quenching of hot, magmatic steam- (Allen et al., 2008) or air-charged (Whitham and Sparks, 1986) pumice accelerates water ingestion and attainment of negative buoyancy, resulting in rapid fall-out from subaqueous eruption plumes as eruption-fed density currents (Cashman and Fiske, 1991; White, 2000). In contrast, air-cooled fragments of pumice float for long periods (Richards, 1958; Coombs and Landis, 1966; Frick and Kent, 1984; Risso et al., 2002; Bryan et al. 2004; Jutzeler et al., 2014) due to their low permeability, with the time to saturation being proportional to either the square of the clast radius (small clasts: Manville et al., 1998) or its radius alone (large clasts: Vella and Huppert, 2007), or to the clasts' c-axis (Risso et al., 2010). More challenging to explain are subaqueously erupted pumice clasts that float for a long time (Bryan et al., 2012,), or out-sized vesicular blocks that avoid quench fragmentation or thermal decrepitation. Here we analyse such blocks from deposits around Lake Taupo, New Zealand (Fig. 1)

1.1 Giant rafted pumice blocks

Observed subaqueous pumice-producing eruptions fall into two categories: explosive ones from shallow depths that breach as vapor-laden tephra jets; and passive upwelling of pumice blocks and lapilli, discoloured hot water, and bubbles from deep water (Kano 2003), with only a single, recent, satellite-observed large, deep-water explosive pumice-forming eruption (Carey et al., 2014). The 1952-53 eruption of Myojinsho, Japan, involved dome growth, submarine explosions including emergent Surtseyan jets, and production of floating pumice blocks and lapilli (Fiske et al. 1998). Most only floated briefly, but the largest, up to 1 m in diameter floated for long periods and were still hot when sampled (Tsuya et al. 1953). The 1953-57 eruption of Tuluman volcano near Papua New Guinea evolved from upwelling of metre-sized pumice clasts (Fig. 2) to phreatomagmatic eruptions and emergence of a number of lava domes (Reynolds and Best 1980; Reynolds et al. 1980). The 1934-35 eruption of Shin-Iwojima (Maeno and Taniguchi 2006), southwest Japan, occurred in 300 m of water, with early activity producing swarms of hot, steaming metre-sized pumice blocks that floated to the surface (Tanakadate 1935). Some floating pumice blocks up to 30 m^3 in volume sank abruptly, but many remained floating and were carried away by ocean currents. The 1924 eruption near Iriomote Island, Japan also produced a gentle but continuous rise of pumice clasts to 2-3 m across that floated for over 1 year (Kano 2003).

Large blocks of subaqueously erupted pumice have also been reported in a range of marine (Kano et al. 1991; Kano et al. 1996; Allen and McPhie 2000; Allen and Stewart 2003; Binns 2003) and lacustrine geological settings (Clough et al. 1981; Mann et al. 2004; Barker et al. 2012), including Lake Taupo (Wilson and Walker 1985). In most cases, such pumice blocks are contained within populations of more finely fragmented pumice, suggesting relatively energetic, explosive eruption processes (Raos and McPhie 2003), but sometimes they occur in depositional setttings that are clearly remote and decoupled from where they formed, presumably as a result of flotation and transport. Recorded examples include a bed of giant pumices at La Primaevera caldera (Clough et al. 1981), the San Agustin deposit at Ilopango (Mann et al. 2004), and the Green Lake pumice at Raoul Island (Barker et al. 2012). The observed and inferred prolonged buoyancy of hot fragments of vesicular dome-derived rhyolite formed under natural conditions thus contrasts markedly with laboratory experiments on hot subaerially and subaqueously erupted pumice clasts, which sink almost instantly through ingestion of water caused by thermal contraction of the cooling vesicle-filling gases (Whitham and Sparks 1986; Dufek et al., 2007; Allen et al. 2008). This contrast in behaviour must reflect either a scale-dependent effect or a fundamental difference in pumice properties such as vesicle interconnectivity produced by fragmentation of degassing magma ascending in a conduit versus that produced by effervescence as part of a growing lava dome (Manville et al., 1998; Bryan et al., 2004).

2.0 GEOLOGICAL SETTING

The Taupo Volcanic Zone (TVZ) is a 300 x 50 km region of intense, predominantly silicic, Quaternary volcanism (Houghton et al. 1995; Wilson et al. 1995) and extensional normal faulting (Rowland and Sibson 2001; Villamor and Berryman 2001) in the central North Island of New Zealand (Fig. 2). Two volcanic centres are presently active in the central, rhyolite-dominated segment of the TVZ, Okataina to the north (Nairn 2002) and Taupo to the south (Wilson 1993). Taupo volcano lies beneath Lake Taupo (Lowe and Green 1992), one of the largest bodies of fresh water in Australasia (area 616 km^2, volume 60 km^3), which was largely formed in its current configuration by caldera collapse and pyroclastic flow emplacement during the 26.5 ka Oruanui eruption (Davy and Caldwell 1998; Wilson 2001).

The Taupo 1.8 ka eruption (Wilson and Walker 1985) was the most recent explosive one at Taupo volcano. The complex multiphase eruption generated a number of fall deposits (Wilson, 1993) before culminating in emplacement of the c. 30 km^3 Taupo ignimbrite (Wilson 1985) which blocked the outlet to the intracaldera basin. Lake Taupo refilled in the decades after the eruption to a mean highstand level c. 34 m (Manville et al. 2009) above its present elevation of 357 mASL[1] before breaking out catastrophically (Manville et al. 1999). Several decades after the climactic phase of the eruption (eruption Y6: Wilson, 1993), based on inferred filling rates (Smith 1991; Manville et al. 1999), two subaqueous lava domes (eruption Z: Wilson 1993) composed of magma geochemically indistinguishable from that erupted in the explosive eruption, were extruded beneath the refilling lake to form Horomatangi Reefs (c. 0.25 km^3 volume), Waitahanui Bank (c. 0.03 km^3), and the giant pumice blocks themselves (Fig. 1), from which the eruption Z geochemistry is known (Sutton et al., 2000). Horomatangi Reefs comprises a pair of arcuate ridges oriented NE-SW, parallel with the regional tectonic grain and alignment of Holocene vents (Wilson 1993), that rise from the deepest part of the lake basin to within <5 m of the modern lake surface and are associated with an active geothermal system (de Ronde et al. 2001, 2002). Published bathymetric charts show steep-sided topography (https://data.linz.govt.nz/layer/1466-chart-nz-232-lake-taupo-taupomoana-horomatangi-reef/), but we know of no detailed observations of the submerged domes, which are culturally sensitive; even the most recent papers do not document dome form (Davy and Caldwell, 1998; de Ronde et al., 2002).

During eruption, blocks of vesicular material from one or both of these domes reached the surface of Lake Taupo then drifted onto its northeastern shores between Te Kumi Bay and Motutere, mostly in the Five Mile Bay area, where they lie embedded in transgressive lacustrine shoreline sediments (Fig. 3; see also supplementary file 1). These blocks of grey vesicular rhyolite are herein referred to as ‘pumice’, a term applied to very vesicular volcanic glass foam (Fisher and Schmincke 1984), although Manville et al. (1998)

[1] Elevations are expressed either as mASL (metres above mean sea level) or + x.y m (metres above modern lake level of 357 mASL). Lake Taupo water levels have been artificially controlled since 1941 AD for hydroelectric purposes when the lake was raised by about 1.5 m: the natural minimum and maximum levels being 355.84 and 357.72 mASL respectively; normal operating levels are around 357 mASL.

restricted the definition to micro-vesicular pyroclastic fragments of generally silicic composition that will float on water when dry and cold. Clasts range from 2 mm to 20 m long and are angular and blocky, especially at the smaller (< 0.5 m) sizes. Complex jointing patterns are present on blocks larger than c. 0.5 m, including surficial polygonal fracture patterns and interior herring-bone and rosette structures. The smaller grey pumice clasts form a secondary population that is only found associated with the giant blocks, and were presumably broken off the large blocks by wave action or collision during residence along the shoreface. In addition to its distinctive grey colour, which reflects textural properties rather than a distinct geochemistry, the dome-derived pumice has a more variable and generally lower vesicularity than the white, tube-walled pumice that forms the bulk of the Taupo eruption's products (Houghton and Wilson 1989; Houghton et al. 2003; Houghton et al. 2010) and is chemically identical in both major and minor element abundances (Sutton et al. 1995; Sutton et al. 2000). Measured volatile contents, in glass inclusions trapped in crystals, are uniform throughout all phases of both the 1.8 ka Taupo eruption and the eruption Z dome-derived pumice at 3.6-4.3 wt.% H_2O (Dunbar and Kyle 1993).

3.0 SEDIMENTOLOGY

Grey, dome-derived giant pumice clasts, with aggregate volume of approximately 4,000 m^3, are exposed along 42 km of the northeastern shoreline of Lake Taupo (Fig. 1 includes all known giant pumice clasts), predominantly in the Five Mile Bay area where they crop out in the toe and face of a lowstand shoreline terrace. This terrace was cut into primary deposits of the Taupo eruption by wave action after the level of Lake Taupo dropped from its highstand at c. +34 m when the intracaldera was breached and released a break-out flood (Manville et al. 2007; Manville et al. 1999). Wind-driven waves represent the most important sediment transport process at modern Lake Taupo (Riggs et al. 2001), and wave energy varies significantly around the lake. Prevailing winds are from the south and southwest (Thompson 1984), which coincides with the long axis of the lake, maximizing wave energy along the exposed Five Mile Bay beaches where most giant rafted pumice is now exposed *in situ* within eroding lacustrine deposits. Long-shore drift generally moves sediment from stream mouths north-north-east along the lake.

3.1 Lacustrine and shoreface sediments

Transgressive lacustrine shoreline deposits are developed extensively around the Lake Taupo basin as a result of the lake overfilling by c. 34 m following damming of the outlet during the 1.8 ka Taupo eruption (Wilson et al. 1997; Manville et al. 1999). Efficient hydraulic segregation of the different size and density components in the reworked pyroclastic materials gave rise to a suite of distinctive litho- and petrofacies (Manville, 2001; Manville et al. 2002). These sediments overlie an erosional unconformity cut into the top of the Taupo ignimbrite and comprise a deepening upward sequence that broadly corresponds to the shoreface-offshore succession developed along the modern lake shoreline, although the back-beach berm of rounded pumice pebbles and cobbles is usually absent from the transgressive sequence except at the highstand shoreline (Clarkson 1996; Riggs et al. 2001). Swash-zone sands lie above the unconformity and are represented by 10-20 cm of plane-parallel bedded and low-angle cross-stratified coarse sands and fine gravels that dip lakeward at 1-5^{o}: componentry is dominated by dense clasts, principally lithic fragments (rhyolite lavas and obsidian) and crystals (quartz, feldspar, hornblende and magnetite). Bedding is defined by sharp changes in grain-size, and pebble bands, which commonly include sub-rounded pumice clasts, are normally graded. In the zone of shoaling waves (surf zone) beds are tabular and thicker, comprising 30-60 cm of decimetre-bedded onlapping lenses of matrix-free, normally graded, moderately to well-rounded pumice gravel. These grade upward into nearshore (lower shoreface or transition zone sediments developed above fair-weather wave-base; Riggs et al. 2001). This sub-environment is characterised by rippled fine to medium pumice sands 20-50 cm thick. Symmetrical oscillatory ripples dominate, but slightly asymmetric or trochoidal ripples also occur. Fine dense component sands may be concentrated at ripple crests, while occasional ripple sets are entirely composed of crystals and lithics. Wavelengths vary between 35-100 mm and amplitudes between 3.5-14 mm. As water depth increased during the transgression, the rippled facies passes up into offshore sediments developed above storm wave-base, including massive and laminated vitric (pumice glass-shard) silts. Interbedded lenses of dense-component-rich coarse-sands and fine gravels are interpreted as material eroded from the shoreface and transported into deeper water by storm waves and rip currents. Deep water sediments accumulated below wave base are dominated by massive and laminated fine pumice sands and silts. In general, this sequence reflects partitioning of different density material during reworking of the Taupo ignimbrite by wave action: high-density components are concentrated as a lag on the high-energy shoreface, whilst lower density, more easily remobilised material is transported into the quieter offshore. The transgressive succession is remarkably consistent around the lake, being largely unaffected by variations in sediment flux and wave energy. High-energy settings are marked by more-common lithic-enriched storm facies in offshore as well as onshore sub-environments, while in high sediment supply areas sedimentation rate kept pace with the rate of lake deepening giving rise to thicker sequences with weaker deepening-upward trends (Riggs et al. 2001).

The giant rafted pumice blocks occur in a number of transgressive shoreline sub-environments. Grey clasts that are sub-rounded, in contrast to the generally angular margins of the large pumice clasts, and associated with shoreface dense-component-rich sands are inferred to indicate abrasion in the surf-zone, while those embedded in nearshore pumice gravels and sands were probably transported into deeper water by wave action (Fig. 4). There is very little or no deformation of the sediments below even the largest grey pumice clasts (Fig. 5), suggesting that they did not sink rapidly into place, and were almost neutrally buoyant when deposited (Manville et al. 1998; White et al. 2001; Manville et al. 2002). Assuming neutral buoyancy and given the c. 1:10 to 1:50 gradient of the shoreface, typical blocks c. 2 to 4 m in minimum to maximum diameter would have run aground 20-200 m offshore of the shoreline. Enclosing sediments show no evidence, such as fluidisation structures or thermal modification, of having been in contact with hot pumice, and this suggests that block exteriors were cool at the time of final lodgement and burial. Rates of accumulation for the sediment enclosing the pumice blocks varied around the lake, with relatively high rates inferred for the Five Mile Bay area (Riggs et al. 2001). If a maximum rate of 5 m/yr is accepted (as determined and defended by Riggs et al. 2001), burial of the largest blocks within the enclosing sediment would have required about a year once they ceased movement. Lower rates would imply slower burial.

The lake is inferred to have drained rapidly in response to breaching of the outlet-blocking ignimbrite barrier when the rising lake overtopped it (Manville et al. 1999). High drawdown rates estimated at c. 1.5 m/day minimised reworking of the transgressive shoreline and lacustrine sediments during regression, although in some areas small intermediate-elevation wave-cut terraces occur and local rounded-pumice gravels are interpreted as stranded pumice rafts (Riggs et al. 2001). Most of the giant rafted pumices in the Five Mile Bay area crop out in the lowstand shoreline terrace: post-breakout downcutting at the outlet lowered lake level by a further 2-4 m, but the level is now controlled by engineering works.

3.2 Distribution of the giant rafted pumice

Differential GPS surveys of grey pumice locations show that their basal elevations range between 6.8 and 12.0 m above modern lake level (Fig. 4; see also supplementary information 2). Expected relative accuracy should be within a couple of decimetres – discussed in Wilson et al. (1997) shoreline atlas cited. This was informally confirmed within longitudinal sections in which the DGPS elevations went up for clasts higher and further from the lake, and down for those in the other direction. Accepting that the DGPS heights are reliable, this variation reflects a combination of distributed and fault-related offsets of the lake shoreline by tectonic movements over the past 1800 years (Wilson et al. 1997; Manville and Wilson 2003), differences in the grounding level of different-sized pumice blocks, and reworking of smaller clasts into the offshore. Many of these small clasts are denser than water, and so cannot have travelled from the dome to the shoreline except as part of larger, more-buoyant blocks. Their presence precludes our obtaining and using a pumice-size distribution to infer how long pumice clasts needed to float in order to reach the shoreline. Even without the grey pumice, however, such a distribution would be deeply compromised by the sampling bias inevitably accompanying size measurements confined to the narrow modern-day outcrop belt.

The interval between the climatic phase of the Taupo eruption and emplacement of the subaqueous lava domes is uncertain. Manville et al. (1999) estimated that the lake refilled from a post-eruption lowstand level of c. -130 m, based on features seen in sub-bottom profiling (Lister 1978), to +34 m in c. 40 years. Smith (1991), put the interval at closer to 15 years, plus an extra couple of years for the lake to rise from its modern level (inferred to approximate the pre-1.8 ka eruption level: Wilson, 1993) to +34 m. Excluding the time required to refill Lake Taupo from an ambiguous post-eruption lowstand elevation to its modern level, a period which is subject to the most uncertainties and assumptions regarding starting points, inflow rates, and establishment of a stable water table in the eruption-impacted catchment (Riggs et al., 2001), and using the modern range of natural annual inflows (minimum 80 m^3/s, mean 125 m^3/s, maximum 170 m^3/s), it is estimated that the lake took c. 4-7 years to fill from +0 to +34 m. This gives an annual filling rate of 5-9 m/yr (Riggs et al. ,2001).

At individual sites, giant grey pumice clasts occur over narrow elevation ranges (less than 1 m), implying that they were emplaced during a single, short-lived stranding event (Riggs et al. 2001). Correction for post-1.8 ka tectonic movements (Otway, 1986; Wilson et al., 1997) and grounding-line variations suggests emplacement occurred over less than one year. This implies either rapid emplacement of the Horomatangi Reefs dome at a rate (c. 8 m/s) somewhat higher than the historically observed range for modern subaqueous rhyolite dome growth (1-3 m^3/s: (Maeno and Taniguchi 2006)), or more prolonged dome growth and a brief episode of block release from the dome (Kano 2003).

4.0 JOINTING PATTERNS

The giant rafted pumice blocks (labelled GRP## in this paper) at Taupo show complex, heterogeneous, jointing patterns. Block surfaces and rims are marked by a distinct zone of fine surface-normal joints approximately 10 cm deep, with joint spacings decreasing towards the outer perimeter to a minimum of 5-10 mm. These form polygonal (tortoise-shell) crack patterns on the block surfaces. Larger joints are spaced c. 30 cm apart and traverse a transitional zone where they are oriented perpendicular to the clast margins to penetrate up to 0.5 m into the interiors of the largest blocks. Here they typically merge into more closely spaced 'herringbone' (sample from GRP29) or chaotic joint sets. In some more-equant blocks (i.e. GRP40; Fig. 2) surface-normal joints converge inward to a central point in a rosette-like structure that becomes less chaotic inwards. Jointing patterns are generally identical on all exposed sides of the observed blocks, although the short side of GRP40 has a smaller and less prominent transition zone and a wider rim with more-irregular joints than do the two longer faces.

The bimodal depths of cracks extending inward from the block rims is indicative of formation by two processes. First, the fine polygonal cracks are inferred to result from thermal contraction of the block surfaces during rapid cooling and quenching by contact with water (Yamagishi 1991), as observed in pillow (Yamagishi 1985) and ice-contact lavas (Lescinsky and Fink 2000; Spörli and Rowland 2006). When thermally-generated stresses exceed the tensile strength of the rock, fractures develop perpendicular to the surface of equal tensile strength, i.e. parallel to the thermal gradient, forming columnar joints (DeGraaf and Aydin 1987; Saliba and Jagla 2003). Crack spacing is inversely proportional to cooling rate (Toramaru and Matsumoto 2004). Second, the wider-spaced and larger open joints are interpreted as tensional features developed by inflation of the block interior (Yamagishi

1991), most likely as a result of continued vesiculation, similar to the process that produces bread-crust bombs (Wright et al. 2007).

Smaller grey pumice clasts lack complex jointing patterns, but often have curvilinear faces or polygonal cracking on one surface only, suggesting that they were formed by the break-up of larger blocks along thermal contraction fractures, possibly due to wave action or thermal decrepitation. Reworking in the swash-zone caused partial rounding of some blocks.

5.0 VESICULARITY

A number of qualitative and quantitative techniques were used to characterise the vesicularity of the giant rafted pumice blocks, and complement data on vesicle populations from imagery studies (Houghton et al., 2003; 2010). BET (Brunauer, Emmett and Teller) analysis and mercury porosimetry are common quantitative industry techniques applied to porous materials, but have rarely been used on pumice (Whitham and Sparks 1986). BET analysis provides information on the internal surface area of a pumice clast while mercury porosimetry yields data on the dimensions of pore throats: in combination they yield information on pore-size distribution and abundance, and a measure of interconnectedness. While vesicularity governs the bulk density of a pumice clast (Houghton & Wilson 1989) and determines whether it will float at all (Manville et al. 1998), total porosity, interconnected porosity, and pore geometry all influence permeability (Klug and Cashman 1996), which controls its ability to become saturated with water, and the time required to do so. This in turn controls the buoyancy history of the clast (White et al. 2001).

The large grey pumice blocks display obvious variations in vesicularity, with 'core' domains nearer the clast centres being most vesicular, outer edges least vesicular, and zones of transitional vesicularity occurring between (Fig. 5). Overall, the grey pumice has a more varied, domainal, and generally lower vesicularity than the white tube-walled pumice (71%-79%; Houghton & Wilson, 1989; Houghton et al. 2010) which dominates the surrounding nearshore pumiceous gravels and was reworked from the Taupo ignimbrite. Measurements were conducted on eight 1 cm cubic samples taken from the giant rafted pumice blocks, and a number of scanning electron microscope (SEM) inspections were made. Exterior and interior samples were taken from two large clasts (>5 m; GRP29 and GRP40 which also has a transitional sample). The transitional zone of GRP23 was also sampled.

5.1 Results of vesicularity analysis

In hand specimen, consistent macroscopic trends in vesicularity are apparent in the larger giant rafted pumice blocks (Table 1), but with inhomogeneous vesicle populations in all zones; rim, transitional and core. Specific area, from BET analysis (Table 2) is greatest in transitional zones because of the presence of both small and large bubbles and greater connectivity: although rim zones have more numerous and smaller vesicles, measured specific area is reduced by isolation of some vesicles and poor connectivity among others (See also supplementary information #3). Conversely, specific area in core zones is reduced by the presence of abundant large and composite pores. Quantitative data from Hg porosimetry yields a rather noisy pattern revealing no dominant vesicle size (Table 3; Fig. 6; supplementary information). This contrasts with the SEM-observed peak in vesicle abundance at 25 μm in all samples examined, which matches the "low vesicularity" mode identified for these pumices using image analysis and stereology (Houghton et al., 2010). No other peaks or troughs are shared across all our pumice samples. Mercury porosimetry consistently overestimates potential specific area because of the abundance and frequency of non-spherical and ink-bottle-shaped vesicles (pores) in all samples. We now describe vesicularity of three giant pumice clasts in more detail.

Pumice clast GRP23: The centre of the clast shows the highest macro-vesicularity, with patchily distributed sub-spherical to tubular pores, including large cavities up to 4 cm in diameter spanned by fibrous glass bridges. SEM examination of sample T71 from the transitional zone shows multiple generations of slightly elongate vesicles down to minimum size of 1 μm. BET analysis of this sample (Table 2) records a low vesicularity but high specific area, indicating lots of very small vesicles. Mercury porosimetry results (Table 3) show low injected volumes and moderate retention on extrusion, indicating low pore volumes and an intermediate number of bottle-shaped pores.

Pumice clast GRP29: Sample T89 from the clast interior is very porous, with a minimum (SEM) vesicle size of 4 μm. BET analysis (Table 2) shows a low specific area relative to the rim sample (T91), whilst mercury porosimetry (Table 3) shows lower intruded volumes but greater retention on extrusion. The minimum vesicle size seen under SEM in T91 is 0.3 μm.

Since both samples have similar vesicularities based on sample density, it is inferred that although T89 contains more bottle-shaped pores, and that T91 has more pores of a given-size than T89, many of those in the rim are unconnected and hence not measured by either BET or mercury porosimetry techniques.

Pumice clast GRP40: BET and porosimetry analysis of sample T134 from the clast interior underestimate total vesicularity (Tables 2, 3) because, as with the other interior cube samples, the measured sample lacks the multi-centimetre diameter cavities that occur dispersed through the clast central domain. BET analysis gives an intermediate specific area between the lowest (rim sample T137) and the highest (transitional sample T135). Mercury porosimetry results (Table 3) indicate that the interior sample accepted and retained the least mercury. T135 (transitional) accepted the most mercury, indicating good connectivity, and in conjunction with the BET results, a mixed population of large and small pores. T137 (rim) had the greatest mercury retention: combined with the BET data this indicates abundant small but poorly connected pores with many closed voids. SEM analysis shows few broken bridges.

6.0 PALEOMAGNETIC ANALYSIS

Early paleomagnetic studies of the grey pumice blocks showed that they shared the same remanent magnetic orientation as the Earth’s current magnetic field, which was interpreted, along with the surface-normal jointing patterns, to result from in-place cooling as miniature rhyolitic intrusions or ‘necks’ intruded along an arcuate structure (Northey 1983). More detailed field work revealed that the pumice blocks are surrounded on all sides by lacustrine sediments and that the arcuate lineament on which they appear to be aligned is a lowstand shoreline associated with the post-eruption rise and fall of Lake Taupo (Wilson and Walker 1985). The absence of a chilled glassy rim on the pumice blocks or thermal alteration of the surrounding sediments also indicates that their exteriors were cool at the time of final lodgement and burial.

We conducted more-detailed magnetic analyses to determine the emplacement temperatures of the giant pumice blocks. In igneous rocks ferromagnetic minerals, principally Fe-Ti oxides, generally record the orientation of Earth’s geomagnetic field as they cool below the Curie temperature (T_c) (e.g. Butler 1992; Dunlop and Özdemir 1997) which is known as a thermoremanent magnetisation (TRM). Different minerals have different Curie temperatures and coercivities (ease of demagnetization), for example the T_c of magnetite is c. 575°C and that of hematite c. 675°C. Rock magnetic vectors are described in declination (angular difference between grid north and magnetic north), inclination (dip angle relative to the horizontal plane of the Earth's surface), and intensity of magnetisation. Progressively reheating an oriented sample (thermal demagnetisation) of igneous rock will cause it to demagnetize as the constituent magnetic minerals exceed the unblocking temperature or Curie temperature. The aim of progressive thermal demagnetisation is to remove low stability components, which often are late stage overprints until only the high stability ones remain, which are referred to the as primary magnetisation and most representative of the time of cooling below the curie temperature. Between each heating step magnetic moment measurements are made that track the demagnetisation process. Magnetic moment data are typically plotted on orthogonal component vector diagrams where principal component analysis (PCA) is conducted to deconvolve low and high temperature/stability magnetic components (Fig. 7).

6.1 Paleomagnetic Methods

Thirty-eight orientated samples were collected from ten large (>4 m) rafted pumice blocks for which samples could be confidently assigned to the rim, transition or interior zones. To minimise any iron hydroxides such as goethite in analysed samples, less weathered and soil free/poor locations were selected for sampling. Pumice blocks were set in plaster and 188 oriented cores (at least two from each block) drilled using a standard 2.25 cm diameter, non-magnetic diamond tipped drill. Magnetic moment measurements were made using a Molspin minispin spinner magnetometer or with the 2G Enterprises DC 760.5, pass-through superconducting rock magnetometer, both of which are housed in a magnetically shielded room at the Otago Paleomagnetic Research Facility (OPRF). Thermal demagnetisation was conducted using the triple shielded, ASC-Scientific® demagnetising oven housed at the OPRF and Alternating Field (AF) demagnetisation was conducted using the inline demagnetising coils on the 2G Enterprises magnetometer, induced remanent magnetisations (IRMs) were imparted using an ASC-Scientific® impulse magnetiser and hysteresis analyses were conducted using a Princeton Measurements Corporation Vibrating Sample Magnetometer (VSM).

6.2 Magnetic mineralogy

Alternating Field (AF) demagnetisation, saturation-isothermal-remanent magnetisation (IRM) analyses and hysteresis analyses were conducted to determine magnetic mineralogy samples. Eighteen cores were AF demagnetized at 5 mT increments in fields between 5 mT and 50 mT, then at 60 mT, 80 mT and finally at 100 mT using the in-line AF demagnetization coils of the 2G magnetometer. Magnetic moment measurements were made between each demagnetisations step. IRM analyses were conducted on 17 samples using an ASC Scientific impulse magnetiser where samples were magnetised at 10 mT increments to 100 mT, 20 mT increments to 200 mT, 50 mT increments to 1T (saturation) at which point the orientation of samples was reversed and the process repeated. Magnetic moment measurements between magnetising steps were made using the Molspin minispin magnetometer. Hysteresis analyses were conducted using a Princeton Measurements Corporation VSM with maximum applied fields of 500 mT which was sufficient to saturate samples.

AF demagnetisation revealed a rapid decrease in magnetisation with most samples reducing to an average of a quarter of the natural remanent magnetisation (NRM) at 100 mT (Figure 9) indicating that the dominant magnetic mineral is likely to be magnetite (*cf.* Lowrie and Fuller 1971; Dunlop and Özdemir 1997). The remaining remanence above the 100 mT demagnetisation step indicates the presence of small quantities of one or more 'hard' magnetic minerals such as haematite, goethite, or oxidised magnetite. IRM analyses (Figure 7) revealed a rapid increase in magnetisation within the first 50 mT and complete saturation by the 300 mT step. Mean sample coercivity was 21 mT, which indicates a magnetite dominated mineralogy (Dunlop and Özdemir 1997) with a dominance of small Pseudo Single Domain (PSD) or Single Domain (SD) grains (Dunlop 1973; Wasilewski 1973). A few samples had higher coercivities and saturated at higher fields indicating the presence of minor quantities of higher coercivity minerals in agreement with AF demagnetisation (Dunlop and Özdemir 1997). Hysteresis analysis (Figure 7) indicates samples saturate at relatively low fields and indicating the dominance of magnetite. The closed nature of hysteresis data likely indicates the presence of large, multi domain grains with a minor component of single domain grains.

6.3 Thermal demagnetisation and magnetic moment measurements

The thermal demagnetization was conducted in two parts: a pilot study of 38 cores, one from each sample and a follow-up study, which analysed a further 19 cores at smaller temperature increments. The natural remnant magnetisation (NRM) was measured before thermal demagnetisation was started. Samples were then subjected to stepwise thermal demagnetisation with magnetic moment measurements made between demagnetisation steps using the spinner magnetometer. Thermal demagnetization data were plotted on orthogonal component vector plots using PuffinPlot (Lurcock and Wilson, 2012). Magnetisation directions were calculated using principal component analyses (PCA, Kirschvink, 1980). Thermal alteration of samples was monitored by measuring magnetic susceptibility using a Bartington MS2B magnetic susceptibility meter.

Most samples completely demagnetised by c. 590°C indicating magnetite is the dominant remanence carrier (Lowrie and Fuller 1971). Some samples exhibited minor, very low blocking temperature components (20 to 143°C) which may indicate small amounts of a magnetic mineral with a very low Curie temperature, such as goethite. The remaining intensity measured at temperatures higher than 590°C, can be attributed to small amounts of hematite.

6.4 Interpretation of thermal demagnetisation data

We analyse the orientation of the primary TRM to determine whether selected blocks have experienced rotation since cooling below the Curie temperature. The geomagnetic field at the time of eruption was similar to the modern geomagnetic field with a declination of approximately 000° and an inclination of between -50° and -60° (Turner and Lillis 1994). Results for other blocks are given as Supplementary information (supplementary information #4).

Clast GRP23: Three samples from span the interior to the rim (Fig. 8a). Sample T237, from the interior displays a primary remanence direction that is similar to the modern geomagnetic field indicating that the sample cooled below the Curie temperature in its current position (Fig. 8a). In contrast, sample T238 from the transition zone has a dominant remanence declination of 069° indicating this sample had cooled beneath the Curie temperature and was then reoriented before emplacement. A minor low temperature component aligned approximately north-south demagnetises by c. 200°C and is probably a recent overprint. T239 is from the rim of the block and displays more complex demagnetisation behaviour with a north-south oriented shallow inclination component (-43°) that is offset from the origin and persists to above 500°C. The north-south orientation of the component indicates that this block has not rotated in the horizontal plane since cooling beneath the Curie temperature of magnetite. However, the sample may have been rotated in the vertical plane, possibly when it settled in its final position. Early in its history, however, GRP23 did experience rotation in the horizontal plane, which is recorded by sample T238, but it is probable that parts of the block remained well above the Curie temperature after the block settled in its final position. Sample T239 has a more-complex multi-component demagnetisation path with low-temperature magnetic components, which indicates some degree of rotation.

Clast GRP40: All samples have steep inclinations (Fig. 8b), which indicates that this block has not been overturned. However, the declination of primary remanence varies from place to place through the block, indicating that different parts cooled at different times. The declination of interior sample T219 is rotated 073° indicating that this part of the block had cooled below the Curie point prior to lodging in its current position. Sample T220, taken inward from the small-normal-jointed margin and lacking transitional textural characteristics, has a primary remanence direction that approximates the modern geomagnetic field, indicating that it was above the Curie temperature when it lodged in its current position. Samples T221 and T218 have very similar remanence directions that are mildly rotated with respect to geographic north, but sample T217, from the rim of the block, has been rotated 170° indicating that the outer surface had cooled and the clast rotated significantly prior to emplacement in its current position.

Clast *GRP104*: Samples show a wide range of magnetisation directions (Fig. 8c). Overall inclination and declination are quite varied, and indicate that the block had cooled below the

Curie temperature before emplacement. The shallow inclinations (T243 and T244) also indicate that the tabular 5.1 m long block was overturned after cooling.

Principal component analysis (PCA) of magnetisation directions demonstrate that some large blocks record significant re-orientations during their cooling history. In all instances samples from the dense pumice rim, which forms shortly after initial extrusion, display the greatest degree of mis-orientation with respect to the expected geomagnetic field. This indicates that, unsurprisingly, they had cooled below 580°c prior to emplacement and burial along the lakeshore. Systematic interpretation of the transitional and interior samples is more difficult. In GRP23 and GRP40 the mean inclination of all samples is c. -60° which is similar to the expected geomagnetic field at the time of eruption (Turner and Lillis 1994) suggesting that these blocks experienced horizontal rotations only. A systematic relationship between declination and the position within a block (interior vs transition) is not clear with some interior samples showing evidence for emplacement at temperatures above 580°C and others showing a emplacement at cooler temperatures. It is likely that water entering fractures or open permeability pathways (e.g. Manville et al., 1998) in the blocks, or even in the pumice carapace prior to block separation, caused some interior parts to be cooled earlier than others. One simple relationship can be seen. Magnetisation at the exteriors of the blocks, which developed in the dense pumice rims shortly after initial extrusion, rarely matches the expected field, indicating rotations of the clasts after their rims had cooled below the Curie temperature. Other samples, from transitional texture zones and from the interiors of the blocks, show a variety of magnetic orientations. These developed as irregular, reticulate (Manville et al., 1998), cooling fronts advanced from the surface and from deep fractures and joints. Some of these samples have the expected magnetic orientation, and are from sites that cooled below Curie after the pumice blocks had become lodged and fixed in place at the shoreline. Smaller, blocks display apparently random orientations related to rotations while floating across the lake, especially for higher blocking temperatures.

7.0 DISCUSSION

Synthesis of data from sedimentary features, pumice vesicularity, paleomagnetic analyss, and jointing geometries indicates that the giant rafted pumice blocks at Taupo still had hot domains internally (>575°C) when washed ashore, and finished cooling to ambient temperatures after stranding along the transgressing shoreface of the lake. Block rims show evidence of the most rapid cooling, with the finest polygonal cooling cracks, and the lowest vesicularity, vesicle sizes, and permeability. Transitional zones are cut by cooling joints perpendicular to the outer surface, with a greater spacing than in the rim, indicating slower cooling. Minimum and maximum vesicle sizes, and vesicle-size distributions are intermediate between those of the rim and core zones, and many pores have broken or ragged inter-vesicle bridges. In addition, the thickness of intact bridges is less than that in the rims and many coalesced vesicles are visible in both hand-specimen and SEM. Broken bridges between vesicles, as well as fully coalesced vesicles, result in greater connectivity and permeability. The boundary between the transition zone is not geometrically regular, and the interior is marked by a very abrupt change in the size, character, and orientations of joints. In many places within block interiors, joints are closely spaced in intricate arrangements, such as the rosette shape as seen in GRP40 or the series of intricate chevron-like structures in GRP29 – these are taken to record complex cooling of the interiors in response to local invasion of water. Vesicularity generally increases towards the block centres, and many joint rosettes terminate in this central maximum-vesicularity zone, consistent with their being among the last parts of the blocks to cool. Mercury porosimetry and SEM data show that pore connectivity is greatest in parts of the interiors; walls are thinner and more likely to be broken or fibrous. The longer period of ductility experienced by some inner parts of the blocks, compared to the rims, allowed bubbles to grow and coalesce, resulting in internal expansion and the development of expansion joints in the cooler, more rigid exterior.

Studies of the vesicularity of clasts from all phases of the explosive Taupo 1.8 ka eruption (Houghton et al. 2010) show evidence of bubble coalescence late in the pre-fragmentation degassing history of all magmas, with new bubbles nucleating right up to the point of fragmentation. The magma involved in the late-stage domes that gave rise to the giant rafted pumices remained deep in the plumbing system for an extended period, enabling limited growth of microphenocrysts, before ascent and equilibrium degassing. These samples also show evidence for the onset of permeability development, partial outgassing, limited syn-eruptive crystallization and bubble collapse.

7.1 Pumice from domes vs high-intensity eruptions

Experiments on cold and hot pumice clasts from high-intensity, plinian eruptions demonstrated that cold pumice floated for extended periods of time, whereas hot pumice in the experiments (up to 25 cm^3) sank immediately (Whitham and Sparks 1986), with vesicle interconnectivity (Manville et al. 1998; Scott et al. 2004) strongly mediating saturation rates of cold pumice. Loss of buoyancy for hot pumice resulted from volume reduction and condensation of hot internal gases (Whitham and Sparks, 1986), including magmatic steam (Allen et al. 2008), by cold water that was then drawn inward by the sudden pressure contrast progressively along a variably irregular, reticulate (Manville et al., 1998), cooling front. This behaviour differs from that of large blocks of hot, steaming pumice observed floating at the subaqueous Myojinsho (Tsuya et al. 1953; Fiske et al. 1998), Tuluman (Reynolds and Best 1980; Reynolds et al. 1980), and Shin-Iwojima (Tanakadate 1935; Maeno and Taniguchi 2006) eruptions, and the inferred behaviour of the Taupo giant rafted pumices, or similar ones at La Primavera (Clough et al., 1981) and Ilopongo (Mann et al., 2004). The question is then different buoyancy responses reflect in part some fundamental difference in the porosity and permeability of pumice from high-intensity eruptions versus from domes, or whether hot flotation is entirely a scale-dependent effect.

Pumice from intense eruptions appears to have much greater vesicle connectivity than dome-derived material, due to more-rapid degassing of the ascending magma in a conduit, which culminates at a fragmentation front (Klug and Cashman 1996; Mungall et al. 1996; Kaminski and Jaupart 1997; Wright et al. 2007; Mader 1998; Kremers et al. 2010; Richard et al. 2013). Rhyolite lava domes, by contrast, are formed by the eruption of largely outgassed magma that subaerially may be undercooled by 100 ^{o}C or more below its liquidus temperature (Manley and Fink 1987), and Houghton et al. (2010) report vesicle-population evidence that the Taupo giant pumices are also from "partially degassed" magma. Subaerial domes develop a variety of distinctive surface textures during and after extrusion at the surface as a function of further degassing and devitrification processes (Fink et al. 1992), and the evolving rheology of the cooling flow (Fink 1983; Griffiths and Fink 1992; Griffiths and Fink 1993).

7.2 Subaerial vs subaqueous silicic domes

In contrast with subaerial domes (Fink 1983; Eichelberger et al. 1986; Griffiths and Fink 1993), subaqueously extruded silicic magma is subjected to more-rapid surface cooling due to the much greater heat capacity of water, while hydrostatic pressure reduces vesicle growth (White et al. 2003). Exposures of the internal structure of felsic domes developed underwater show that they take the form of large mounds veneered by dome-derived hyaloclastite that comprises fragments of varying vesicularity and degrees of quenching. The "dome" itself has a complex internal structure defined by mutually crosscutting, more-coherent dykes, pods, and lobes (Furnes et al. 1980; Yamagishi 1991; Scutter et al. 1998; De Rita et al. 2001; Goto and Tsuchiya 2004). The margins of these bodies can be vesicular, and show a range of features, including ropy wrinkles and corrugations, bimodal fractures comprising small polygonal contraction cracks perpendicular to the surface and larger tensional expansion joints (Yamagishi 1991), glassy rims (Furnes et al. 1980; Yamagishi and Dimroth 1985). Contacts of coherent rock with the enclosing hyaloclastite are gradational, passing through areas of more- or less-fragmented monolithologic angular breccia (often resembling a jigsaw puzzle) spalled off from the pseudo-pillows margins. Continuous and well-defined glassy rims are usually absent (Yamagishi and Dimroth 1985), though pumice and obsidian may be present (de Rosen-. Spence et al., 1980), and entire domes/lobes may be aphyric (Hanson, 1991).

Pumiceous textures are favored where confining (hydrostatic) pressures are low (Hunns and McPhie 1999; Gifkins et al. 2002).

7.3 Subaqueous dome disruption processes

Subaqueous rhyolite lava domes, with or without hyaloclastite veneer, have been inferred to be disrupted in various ways to produce floating pumice blocks (Kano, 2003), including by Vulcanian eruptions, phreatomagmatic (steam explosion) eruptions, and non-explosive dome breakup ("dome collapse") eruptions in which effusing rhyolite forms unstable hyaloclastite mounds laced with bodies of coherent rhyolite. The presence of microlites and distorted and deflated bubble shapes in the Taupo giant rafted pumices suggests an extended period of magma storage, ascent and equilibrium degassing, followed by vesicle coalescence and partial collapse.

In Vulcanian eruptions, magmatic gas trapped within coarsely vesicular pumice (Manley and Fink 1987) below a largely impermeable zone at the outer margins of the dome attains pressures sufficient to disrupt the dome carapace, thereby producing a thick bed of coarse pumice with a basal lithic breccia of glassy lava crusts in proximal locations, and potential flotation of coarsely vesicular pumice (Kano 1996).

Phreatomagmatic explosions can be generated when water penetrates cracks in the carapace of a growing lava dome to come into direct contact with molten rhyolite (Allen and

McPhie 2000). The mixing efficiency of cold water with hot rhyolitic magma is low because of the latter's high viscosity (Kokelaar 1986; Wohletz 1986), but explosive interactions can be induced by dynamic fracturing of submerged lava in response to internal dome inflation (Austin-Erickson et al. 2008). Such eruptions are expected to generate dilute volcaniclastic density currents and floating hot pumices, some of which will be derived from the molten dome core and may have fluidal or/and quenched exteriors.

Non-explosive "collapse" of a growing dome (Kano et al. 1991) can occur when the hyaloclastite veneer creeps or slumps gently (because of the small effective density of the fragments in water) in response to growth of the underlying complex dome in which vesiculating lava is intruded into and through a carapace of syn-eruptive hyaloclastite breccia. Thermal gradients are lower in this water-saturated mound, which at least proximally has zones of mechanically-interlocked 'jigsaw' blocks. Dynamic and gravitational destabilisation of the growing pile can result in weak slumping, enabling the release of externally-cooled pseudo-pillows and blocks as a result of buoyancy and thermal and mechanical fragmentation (Kano 2003). Such blocks will have complex cooling histories, with some surfaces that began cooling when they were outer constituents of the dome prior to breakup, and other surfaces newly created at the time of disruption and flotation. Alternatively hot blocks, once detached, can rise through the mobile granular mass to escape; buoyancy forces experienced by the largest blocks at Lake Taupo (>400 m^3) would exceed 60 tonnes for a mean density of 900 kg/m^3, which allows for some saturation of marginal parts of the blocks. Clasts that are sufficiently large retain for long periods the internal heat necessary to preserve vapor in the vesicular core, which allows them to float to the surface and drift ashore. Clasts of pumice with interconnected vesicles, which is the general case (Klug and Cashman, 1996), that cool before stranding will slowly saturate and and may sink before stranding (Whitham and Sparks, 1986; Manville et al., 1998).

We have only the floated blocks to examine at Taupo, so we cannot use the style or fragment types in near-vent deposits to help distinguish among different eruptive styles. The chilled outer margins of floated pumice blocks at Taupo are not coarsely vesicular, nor do they contain bands of obsidian, both of which would be expected for blocks produced by a Vulcanian eruption (Manley and Fink, 1987; Kano, 2003). There is variable but not obviously systematic development of fracture and vesiculation patterns on all sides of the giant rafted pumices, showing that the blocks' internal textures continued to evolve after release from the dome. The finely vesicular rims of the rafted pumice blocks, as well as lack of obsidian interbanded with coarsely vesicular pumice in the blocks, further argues against fully subaqueous Vulcanian disruption. From the transitional to core zones some vesicles become larger and there is clear evidence of coalescence. These are both probably responses to gas expansion, which is most likely to have taken place when pressure was released as the blocks rose from shallow depths to the lake's surface. Without additional information from near-source beds it cannot be determined whether the blocks were released by phreatomagmatic explosions, or by low-energy disruption of a growing dome; the floatable material released would be the same.

8.0 CONCLUSIONS

The giant pumice blocks preserved around the shoreline of Lake Taupo formed during subaqueous dome growth in the decades-long aftermath of the explosive 1.8 ka eruption, floated to the surface and were blown ashore where they became embedded in accumulating transgressive lacustrine shoreface sediments. TRM orientations preserved in rim-to-core profiles record an initial field acquired during dome extrusion or intrusion into an auto-brecciating saturated hyaloclastite mound, more-random vectors developed during flotation and transport across the lake, and in places within block interiors a final stable vector close to the modern geomagnetic field, locked-in during final lodgement and burial. Parts of the blocks thus remained above the Curie temperature of magnetite for an extended period, probably due to their size and the thermal insulation afforded by the vesicular rim, and remained buoyant long enough to cross several kilometres of open water. Surficial fracture patterns include both small thermal-contractional cooling cracks and inflation-expansion joints, indicating rapid cooling of block margins below the brittle-ductile transition while parts of the interiors continued to expand. Denser fragments, including those spalled from floating block exteriors, never reached the shoreline, resulting in efficient hydraulic segregation, and probably a trail of isolated blocks on the lake bed tracing back towards the blocks' source.

The blocks are unlikely to be the product of explosive disruption of an emergent dome by a Vulcanian or phreatomagmatic eruption, because there are no correlative fall deposits associated with the eruption Z dome growth (Wilson 1993). Release of buoyant pods of lava grown into its own fragmental carapace (such as pseudo-pillows: Yamagishi 1991) is envisaged, associated with breakup and possible phreatomagmatic explosions in the unstable edifice. Similar rafted giant pumice blocks are a common product of subaqueous rhyolite dome growth at depths of 200-500 m (Kano 2003), but are rarely observed in the geological record unless trapped within a closed basin such as an intracaldera lake (Clough et al. 1981; Wilson and Walker 1985; Mann et al. 2004; Barker et al. 2012). Of the 26 known post-26.5 ka eruptions at Taupo volcano, 23 have been subaqueous, with the majority showing evidence for late-stage lava extrusion (Wilson 1993). Therefore, the probability that the next eruption at this hyperactive rhyolite caldera will also include a subaqueous dome-forming event are high, potentially generating floating giant pumice blocks with implications for water quality and hazards.

ACKNOWLEDGEMENTS

This study was funded by FRST through GNS contract C05X0006 to Manville, sub-contract 5/HAZ/OU to White, and an Otago University Award to von Lichtan. BET analysis was arranged for us by Bernd Zimanowski, and conducted by Dietmar Schenk using a Nova 1200 Gas Sorption Analyser V.3.00 at the Institut für Geowissenschaften, Johannes-Gutenberg-Universität Mainz, Germany. Mercury porosimetry analysis was conducted at the Particle and Surface Science Application Laboratory, NSW, Australia. Paleomagnetic studies were carried out at the Otago Palaeomagnetic Laboratory at the University of Otago, Dunedin using a Molspin spinner magnetometer (SIRM), an automated pass-through cryogenic magnetometer (AF demagnetisation and magnetic analysis), and Princeton Measurements Corporation VSM. The paper was improved in light of comments from JVGR reviewers Scott Bryan, Kazuhiko Kano, and an anonymous reviewer, and we thank them for their efforts.

Table 1: Generalised trends in vesicularity patterns

Parameter	**Distribution**
Vesicularity	core > transitional > rim
Minimum vesicle size	core > transitional > rim
Maximum vesicle size	core > transitional > rim
Vesicle size variation	core > transitional > rim
Specific area	transitional > core > rim

Table 2: BET results for 1 cm^3 cubes, and granulate fragments 1 mm or 2 mm diameter. Samples are core, rim, core-rim transition (trans), or typical for a sampled clast (typ). Granulate samples labelled by granule size. The Brunauer, Emmett and Teller (BET) analysis was conducted using a Nova 1200 Gas Sorption Analyser V.3.00 through Dietmar Schenk at the Institut für Geowissenschaften, Johannes-Gutenberg-Universität Mainz, Mainz, Germany.

Sample No.	Weight (g)	Surface Area (sq m)	Specific Area (sq m/g)	BET C	Simple Point Surface Area ((sq) m)	Simple Point Specific Area (sq m/g)
T071 trans GRP 23	1.0761	12.3426	11.4698	3.454128	5.9685	5.5464
T089 core GRP 29	0.9162	11.3688	12.4087	3.667106	5.6208	6.1349
T091 rim GRP 29	1.0166	6.8864	6.7739	4.489771	3.6498	3.5902
T134 core GRP 40	0.6414	8.388	13.0776	4.221139	4.3513	6.7841
T135 trans GRP 40	0.6107	10.2709	16.8183	3.969104	5.2258	8.5571
T137 rim GRP 40	0.9209	12.2408	13.2922	3.792754	6.0959	6.6195
T134 core 1mm granulate	0.021	0.0646	3.0779	8.86863	0.0282	1.3428
T134 core 2mm granulate	0.0824	0.131	1.5894	8.975279	0.0706	0.8563
T137 rim 1mm granulate	0.043	0.1335	3.1037	6.999031	0.0659	1.5328
T137 rim 2mm granulate	0.3089	12.5784	40.7201	2.23116	4.5429	14.7067

Table 3: Mercury intrusion porosimetry results for granulated pumice. Samples are core, rim, core-rim transition (trans), or typical for a sampled clast (typ). Data reported from Particle & Surface Sciences Applications Laboratory, Gosford, New South Wales, Australia, 26 September 2002.

Sample ID	Sample Weight (g)	Total Intrusion Volume (cc/g)	Total Pore Area (m^2/g)	Median Pore Diameter (Volume) (μm)	Median Pore Diameter (Area) (μm)	Average Pore Diameter (μm)	Envelope Density (g/cc)	Skeletal Density (g/cc)	Porosity (%)
T71 trans GRP 23	0.6985	0.3584	10.78839	20.2966	0.0129	0.1333	1.2749	2.3473	45.686533
T89 core GRP 29	0.6176	0.3072	9.802458	20.2851	0.0099	0.1256	1.3655	2.3521	41.945496
T91 rim GRP 29	0.5382	0.3195	9.834642	16.5746	0.0089	0.1304	1.3724	2.4439	43.843856
T134 core GRP 40	0.5699	0.4404	10.15727	22.2397	0.01	0.1354	1.1367	2.3092	50.77516
T135 trans GRP 40	0.465	0.5043	14.90674	22.2397	0.01	0.1354	1.0668	2.3092	53.802183
T137 rim GRP 40	0.622	0.4649	11.84878	11.1909	0.0099	0.0955	1.2062	2.357	48.824777

List of figures

Fig. 1: Locations of rafted grey pumice blocks along the NE shore of Lake Taupo. Blue line marks the highstand of Lake Taupo following the 1.8 ka Taupo eruption, with spot elevations marked. Inset shows Lake Taupo near centre of the North Island of New Zealand, with study area boxed. Location of Figure 4 deposits indicated.

Fig. 2: Giant floated pumice. (a) Floating steaming few-m wide pumice blocks from the Tuluman eruption, Papua New Guinea, taken 24th March 1955 (Reynolds and Best, 1957). (b) Giant Rafted Pumice GRP40. Outer cooling joints are perpendicular to the cooling surface, while “rosette style” internal joints centre on the most vesicular area of the clast. (c) SEM of pumice-interior texture of T134. (d) Close-up of transition-zone sample T135

Fig. 3: Photo of giant rafted pumice block (GRP) and lacustrine sediments. Giant rafted pumice resting on undisturbed alternating beds of laminated mineral-rich sand and thin pumice-pebble layers, Five Mile Bay.

Fig. 4: Photo (A) of giant rafted pumice block overlying 10 cm thick bed of pumice pebbles, over normal-graded pumice bed of fine pebbles to sand. B-D are selected measured sections (see online supplement for all sections). Elevations are a.l.l. with error estimated 10-20 cm (within symbol size), grainsize scale in mm. (B) Sections show variability in a small area with many pumice blocks, with 057 showing a cluster of large grey pumice clasts representing a broken-apart rafted block; most of these grey clasts would not float on their own, as tested by putting a group into the lake. (C) Section 171 with giant rafted pumice overlying shoreface pumice and lithic-sand beds. (D) Section 169b giant rafted pumice overlies a more pumice-rich section. (E) Elevation of pumice blocks (sizes indicated by symbols) plotted against distance northward along Five-Mile Bay. Inset illustrates draught ratio of a floating partly saturated block with density ~900 kg/m^3. Note that despite having greater draught, the largest blocks lie at higher elevations further north in the downwind direction – this suggests that they were repeatedly lifted and re-stranded as the shoreline transgressed.

.

Fig. 5: GRP23, in roadcut above Motutere Bay, and vesicularity variations. It has visible jointing, perpendicular joints on the outer margins and a chaotic jointing structure centred on the more vesicular area. Close up scans and SEM images show the variation from: (a) the rim (av.

vesicularity 63%); (b) transitional (av. vesicularity 66%); and (c) the interior (av. vesicularity 67%). Estwing hammer (~33 cm) below “a” for scale.

Fig. 6: Plot of vesicle(-throat) diameter versus incremental vesicle (porosity) volume for selected samples from giant pumice blocks at Taupo obtained using Hg porosimetry. Note large range of pore-throat diameters and lack of distinct measured differences between rims and cores. T89=GRP29 interior; T91=GRP29 rim; T134=GRP40 interior; T137=GRP40 rim

Fig. 7: Saturation isothermal remnant magnetisation (SIRM) and backfield acquisition experiment (A) and AF demagnetisation data (B) from representative samples from large grey pumice blocks. All samples have a low coercivity (Hcr of about 20 mT) and saturate rapidly (below 300 mT) which indicates low coercivity magnetic minerals. AF demagnetisation indicates a rapid decrease in magnetic intensity indicating the presence of magnetite but multiple samples did not fully demagnetise by 100 mT indicating the presence of high coercivity magnetic minerals that do not easily demagnetise in AFs. Hysteresis analysis (C) of GRP29 saturation occurs at low field strength indicative of magnetite and the closed nature of the hysteresis loop indicates that grains are large, multidomain grains.

Fig. 8: Orthogonal component vector plots and PCA of thermal demagnetisation data for samples from selected giant pumice blocks at Taupo. Solid symbols are projections for data in plan view, and hollow symbols are of data projected in the vertical, N-South plane. Magnetisation gradually decreases with increasing temperature steps, which allows for PCA which is used to identify the primary magnetisation. NRM describes the magnetisation of each specimen prior to demagnetisation. Dec and Inc provides the orientation of the dominant and most subtle magnetic component and the MAD3 value provides an estimate of the ‘goodness of fit’ of the PCA where small numbers indicate a better fit. GRP23 and GRP40 display varied cooling histories with some portions of the blocks cooling below the Curie temperature of magnetite before settling in their modern position (e.g. T238, T217) and other portions of the blocks remaining well above the Curie temperature until after emplacement (e.g. T237 and T220). PCA of specimens from GRP104 have anomalously low inclinations and varied declinations which do not align with the expected geomagnetic field indicating that it cooled before emplacement and probably overturned.

Fig. 9: (A) Schematic diagram, after Kano (2003), showing inferred mode of eruption of the giant pumice blocks at Taupo volcano from a subaqueous rhyolite dome. Magma extrudes and fragments to form a loose clastic carapace, formed by quench fragmentation and auto-brecciation at their outer margins, and continues to grow as magma is added from within. Continued addition of magma helps break off still-hot vesicular dome crust, which continues to vesiculate and expand after rising buoyantly from the pile, perhaps aided by partial uncovering of parts of the dome by phreatomagmatic explosions or/and weak avalanching of carapace material down flanks of the growing mound. Some blocks float briefly, either sinking due to quenching and/or the ingestion of water, or are disintegrated by thermal contraction or internal gas expansion as intruding water flashes to steam. (A, B) Survivors drift with the prevailing wind, rotating about horizontal and vertical axes and washing ashore as they progressively cool from their outer surfaces and from cracks and permeable vesicle paths. (C) After initial shoreline lodgement while parts of the interior are still above Curie temperature, they continue periodic movement until (D) they become embedded in transgressive shoreline sediments and cool completely, with the last-cooled parts retaining the 1.8 ka magnetic orientation.

References:

Allen SR, Fiske RS, Cashman KV (2008) Quenching of steam-charged pumice: Implications for submarine pyroclastic volcanism. Earth and Planetary Science Letters 274:40-49

Allen SR, McPhie J (2000) Water-settling and resedimentation of submarine rhyolitic pumice at Yali, eastern Aegean, Greece. Journal of Volcanology and Geothermal Research 95:285-307

Allen SR, Stewart AL (2003) Products of explosive subaqueous felsic eruptions based on examples from the Hellenic Island Arc, Greece. In: White JDL, Smellie JL, Clague JJ (eds) Explosive subaqueous volcanism. American Geophysical Union, Washington, DC, pp 285-298

Austin-Erickson A, Büttner R, Dellino P, Ort M, Zimanowski B (2008) Phreatomagmatic explosions of rhyolitic magma: Experimental and field evidence. Journal of Geophysical Research 113(B11201):12

Barker SJ, Rotella MD, Wilson CJN, Wright IC, Wysoczanski R (2012) Contrasting pyroclast density spectra from subaerial and submarine silicic eruptions in the Kermadec arc: implications for eruption processes and dredge sampling. *Bulletin of Volcanology*, 74**,** 1425-1443.

Binns RA (2003) Deep marine pumice from the Woodlark and Manus Basins, Papua New Guinea. In: White JDL, Smellie JL, Clague JJ (eds) Explosive subaqueous volcanism. American Geophysical Union, Washington, DC, pp 329-343

Blower JD, Keating JP, Mader HM, Phillips JC (2001) Inferring volcanic degassing processes from vesicle size distributions. Geophysical Research Letters 28:347-350

Bryan SE, Cook A, Evans JP, Colls PW, Wells MG, Lawrence MG, Jell JS, Greig A, Leslie R (2004) Pumice rafting and faunal dispersion during 2001-2002 in the Southwest Pacific: record of a dacitic explosive eruption from Tonga. Earth and Planetary Science Letters 227:135-154

Butler RF (1992) Palaeomagnetism. Blackwell Scientific Publications, Oxford

Cantner K, Carey S, Nomikou P (2013) Volcanologic and petrologic analysis of the 1650 AD eruption of Kolumbo submarine volcano, Greece. J. Volcanol. Geoth. Res.: http://dx.doi.org/10.1016/j.jvolgeores.2013.1010.1004

Carey R, Wysoczanski R, Wunderman R, Jutzeler M (2014) The largest historic submarine eruption the world has never seen. Eos 95

Cashman KV, Fiske RS (1991) Fallout of pyroclastic debris from submarine volcanic eruptions. Science 253:275-280

Clarkson RA (1996) Immediate post-c. 1800a Taupo eruption secondary deposits and shorelines. In: Geology. University of Otago, Dunedin, New Zealand, p 156

Clough BJ, Wright JV, Walker GPL (1981) An unusual bed of giant pumice in Mexico. Nature 289(49-50)

Coombs DS, Landis CA (1966) Pumice from the South Sandwich Eruption of March 1962 reaches New Zealand. Nature 209:289-290

Davy BW, Caldwell TG (1998) Gravity, magnetic and seismic surveys of the caldera complex, Lake Taupo, North Island, New Zealand. Journal of Volcanology and Geothermal Research 81:69-89

De Rita D, Giordano G, Cecili A (2001) A model for submarine rhyolite dome growth: Ponza Island (central Italy). Journal of Volcanology and Geothermal Research 107:221-239

de Ronde CEJ, Davy BW, Smith RT, Immenga DKH, Baxter JA (2001) Detailed swath mapping survey of a submarine geothermal system, Lake Taupo, New Zealand. In: Cidu L (ed) Water-Rock Interaction. Swets & Zeitlinger, Lisse, pp 799-802 de Ronde CEJ, Stoffers P, Garbe-Schönberg D, Christenson BW, Jones B, Manconi R, Browne PRL, Hissman K, Botz R, Davy BW, Schmitt M, Battershill CN (2002) Discovery of active hydrothermal venting in Lake Taupo, New Zealand. Journal of Volcanology and Geothermal Research 115:257-275

De Rosen Spence AF, Provost G, Dimroth E, Gochnauer K, Owen V (1980) Archean subaqueous felsic flows, Rouyn-Noranda, Quebec, Canada, and their Quaternary equivalents. In: Early Precambrian volcanology and sedimentology in the light of the Recent. Elsevier, Amsterdam, International, pp 43-77

DeGraaf JM, Aydin A (1987) Surface morphology of columnar joints and its significance to mechanics and direction of joint growth. Geological Society of America bulletin 99:605-617

Dufek J, Manga M, Staedter M (2007) Littoral blasts: Pumice-water heat transfer and the conditions for steam explosions when pyroclastic flows enter the ocean. J. Geophys. Res 112

Dunbar NW, Kyle PR (1993) Lack of volatile gradient in the Taupo plinian-ignimbrite transition: Evidence from melt inclusion analysis. American Mineralogist 78:612-618

Dunlop DJ (1973) Thermoremnant magnetization in submicroscopic magnetite. Journal of Geophysical Research 78:7602-7613

Dunlop DJ, Özdemir Ö (1997) Rock Magnetism: Fundamentals and Frontiers. Cambridge University Press, New York

Eichelberger JC, Carrigan CR, Westrich HR, Price RH (1986) Non-explosive silicic volcanism. Nature 323:598-602

Fink JH (1983) Structure and emplacement of a rhyolitic obsidian flow: Little Glass Mountain, Medicine Lake Highland, northern California. Geological Society of America bulletin 94:362-380

Fink JH, Anderson SW, Manley CR (1992) Textural constraints on effusive silicic volcanism: beyond the permeable foam model. Journal of Geophysical Research 97:9073-9083

Fisher RV, Schmincke H-U (1984) Pyroclastic rocks. Springer-Verlag Berlin, Heidelberg, p 472

Fiske RS (1969) Recognition and significance of pumice in marine pyroclastic rocks. Geol. Soc. Am. Bull. 80:1-8

Fiske RS, Cashman KV, Shibata A, Watanabe K (1998) Tephra dispersal from Myojinsho, Japan, during its shallow submarine eruption of 1952-1953. Bulletin of Volcanology 59:262-275

Fiske RS, Naka J, Iizasa K, Yuasa M, Klaus A (2001) Submarine silicic volcanism at the front of the Izu-Bonin arc, Japan: voluminous seafloor eruptions of rhyolite pumice. Geological Society of America Bulletin 113:813-824

Frick C, Kent LE (1984) Drift pumice in the Indian and South Atlantic oceans. Transactions of the Geological Society of South Africa 87:19-33

Furnes H, Fridleifsson IB, Atkins FB (1980) Subglacial volcanics - on the formation of acid hyaloclastites. Journal of Volcanology and Geothermal Research 8:95-110

Gifkins CC, McPhie J, Allen RL (2002) Pumiceous rhyolitic peperite in ancient volcanic successions. Journal of Volcanology and Geothermal Research 114:181-203

Gilbert JS, Sparks RSJ (1998) The physics of explosive volcanic eruptions. In: Geological Society of London Special Publication. p 186

Goto Y, Tsuchiya N (2004) Morphology and growth style of a Miocene submarine dacite lava dome at Atsumi, northeast Japan. Journal of Volcanology and Geothermal Research 134:255-275

Gregg SJ, Sing SW (1980) Absorption surfaces and porosity. Academic Press, Griffiths RW, Fink JH (1992) Solidification and morphology of submarine lavas: a dependence on extrusion rate. Journal of Geophysical Research 97:19729-19737

Griffiths RW, Fink JW (1993) Effects of surface cooling on the spreading of lava flows and domes. Journal of Fluid Mechanics 252:667-702

Hanson R (1991) Quenching and hydroclastic disruption of andesite to rhyolitic intrusions in a submarine island-arc sequence, northern Sierra Nevada, California. Geol. Soc. Am. Bull. 103:804-816

Houghton BF, Wilson CJN (1989) A vesicularity index for pyroclastic deposits. Bulletin of Volcanology 51:451-462

Houghton BF, Wilson CJN, McWilliams MO, Lanphere MA, Weaver SD, Briggs RM, Pringle MS (1995) Chronology and dynamics of a large silicic magmatic system: central Taupo Volcanic Zone, New Zealand. Geology 23:13-16

Houghton BF, Hobden BJ, Cashman KV, Wilson CJN, Smith RT (2003) Large-scale Interaction of Lake Water and Rhyolitic Magma During the 1.8 ka Taupo Eruption, New Zealand. In: White JDL, Smellie JL, Clague DA (eds) Explosive Subaqueous Volcanism. American Geophysical Union, Washington D.C., pp 97-109

Houghton BF, Carey RJ, Cashman KV, Wilson CJN, Hobden BJ, Hammer JE (2010) Diverse patterns of ascent, degassing, and eruption of rhyolite magma during the 1.8 ka Taupo eruption, New Zealand: Evidence from clast vesicularity. J. Volcanol. Geoth. Res. 195(1):31-47

Hunns SR, McPhie J (1999) Pumiceous peperite in a submarine volcanic succession at Mount Chalmers, Queensland, Australia. Journal of Volcanology and Geothermal Research 88:239-254

Jutzeler M, Marsh R, Carey RJ, White JDL, Talling PJ, Karlstrom L (2014) On the fate of pumice rafts formed during the 2012 Havre submarine eruption. Nature Communications 5:3660:doi: 10.1038/ncomms4660

Kaminski É, Jaupart C (1997) Expansion and quenching of vesicular magma fragments in Plinian eruptions. Journal of Geophysical Research 102(B6):12187-12203

Kano K (1996) A Miocene coarse volcaniclastic mass-flow deposit in the Shimane Peninsula, SW Japan: product of a deep submarine eruption? Bulletin of Volcanology 58:131-143

Kano K (2003) Subaqueous pumice eruptions and their products: a review. In: White JDL, Smellie JL, Clague JJ (eds) Explosive subaqueous volcanism. American Geophysical Union, Washington, DC, pp 213-229

Kano K, Takeuchi K, Yamamoto T, Hoshizumi H (1991) Subaqueous rhyolite block lavas in the Miocene Ushikiri Formation, Shimane Peninsula, SW Japan. Journal of Volcanology and Geothermal Research 46:241-253

Kano K, Yamamoto T, Ono K (1996) Subaqueous eruption and emplacement of the Shinjima Pumice, Shinjima (Moeshima) Island, Kagoshima Bay, SW Japan. Journal of Volcanology and Geothermal Research 71:187-206

Kato Y (1987) Woody pumice generated with submarine eruption. Journal of the Geological Society of Japan 93:11-20

Kirschvink JL (1980) The least-squares line and plane and the analysis of palaeomagnetic data. Geophysical Journal of the Astronomical Society. 62: 699–718.

Klug C, Cashman KV (1996) Permeability development in vesiculating magmas: implications for fragmentation. Bulletin of Volcanology 58:87-100

Kokelaar P (1986) Magma-water interactions in subaqueous and emergent basaltic volcanism. Bulletin of Volcanology 48:275-289

Kremers S, Scheu B, Cordonnier B, Spieler O, Dingwell DB (2010) Influence of decompression rate on fragmentation processes: An experimental study. J. Volcanol. Geoth. Res. 193(3-4):182-188

Lescinsky DT, Fink JH (2000) Lava and ice interaction at stratovolcanoes: use of characteristic features to determine past glacial extents and future volcanic hazards. Journal of Geophysical Research 105(B10):23711-23726

Lister GS (1978) Sedimentology of Lake Taupo. In: Department of Earth Sciences. University of Waikato, Hamilton, New Zealand

Lowe DJ, Green JD (1992) Lakes. In: Soons JM, Selby MJ (eds) Landforms of New Zealand. Longman Paul Ltd., pp 107-143

Lowrie W, Fuller M (1971) On the alternating field demagnetization characteristics of multidomain thermoremnant magnetization in magnetite. Journal of Geophysical Research 76:6339-6349

Lurcock PC, Wilson GS, (2012) PuffinPlot: a versatile, user-friendly program for paleomagnetic analysis. Geochemistry Geophysics Geosystems 13, Q06Z45, http://dx.doi. org/10.1029/2012GC004098.

Mader HM (1998) Conduit flow and fragmentation. In: Gilbert JS, Sparks RSJ (eds) The physics of explosive volcanic eruptions. Geological Scoiety of London, London, pp 51-71

Maeno F, Taniguchi H (2006) Silicic lava dome growth in the 1934-1935 Showa Iwo-jima eruption, Kikai caldera, south of Kyushu, Japan. Bulletin of Volcanology 68:673-688

Mangan MT, Cashman KV, Newman S (1993) Vesiculation of basaltic magma during eruption. Geology 21:157-160

Manley CR, Fink JH (1987) Internal textures of rhyolite flows as revealed by research drilling. Geology 15:549-552

Mann CP, Stix J, Vallance JW, Richer M (2004) Subaqueous intracaldera volcanism, Ilopango Caldera, El Salvador, Central America. In: Rose WIj, Bommer JJ, López DL, Carr MJ, Major JJ (eds) Natural Hazards in El Salvador. Geological Society of America Special Paper, Boulder, Colorado, pp 159-174

Manville VR (2001) Sedimentology and history of Lake Reporoa: an ephemeral supra-ignimbrite lake, Taupo Volcanic Zone, New Zealand. In: White JDL, Riggs NR (eds) Volcanogenic sedimentation in lacustrine settings. pp 109-140

Manville V, White JDL, Houghton BF, Wilson CJN (1998) The saturation behaviour of Taupo 1800a pumice and some sedimentological implications. Sedimentary Geology 119:5-16

Manville VR, White JDL, Houghton BF, Wilson CJN (1999) Paleohydrology and sedimentology of a post-1800a breakout flood from intracaldera Lake Taupo, North Island, New Zealand. Geological Society of America Bulletin 111:1435-1447

Manville V, Segschneider B, White JDL (2002) Hydrodynamic behaviour of Taupo 1800a pumice: implications for the sedimentology of remobilised pyroclastic deposits. Sedimentology 49:955-976

Manville V, Wilson CJN (2003) Interactions between volcanism, rifting and subsidence: implications of intracaldera palaeoshorelines at Taupo volcano, New Zealand. Journal of the Geological Society of London 160:3-6

Manville V, Hodgson KA, Nairn IA (2007) A review of break-out floods from volcanogenic lakes in New Zealand. New Zealand Journal of Geology and GeophysicBassds 52:131-150

Manville V, Segschneider B, Newton E, White JDL, Houghton BF, Wilson CJN (2009) Environmental impact of the 1.8 ka Taupo eruption, New Zealand: Landscape responses to a large-scale explosive rhyolite eruption. Sed. Geol. 220(3-4):318-336

Mungall JE, Bagdassarov NS, Romano C, Dingwell DB (1996) Numerical modelling of stress generation and microfracturing of vesicle walls in glassy rocks. Journal of Volcanology and Geothermal Research 73:33-46

Nairn IA (2002) Geology of the Okataina Volcanic Centre. Institute of Geological & Nuclear Sciences, geological map no. 25 (1:50 000) (Lower Hutt, New Zealand):1 sheet + 156 pp.

Nishimura A, Marsaglia KM, Rodolfo KS, Colella A, Hiscott RN, Tazaki K, Gill JB, Janecek T, Firth J, Isiminger-Kelso M, Herman Y, Taylor RN, Taylor B, Fujioka K, Party LS (1991) Pliocene-Quaternary submarine pumice deposits in the Sumisu Rift area, Izu-Bonin Arc. In: Fisher RV, Smith GA (eds) Sedimentation in Volcanic Settings. Society of Economic Paleontologists and Mineralogists Special Publications, pp 201-208

Noguchi S, Toramaru A, Shimano T (2006) Crystallization of microlites and degassing during magma ascent: Constraints on the fluid mechanical behavior of magma during the Tenjo eruption on Kozu Island, Japan. Bulletin of Volcanology 68:432-449

Northey DJ (1983) Seismic studies of the structure beneath Lake Taupo. In: Institute of Geophysics. Victoria University of Wellington, Wellington, New Zealand

Otway PM (1986) Vertical deformation associated with the Taupo earthquake swarm, June 1983. Royal Society of New Zealand Bulletin 24:187-200

Raos AM, McPhie J (2003) The submarine record of a large-scale explosive eruption in the Vanuatu Arc: ~ 1 Ma Efaté Pumice Formation. In: White JDL, Smellie JL, Clague DA (eds) Subaqueous explosive volcanism. American Geophysical Union, Washington D.C., pp 273-283

Reynolds MA, Best JG (1980) Summary of the 1953-57 eruption of Tuluman Volcano, Papua New Guinea. In: Johnson RW (ed) Volcanism in Australasia. Elsevier, pp 287-295

Reynolds MA, Best JG, Johnson RW (1980) 1953-57 eruption of Tuluman Volcano: rhyolitic volcanic activity in the Northern Bismarck Sea. Geological Survey of Papua New Guinea Memoir 7:5-44

Richard D, Scheu B, Mueller SP, Spieler O, Dingwell DB (2013) Outgassing: influence on speed of magma fragmentation. Journal of Geophysical Research: Solid Earth:n/a-n/a

Richards AF (1958) Transpacific distribution of floating pumice from Isla San Benedicto, Mexico. Deep Sea Research 5:29-35

Riggs NR, Ort M, White JDL, Wilson CJN, Clarkson R (2001) Post-1.8-ka marginal sedimentation in Lake Taupo, New Zealand: effects of wave energy and sediment supply in a rapidly rising lake. In: White JDL, Riggs NR (eds) Volcanogenic sedimentation in lacustrine settings. International Association of Sedimentologists Special Publication, Oxford, pp 151-177

Risso C, Scasso RA, Aparicio A (2002) Presence of large pumice blocks on Tierra del Fuego and South Shetland Islands shorelines, from 1962 South Sandwich Islands eruptions. Marine Geology 186:413-422

Rotella MD, Wilson CJN, Barker SJ, Wright IC (2013) Highly vesicular pumice generated by buoyant detachment of magma in subaqueous volcanism. *Nature Geoscience,* 6**,** 129-132.

Rotella MD, Wilson CJN, Barker SJ, Cashman KV, Houghton BF, Wright IC (2014) Bubble development in explosive silcic eruptions: insights from pyroclast vesicularity textures from Raoul volcano (Kermadec arc). *Bulletin of Volcanology,* 76**,** 826.

Rowland JV, Sibson RH (2001) Extensional fault kinematics within the Taupo Volcanic Zone, New Zealand: soft-linked segmentation of a continental rift system. New Zealand Journal of Geology and Geophysics 44:271-284

Saliba R, Jagla EA (2003) Analysis of columnar joint patterns from three-dimensional stress modeling. Journal of Geophysical Research 108:ECV 5-1

Scutter CR, Cas RAF, Moore CL (1998) Facies achitetcure and origin of a submarine rhyolitic lava flow-dome complex, Ponza, Italy. Journal of Geophysical Research 103:27551-27566

Smith RCM (1991) Post-eruption sedimentation on the margin of a caldera lake, Taupo Volcanic Centre, New Zealand. Sedimentary Geology 74:89-138

Spörli KB, Rowland JV (2006) 'Column on column' structures as indicators of lava/ice interaction, Ruapehu andesite volcano. Journal of Volcanology and Geothermal Research 157:294-310

Sutton AN, Blake S, Wilson CJN (1995) An outline geochemistry of rhyolite eruptives from Taupo volcanic centre, New Zealand. Journal of Volcanology and Geothermal Research 68:153-175

Sutton AN, Blake S, Wilson CJN, Charlier BLA (2000) Late Quaternary evolution of a hyperactive rhyolite magmatic system: Taupo volcanic centre, New Zealand. Journal of the Geological Society of London 157:537-552

Tanakadate H (1935) Preliminary report of the eruption of Iwojima, Kagoshima Prefecture. Bulletin of the Volcanological Society of Japan, Series 1 2:188-209 (in Japanese)

Thompson CS (1984) The weather and climate of the Tongariro Region. In, p 35 p.

Toramaru A (1989) Vesiculation process and bubble size distributions in ascending magmas with constant velocities. Journal of Geophysical Research 94(B12):17523-17542

Toramaru A, Matsumoto T (2004) Columnar joint morphology and cooling rate: A starch-water mixture experiment. Journal of Geophysical Research 109:B02205

Tsuya H, Morimoto R, Ossaka G (1953) A brief note on the petrography of the pumice ejected from Myojin-Sho (reef), near the Bayonnaise Rocks, Sept. 23, 1952. Journal of the Tokyo University of Fisheries 40:16-18

Turner, G. M. and Lillis, D. A. (1994). A palaeomagnetic secular variation record for New Zealand during the past 2500 years. Physics of the Earth and Planetary Interiors, 83:265–282.

Vella D, Huppert HE (2007) The waterlogging of floating objects. Journal of Fluid Mechanics 585:245-254

Villamor P, Berryman KR (2001) A late Quaternary extension rate in the Taupo Volcanic Zone, New Zealand, derived from fault slip data. New Zealand Journal of Geology and Geophysics 44:243-270

Wasilewski PJ (1973) Magnetic hysteresis in natural materials. Earth and Planetary Science Letters 20:67-72

Webb, P.A. (2001) An introduction to the physical characterization of materials by mercury intrusion porosimetry with emphasis on reduction and presentation of experimental data, pp. 23. Micromeritics Instrument Corp., Norcross, Georgia USA. http://www.micromeritics.com/pdf/app_articles/mercury_paper.pdf

White JDL (2000) Subaqueous eruption-fed density currents and their deposits. Precambrian Research 101:87-109

White JDL, Manville VR, Wilson CJN, Houghton BF, Riggs N, Ort M (2001) Settling and deposition of 181 A.D. Taupo pumice in lacustrine and associated environments. In: White JDL, Riggs NR (eds) Volcanogenic sedimentation in lacustrine settings. International Associations of Sedimentologists, pp 141-150

White JDL, Smellie JL, Clague DA (2003) Introduction: A deductive outline and topical overview of subaqueous explosive volcanism. In: White JDL, Smellie JL, Clague DA (eds) Subaqueous explosive volcanism. American Geophysical Union, Washington D.C., pp 1-23

Whitham AG, Sparks RSJ (1986) Pumice. Bulletin of Volcanology 48:209-223

Wilson CJN (1985) The Taupo eruption, New Zealand. II. The Taupo Ignimbrite. Philosophical Transactions of the Royal Society of London A314:229-310

Wilson CJN (1993) Stratigraphy, chronology, styles and dynamics of late Quaternary eruptions from Taupo volcano, New Zealand. Philosophical Transactions of the Royal Society of London A343:205-306

Wilson CJN (2001) The 26.5 ka Oruanui eruption, New Zealand: an introduction and overview. Journal of Volcanology and Geothermal Research 112:133-174

Wilson CJN, Houghton BF, McWilliams MO, Lanphere MA, Weaver SD, Briggs RM (1995) Volcanic and structural evolution of Taupo Volcanic Zone, New Zealand: a review. Journal of Volcanology and Geothermal Research 68:1-28

Wilson CJN, Riggs NR, Ort MH, White JDL, Houghton BF (1997) An annotated atlas of post-1.8 ka shoreline features at Lake Taupo, New Zealand. In: Institute of Geological and Nuclear Sciences, Lower Hutt, New Zealand, p 35

Wilson CJN, Walker GPL (1985) The Taupo eruption, New Zealand. I. General aspects. Philosophical Transactions of the Royal Society of London A314:199-228

Wohletz KH (1986) Explosive magma-water interactions: thermodynamics, explosion mechanisms, and field studies. Bulletin of Volcanology 48:245-264

Wright HMN, Cashman KV, Rosi M, Cioni R (2007) Breadcrust bombs as indicators ov Vulcanian eruption dynamics at Guagua Pichincha, Ecuador. Bulletin of Volcanology 69:281-300

Wright IC, Gamble JA, Shane PAR (2003) Submarine silicic volcanism of the Healy caldera, southern Kermadec arc (SW Pacific): I - volcanology and eruption mechanisms. Bulletin of Volcanology 65:15-29

Yamagishi H (1985) Growth of pillow lobes - Evidence from pillow lavas of Hokkaido, Japan, and North Island, New Zealand. Geology 13:499-502

Yamagishi H (1991) Morphological and sedimentological characteristics of the Neogene submarine coherent lavas and hyaloclastites in Southwest Hokkaido, Japan. Sedimentary Geology 74:5-23

Yamagishi H, Dimroth E (1985) A comparison of Miocene and Archaean rhyolite hyaloclastites: Evidence for a hot and fluid rhyolite lava. Journal of Volcanology and Geothermal Research 23:337-355

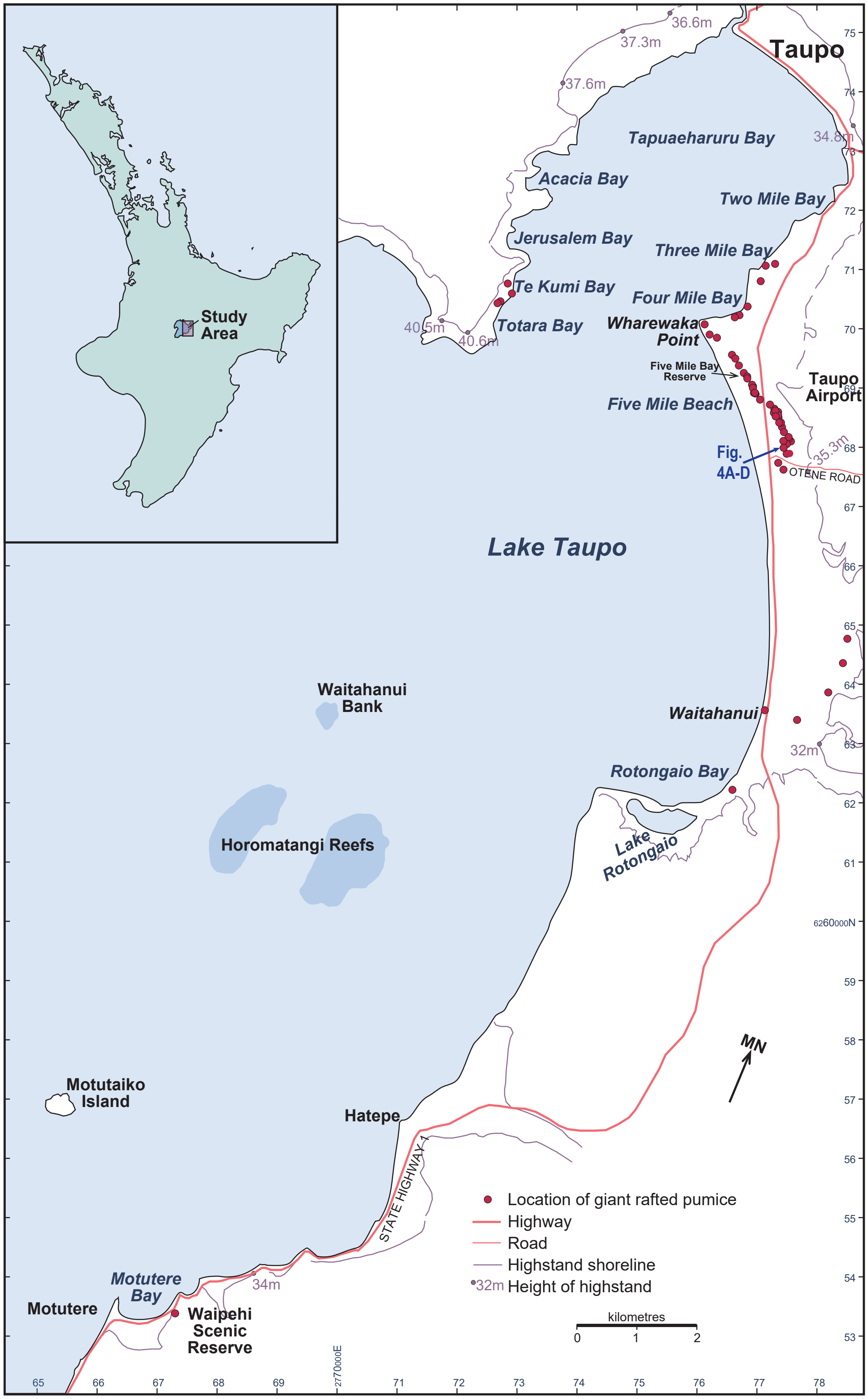

Study Area
Taupo
36.6m
37.3m
37.6m
Tapuaeharuru Bay
34.8m
Acacia Bay
Two Mile Bay
Jerusalem Bay
Three Mile Bay
Te Kumi Bay
Four Mile Bay
40.5m
40.6m
Totara Bay
Wharewaka Point
Five Mile Bay Reserve
Taupo Airport
Five Mile Beach
Fig. 4A-D
35.3m
OTENE ROAD
Lake Taupo
Waitahanui Bank
Waitahanui
32m
Rotongaio Bay
Horomatangi Reefs
Lake Rotongaio
6260000N
MN
Motutaiko Island
Hatepe
STATE HIGHWAY 1
Location of giant rafted pumice
Highway
Road
Highstand shoreline
32m Height of highstand
Motutere Bay
34m
Motutere
Waipehi Scenic Reserve
kilometres
0 1 2
2770000E

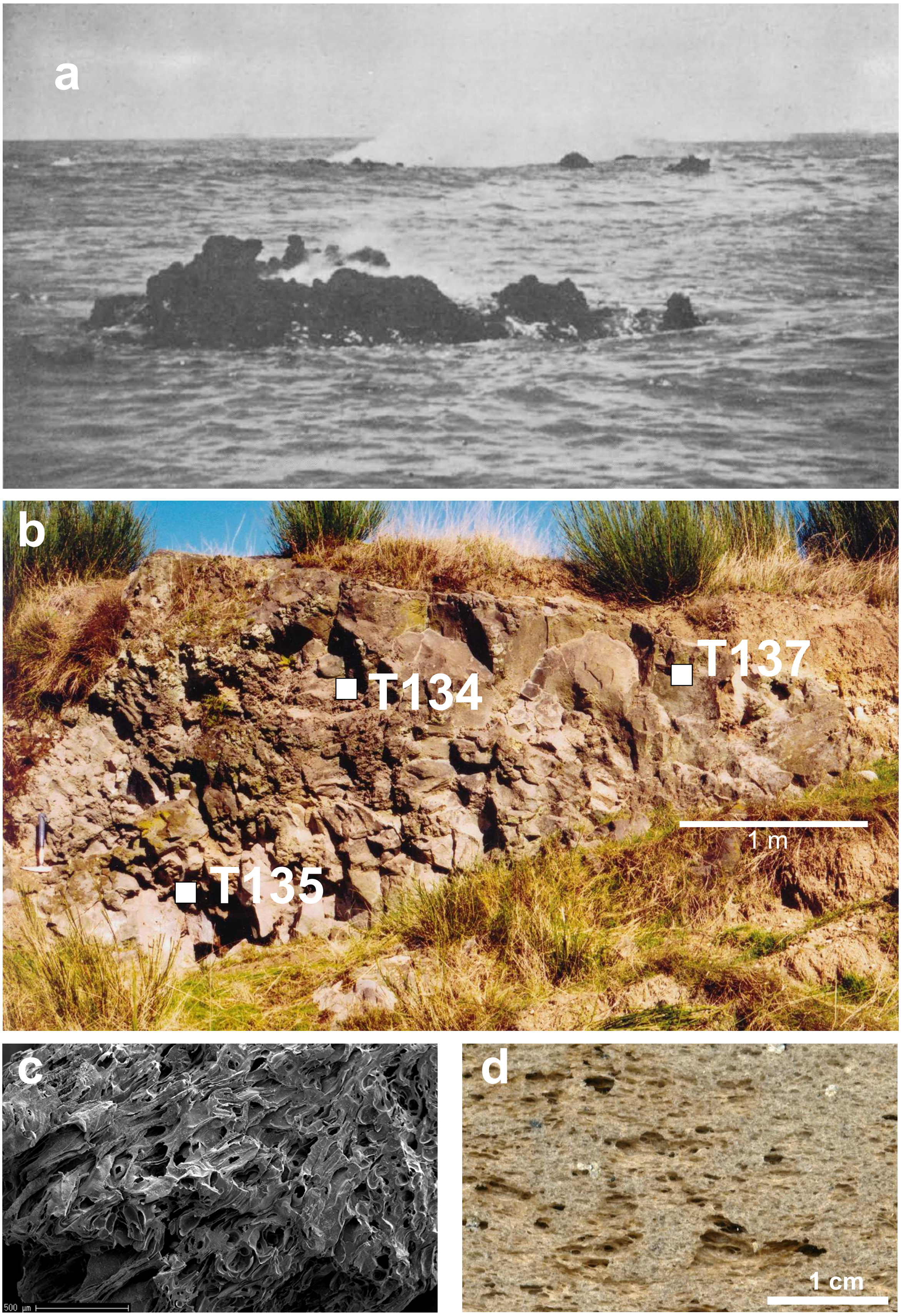

Figure 2 (a) Floating steaming pumice block from the Tuluman eruption, taken 24th March (Reynolds and Best, 1957). (b) Giant Rafted Pumice #40. Outer cooling joints are perpendicular to the cooling surface, while "rosette style" internal joints centre on the most vesicular area of the clast. (c) SEM of pumice-interior texture of T134. (d) Close-up of transition-zone sample T135

Figure 3. Giant rafted pumice block (GRP) and lacustrine sediments. Giant rafted pumice resting on undisturbed alternating beds of laminated mineral-rich sand and thin pumice-pebble layers, Five Mile Bay.

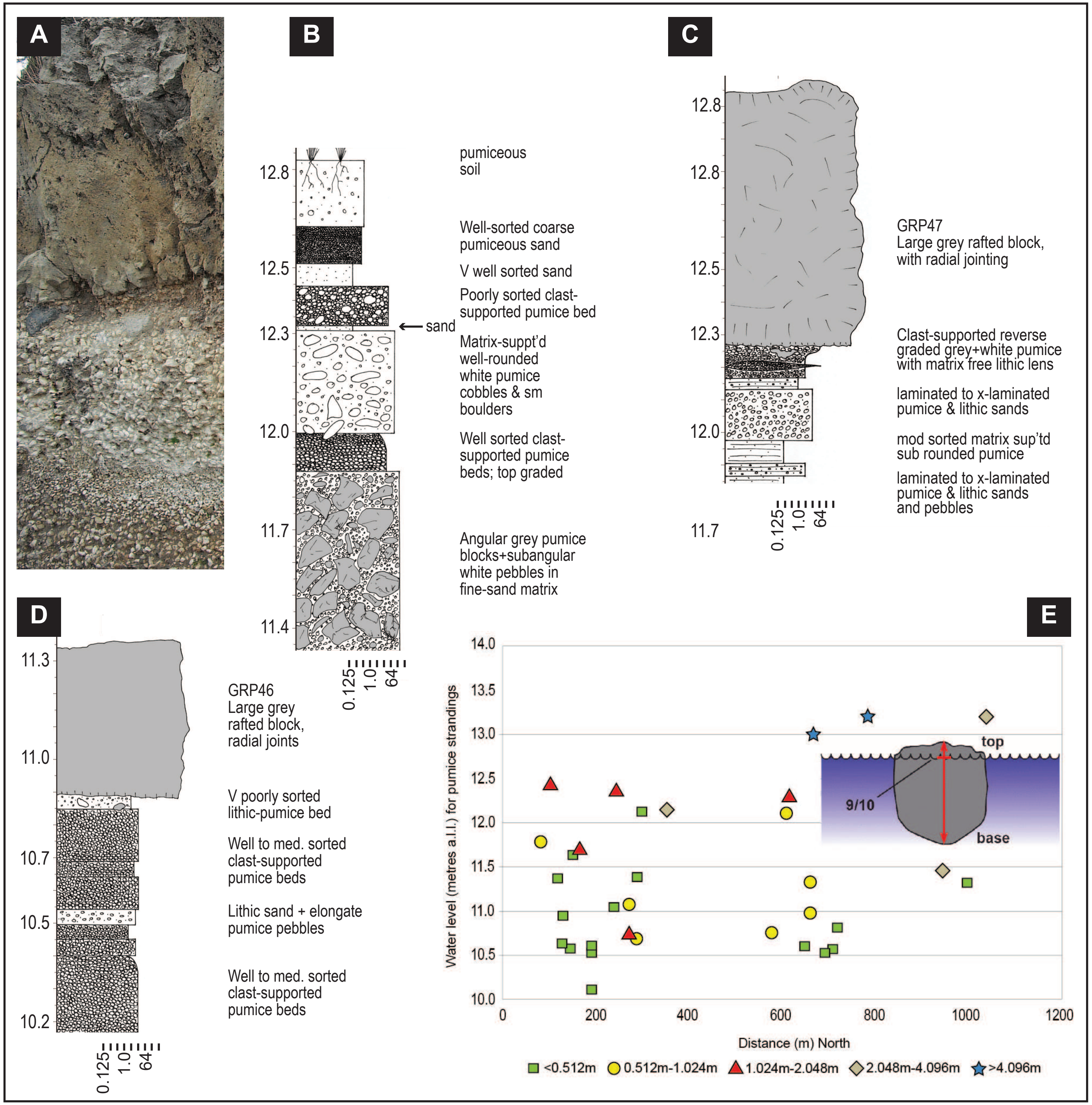
A
B
C
D
E
pumiceous soil
Well-sorted coarse pumiceous sand
V well sorted sand
Poorly sorted clast-supported pumice bed
sand
Matrix-suppt'd well-rounded white pumice cobbles & sm boulders
Well sorted clast-supported pumice beds; top graded
Angular grey pumice blocks+subangular white pebbles in fine-sand matrix
12.8
12.5
12.3
12.0
11.7
11.4
0.125
1.0
64
GRP47
Large grey rafted block, with radial jointing
Clast-supported reverse graded grey+white pumice with matrix free lithic lens
laminated to x-laminated pumice & lithic sands
mod sorted matrix sup'td sub rounded pumice
laminated to x-laminated pumice & lithic sands and pebbles
GRP46
Large grey rafted block, radial joints
V poorly sorted lithic-pumice bed
Well to med. sorted clast-supported pumice beds
Lithic sand + elongate pumice pebbles
Well to med. sorted clast-supported pumice beds
11.3
11.0
10.7
10.5
10.2
Water level (metres a.l.l.) for pumice strandings
Distance (m) North
top
9/10
base
<0.512m
0.512m-1.024m
1.024m-2.048m
2.048m-4.096m
>4.096m

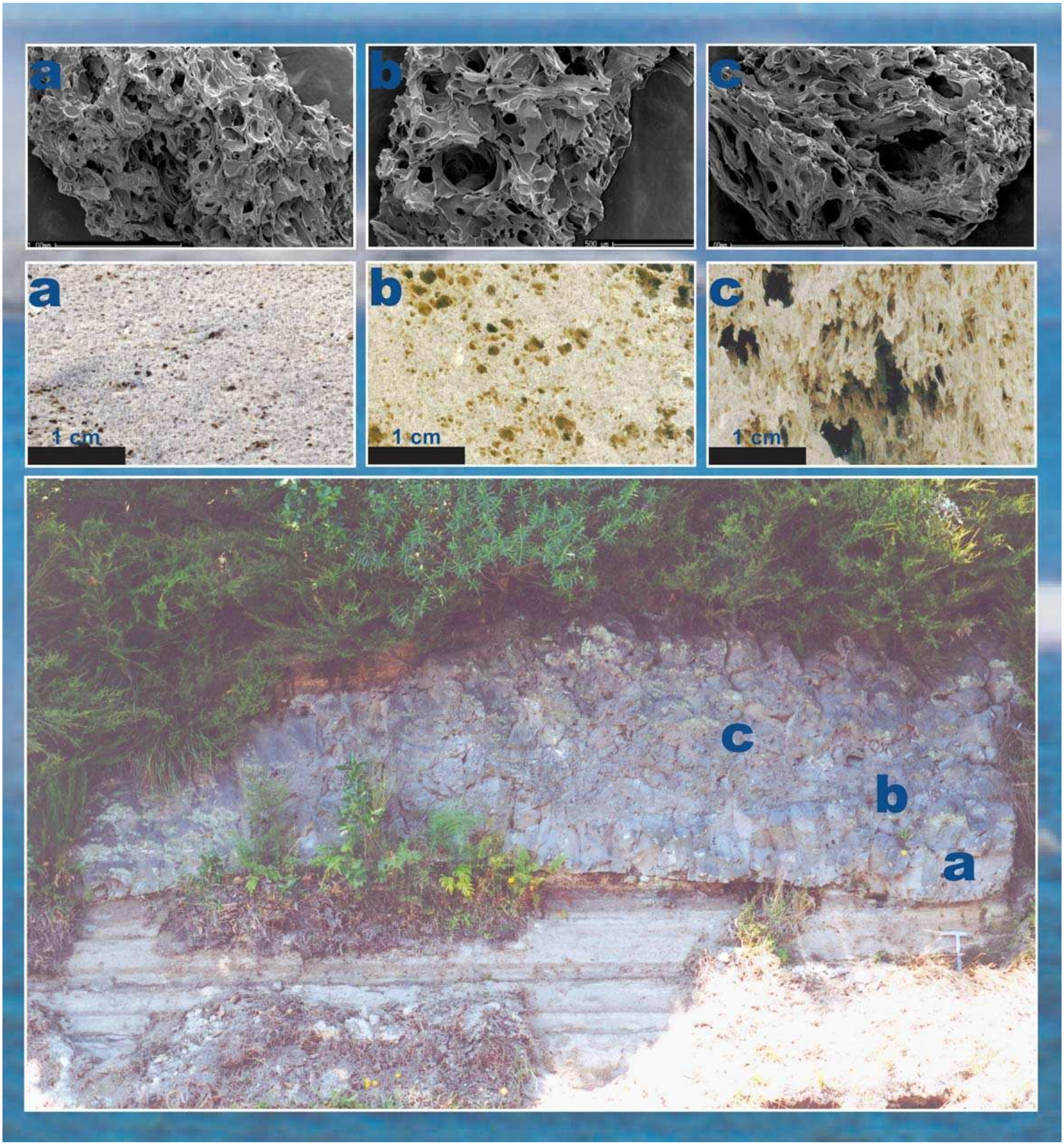
a
b
c
a
1 cm
b
1 cm
c
1 cm
c
b
a

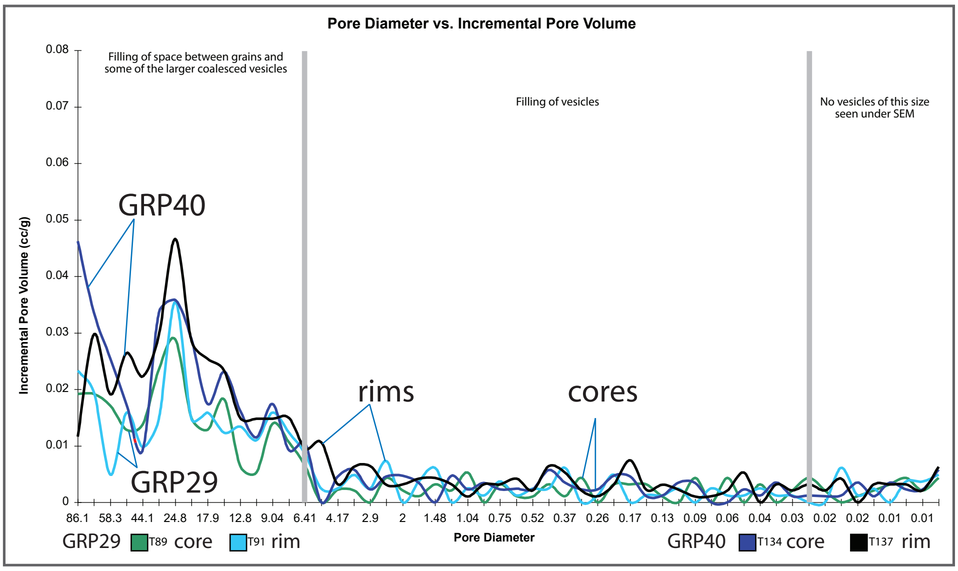

Figure 6: Plot of vesicle(-throat) diameter versus incremental vesicle (porosity) volume for selected samples from giant pumice blocks at Taupo obtained using Hg porosimetry. Note large range of pore-throat diameters and lack of distinct measured differences between rims and cores. T89=GRP29 interior; T91=GRP29 rim; T134=GRP40 interior; T137=GRP40 rim

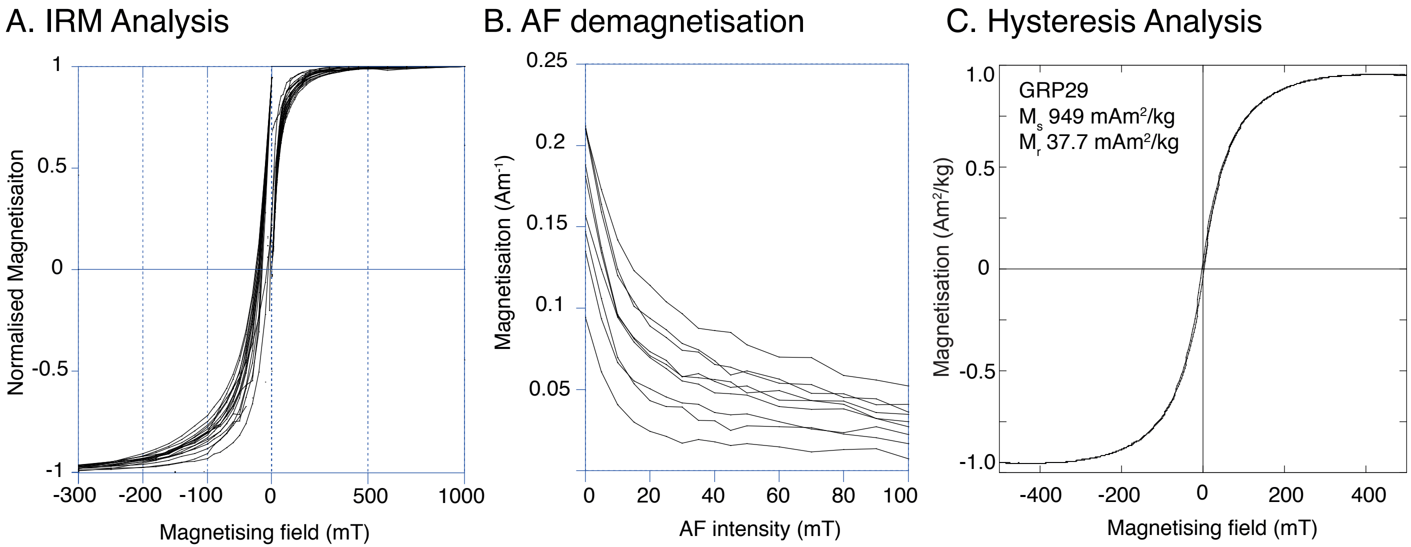
A. IRM Analysis
B. AF demagnetisation
C. Hysteresis Analysis
1
0.5
0
-0.5
-1
Normalised Magnetisaiton
-300
-200
-100
0
500
1000
Magnetising field (mT)
0.25
0.2
0.15
0.1
0.05
Magnetisaiton (Am-1)
0
20
40
60
80
100
AF intensity (mT)
GRP29
Ms 949 mAm2/kg
Mr 37.7 mAm2/kg
1.0
0.5
0
-0.5
-1.0
Magnetisation (Am2/kg)
-400
-200
0
200
400
Magnetising field (mT)

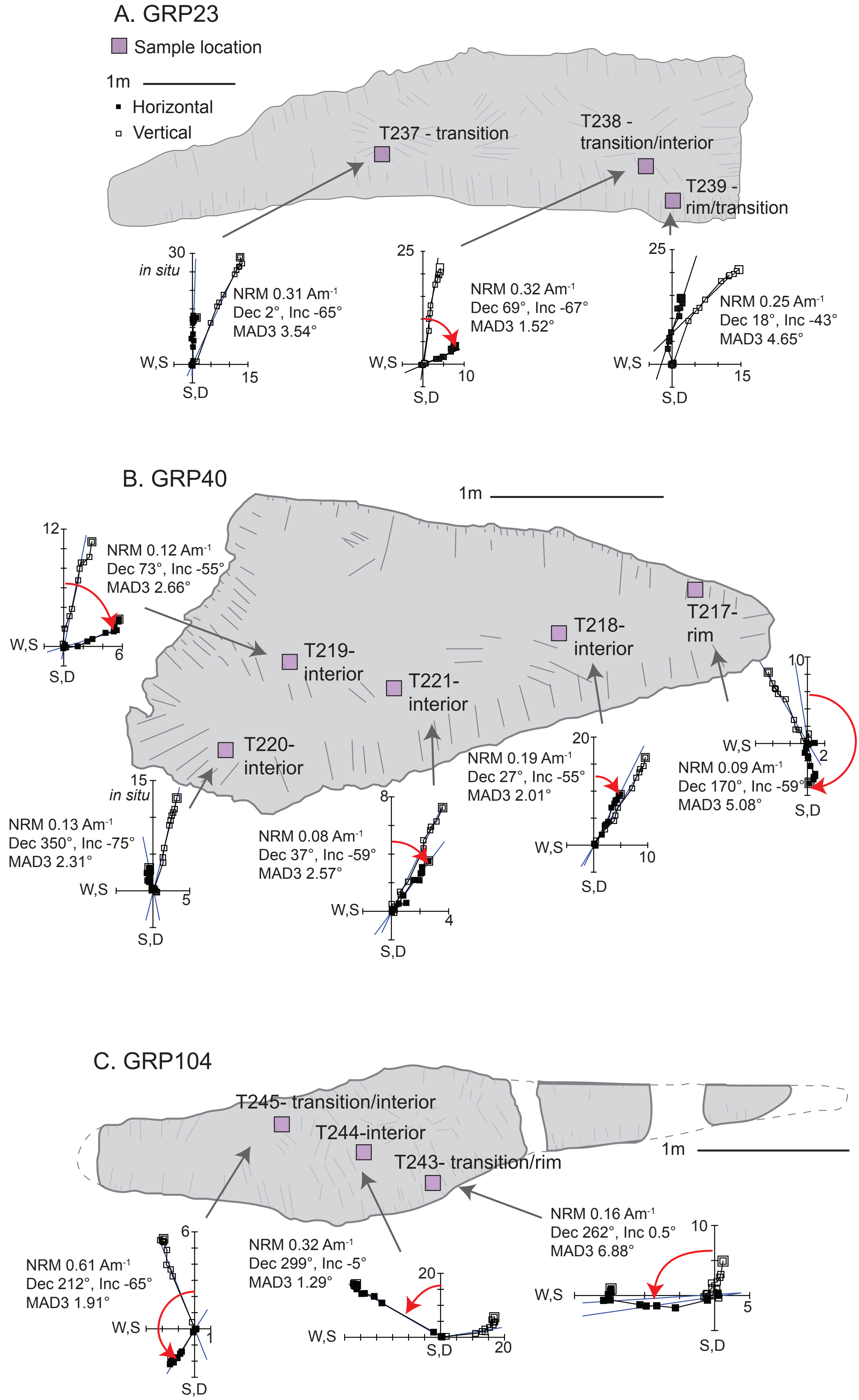

A. GRP23
Sample location
1m
Horizontal
Vertical
T237 - transition
T238 - transition/interior
T239 - rim/transition
30
in situ
NRM 0.31 Am-1
Dec 2°, Inc -65°
MAD3 3.54°
W,S
15
S,D
25
NRM 0.32 Am-1
Dec 69°, Inc -67°
MAD3 1.52°
10
NRM 0.25 Am-1
Dec 18°, Inc -43°
MAD3 4.65°
B. GRP40
1m
12
NRM 0.12 Am-1
Dec 73°, Inc -55°
MAD3 2.66°
6
T219- interior
T221- interior
T218- interior
T217- rim
T220- interior
15
in situ
NRM 0.13 Am-1
Dec 350°, Inc -75°
MAD3 2.31°
5
8
NRM 0.08 Am-1
Dec 37°, Inc -59°
MAD3 2.57°
4
20
NRM 0.19 Am-1
Dec 27°, Inc -55°
MAD3 2.01°
10
NRM 0.09 Am-1
Dec 170°, Inc -59°
MAD3 5.08°
2
C. GRP104
T245- transition/interior
T244-interior
T243- transition/rim
1m
6
NRM 0.61 Am-1
Dec 212°, Inc -65°
MAD3 1.91°
1
NRM 0.32 Am-1
Dec 299°, Inc -5°
MAD3 1.29°
20
NRM 0.16 Am-1
Dec 262°, Inc 0.5°
MAD3 6.88°
5

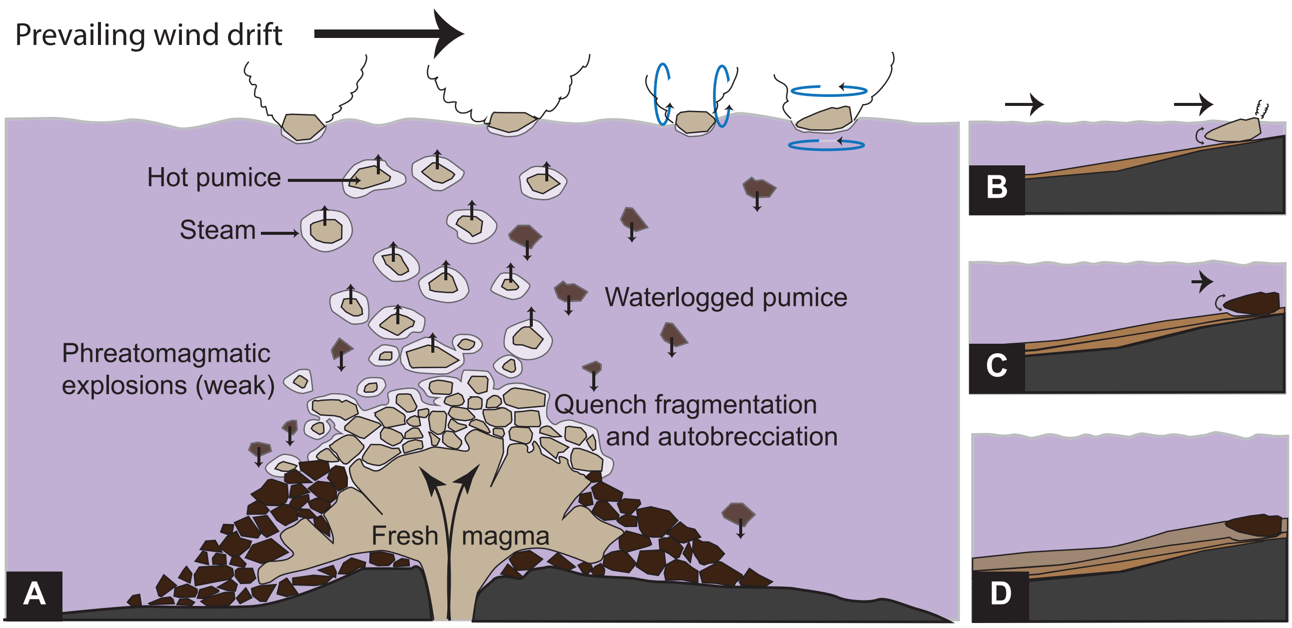
Prevailing wind drift
Hot pumice
Steam
Waterlogged pumice
Phreatomagmatic explosions (weak)
Quench fragmentation and autobrecciation
Fresh
magma
A
B
C
D

A1.1 Introduction

Twenty-five stratigraphic logs were drawn of the lacustrine gravels that encase or underlie grey pumice clasts. The detailed logs with descriptions are included in this appendix. Below is a key associated with the graphic logs.

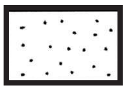
Sands

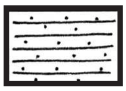
Laminated sands


Sands with crossbedding


Grey pumice clasts

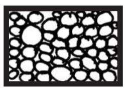
White & beige pumice clasts

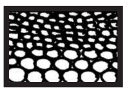
Clast supported, matrix poor, normally graded

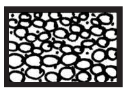
Clast supported with sandy matrix

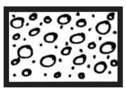
Matrix supported

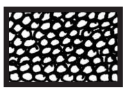
Very well sorted

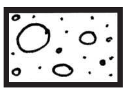
Poorly sorted

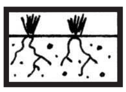
Podsol

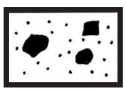
Lithic clasts in sand

Height above a.l.l.	Log	Section: 024	Logged by: Isabella J. von Lichtan
		Grainsize	Descriptions and comments

6268775.76, 2777061.21, 367.12 m, 11.27 m
[Northing, Easting, elevation, elevation above lake level]

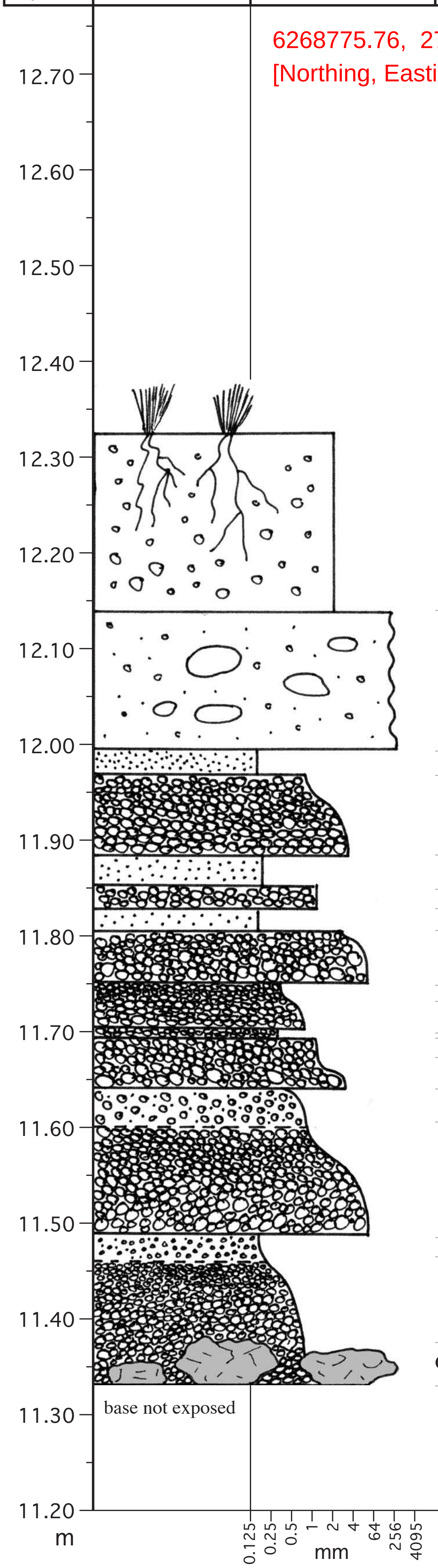

Matrix supported, poorly sorted podsol

Matrix supported, very poorly sorted
contains large rounded pumice cobbles

Matrix supported, medium sorted

Clast supported, very well sorted

Matrix supported, very well sorted

Clast supported, very well sorted

Matrix supported, medium sorted

Clast supported, medium sorted

Clast supported, well sorted

Clast supported, poorly sorted

Clast supported, well sorted

Clast supported, well sorted

Clast supported, poorly sorted

Matrix supported

Clast supported
medium sorting

Matrix supported

Clast supported
very well sorted

Grey pumice clasts

Height above a.l.l.	Log	Section: 045	Logged by: Isabella J. von Lichtan
		Grainsize	Descriptions and comments

6268823.57, 2777024.87, 365.83 m, 9.98 m
[Northing, Easting, elevation, elevation above lake level]

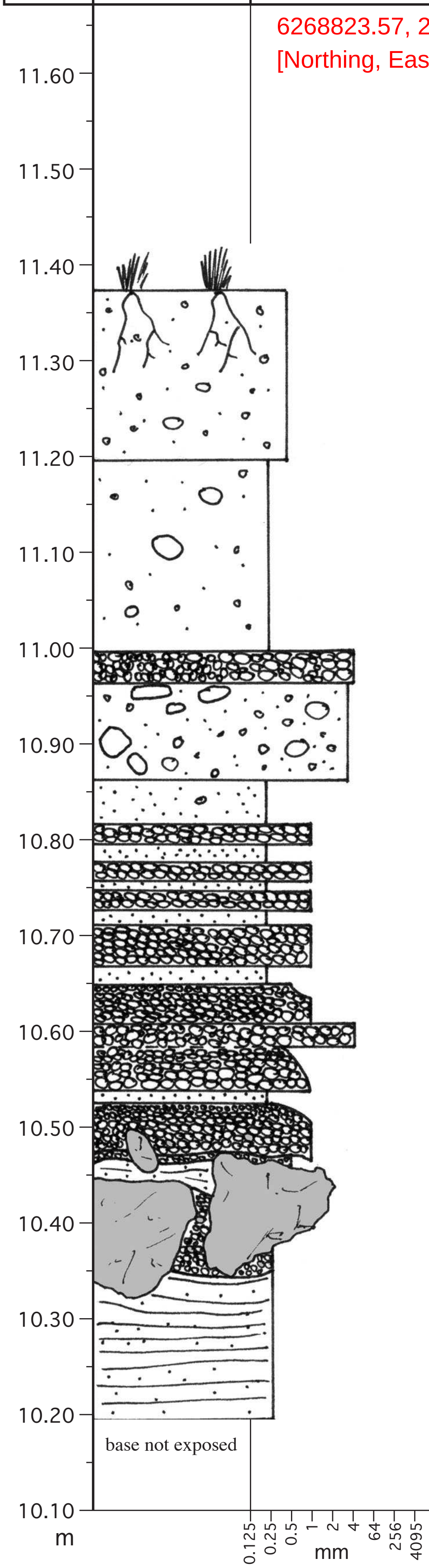

Matrix supported, poorly sorted podsol

Matrix supported, very poorly sorted
contains larger pumice clasts - 'drop pumice'

Clast supported, matrix poor, well sorted

Matrix supported, poorly sorted

Sand
Clast supported, matrix poor, well sorted
Sand
Clast supported, matrix poor, well sorted
Sand
Clast supported, matrix poor, well sorted
Sand
Clast supported, matrix poor, well sorted
Sand
Clast supported, matrix poor, well sorted
grading towards the top
Clast supported, matrix poor, well sorted
Clast supported, matrix poor, well sorted
grading towards the top
Sand

Alternating beds of clast supported, matrix poor, well sorted gravels and sand encasing grey pumice blocks. Grey clats are angular to sub-angular with large vesicles contained within some of the clasts. Some minor bed distruption is visiable around the small blocks. They appear as if the blocks fell into soft sediment and were later incased by further sediment.

Alternating layers of dark grey, lithic rich sands with lighter grey, more pumiceous sands. Well sorted.

Height above a.l.l.	Log	Section: 057	Logged by: Isabella J. von Lichtan
		Grainsize	Descriptions and comments

6268861.18, 2777009.93, 367.17 m, 11.32 m
[Northing, Easting, elevation, elevation above lake level]

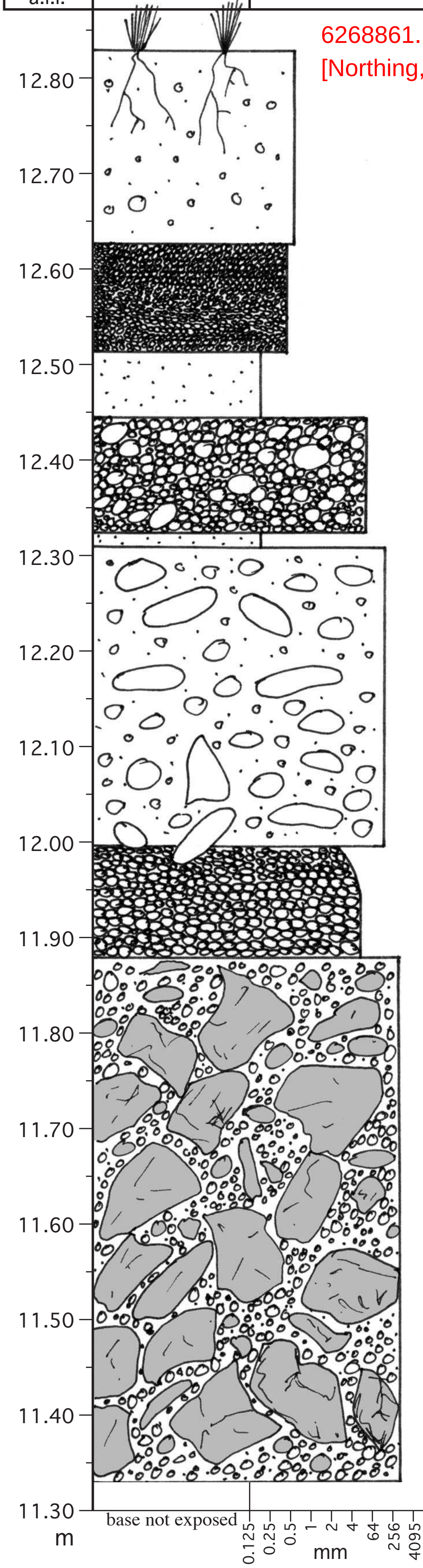

Matrix supported, poorly sorted podsol

Clast supported, very well sorted
pumiceous sand

Sand
very well sorted

Clast supported, poorly sorted
very vesicular pumice clasts

Sand

Matrix supported
very poorly sorted
rounded white pumice clasts
clasts are very vesicular

Clast supported, matrix poor, well sorted
grading towards the top

Angular grey pumice blocks within smaller rounded and sub-angular white pebbles (white pebbles from 0.5cm to 5 cm, average 1cm across).
Matrix is a fine sand
very poorly sorted
matrix supported
grey pumice clasts tend to be tabular, have a non-homogenous vesicularity, distribution of clasts is chaotic

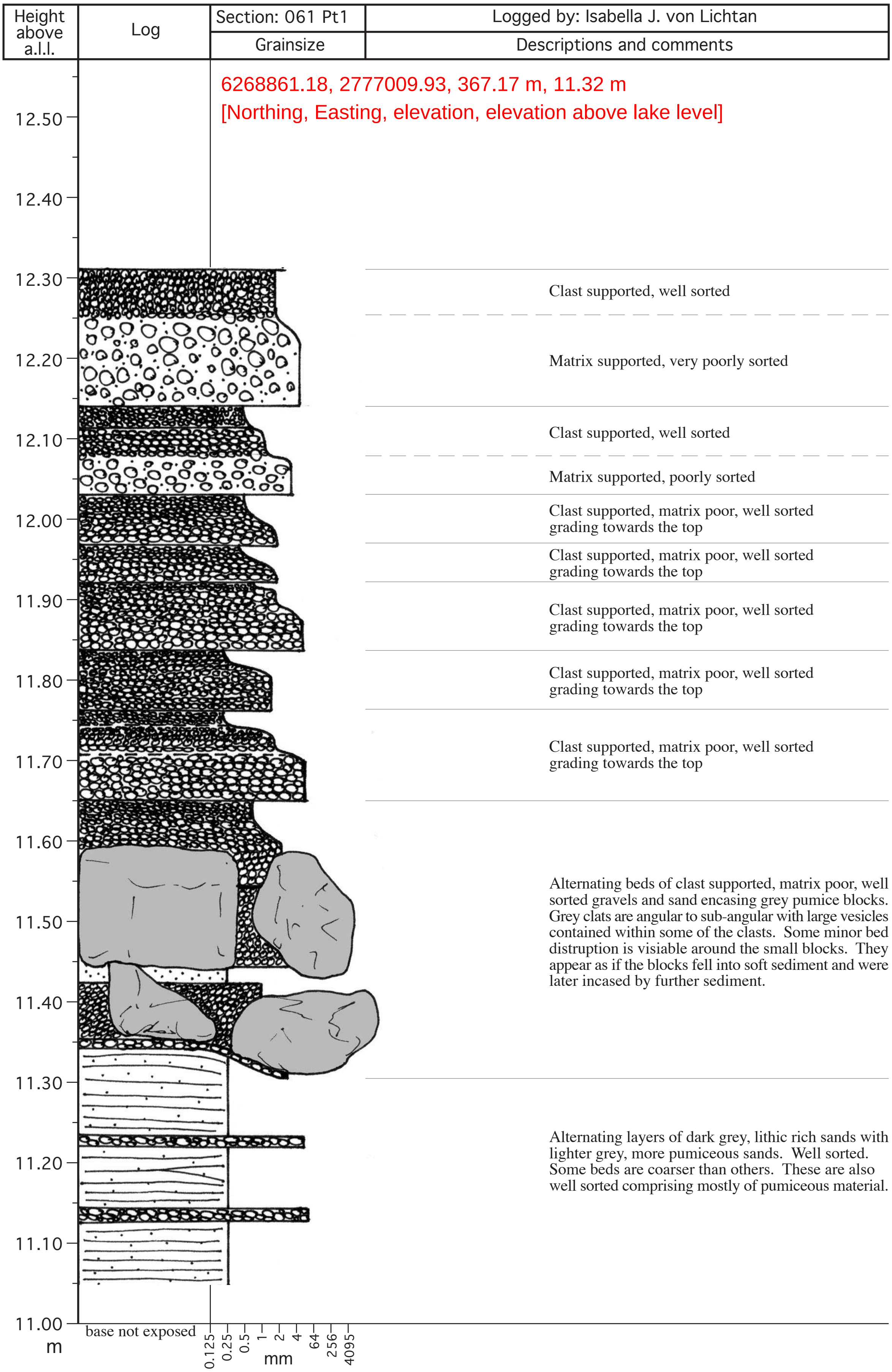
Height above a.l.l.
Log
Section: 061 Pt1
Grainsize
Logged by: Isabella J. von Lichtan
Descriptions and comments
6268861.18, 2777009.93, 367.17 m, 11.32 m
[Northing, Easting, elevation, elevation above lake level]
12.50
12.40
12.30
12.20
12.10
12.00
11.90
11.80
11.70
11.60
11.50
11.40
11.30
11.20
11.10
11.00
m
Clast supported, well sorted
Matrix supported, very poorly sorted
Clast supported, well sorted
Matrix supported, poorly sorted
Clast supported, matrix poor, well sorted grading towards the top
Clast supported, matrix poor, well sorted grading towards the top
Clast supported, matrix poor, well sorted grading towards the top
Clast supported, matrix poor, well sorted grading towards the top
Clast supported, matrix poor, well sorted grading towards the top
Alternating beds of clast supported, matrix poor, well sorted gravels and sand encasing grey pumice blocks. Grey clats are angular to sub-angular with large vesicles contained within some of the clasts. Some minor bed distruption is visiable around the small blocks. They appear as if the blocks fell into soft sediment and were later incased by further sediment.
Alternating layers of dark grey, lithic rich sands with lighter grey, more pumiceous sands. Well sorted. Some beds are coarser than others. These are also well sorted comprising mostly of pumiceous material.
base not exposed
0.125
0.25
0.5
1
2
4
64
256
4095
mm

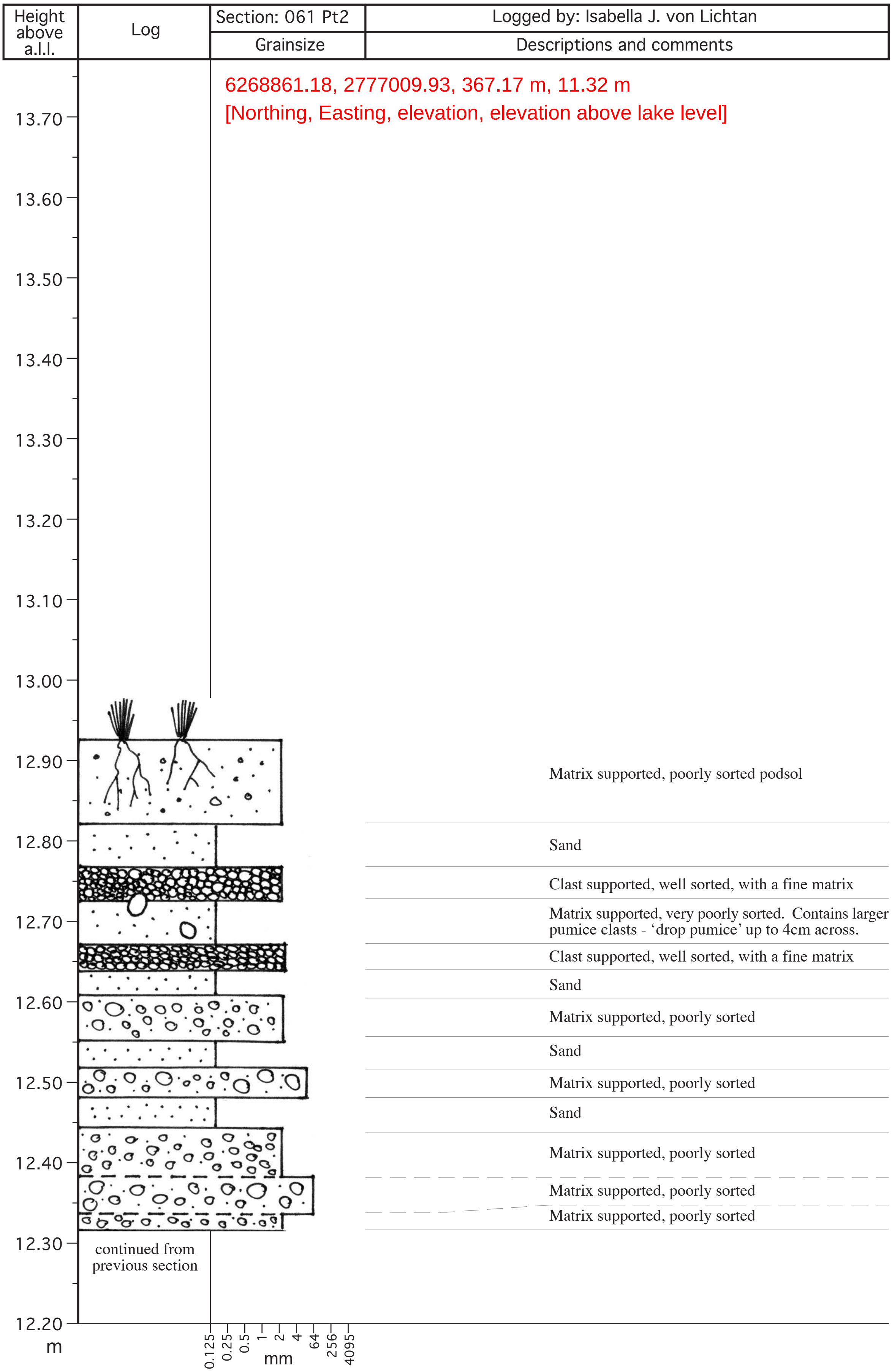
Height above a.l.l.
Log
Section: 061 Pt2
Logged by: Isabella J. von Lichtan
Grainsize
Descriptions and comments
6268861.18, 2777009.93, 367.17 m, 11.32 m
[Northing, Easting, elevation, elevation above lake level]
13.70
13.60
13.50
13.40
13.30
13.20
13.10
13.00
12.90
12.80
12.70
12.60
12.50
12.40
12.30
12.20
m
Matrix supported, poorly sorted podsol
Sand
Clast supported, well sorted, with a fine matrix
Matrix supported, very poorly sorted. Contains larger pumice clasts - ‘drop pumice’ up to 4cm across.
Clast supported, well sorted, with a fine matrix
Sand
Matrix supported, poorly sorted
Sand
Matrix supported, poorly sorted
Sand
Matrix supported, poorly sorted
Matrix supported, poorly sorted
Matrix supported, poorly sorted
continued from previous section
0.125
0.25
0.5
1
2
4
64
256
4095
mm

Height above a.l.l.	Log	Section: 079 Pt 1	Logged by: Isabella J. von Lichtan
		Grainsize	Descriptions and comments

6268888.97, 2776991.03.93, 366.96 m, 11.11 m
[Northing, Easting, elevation, elevation above lake level]

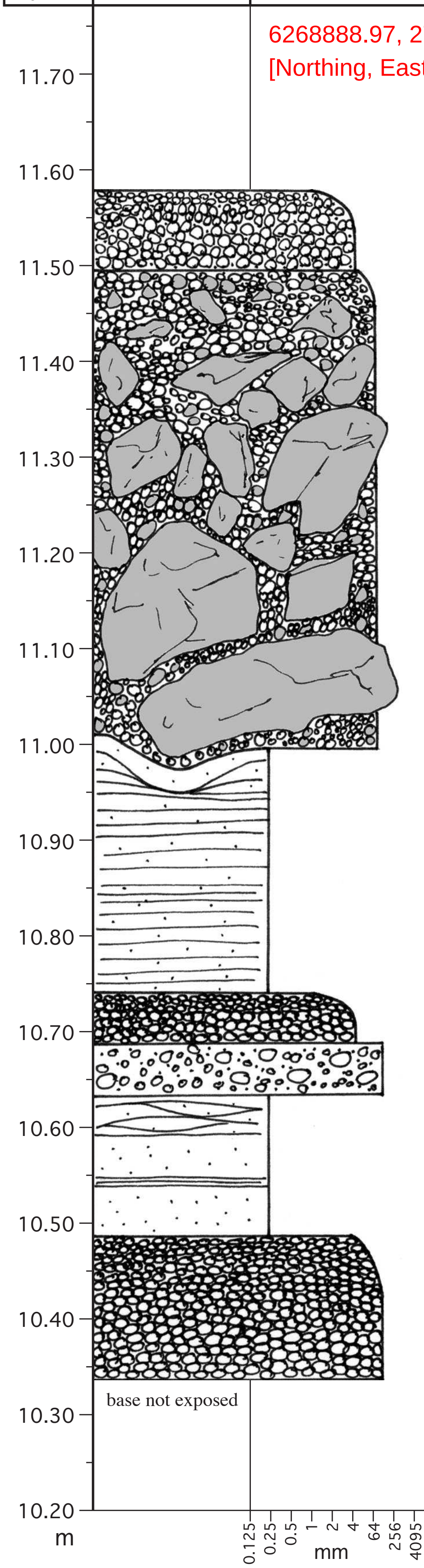

Clast supported, well sorted, pumiceous gravel
clasts are sub-rounded to rounded
contains a matrix

Very poorly sorted, clast supported containing grey pumice clasts of varing sizes in amongst smaller white pumice. Grey pumice clasts/blocks are angular to sub-rounded, and of a lower vesicularity to the white pumice. Matrix is predominetly sand-sized.

Alternating layers of dark grey, lithic rich sands with lighter grey, more pumiceous sands.
Planar beded.

Matrix poor, well sorted, rounded pumice clasts

Matrix supported, poorly to medium sorted, pumiceous clasts

Alternating layers of dark grey, lithic rich sands with lighter grey, more pumiceous sands.
Contains planar and wavy bedding.

Clast supported, very well sorted, matrix poor, pumiceous gravel
clasts are sub-rounded to rounded

Height above a.l.l.	Log	Section: 079 Pt 2	Logged by: Isabella J. von Lichtan
		Grainsize	Descriptions and comments

6268888.97, 2776991.03.93, 366.96 m, 11.11 m
[Northing, Easting, elevation, elevation above lake level]

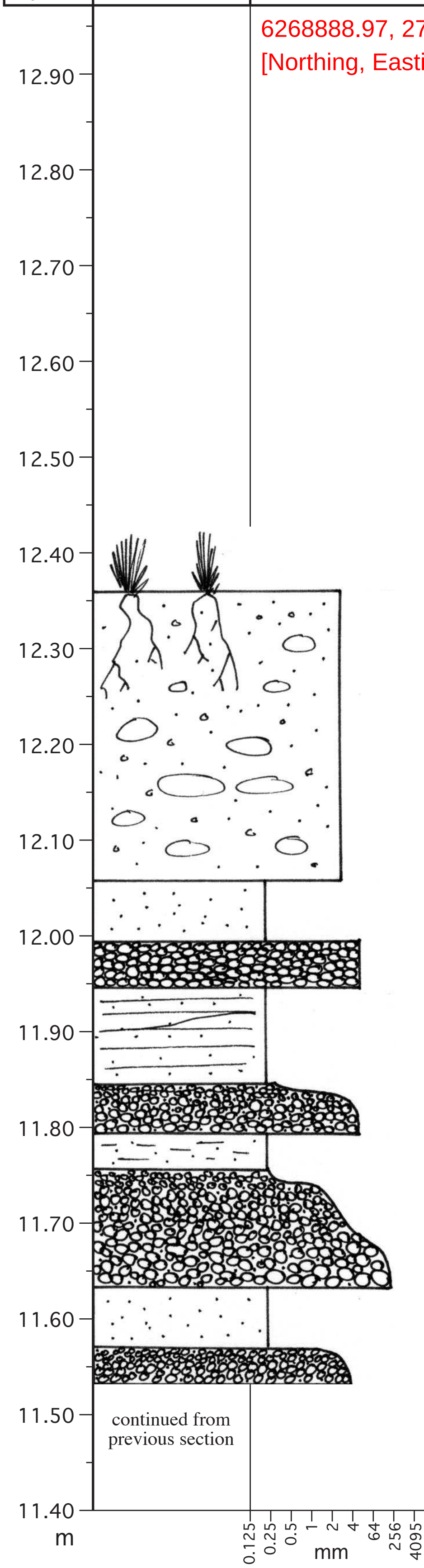

Matrix supported, very poorly sorted podsol

Pumiceous sand

Matrix poor, well sorted, rounded pumice clasts

Alternating layers of dark grey, lithic rich sands with lighter grey, more pumiceous sands.
Planar bedded.

Clast supported, well sorted, pumiceous gravel
clasts are sub-rounded to rounded
contains a matrix

Alternating layers of dark grey, lithic rich sands with lighter grey, more pumiceous sands.
Planar bedded.

Clast supported, well sorted, pumiceous gravel
clasts are sub-rounded to rounded
contains a matrix

Pumiceous sands.

Clast supported, well sorted, pumiceous gravel
clasts are sub-rounded to rounded
contains a matrix

Height above a.l.l.	Log	Section: 096	Logged by: Isabella J. von Lichtan
		Grainsize	Descriptions and comments

6268482.61, 2777231.17, 365.51 m, 9.66 m
[Northing, Easting, elevation, elevation above lake level]

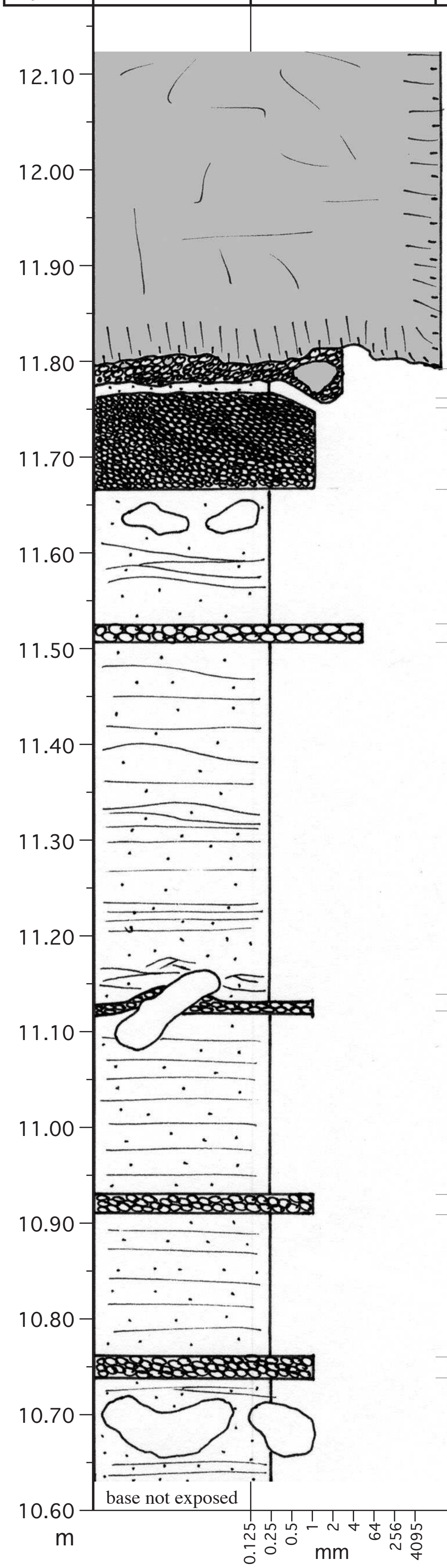

GRP23
Large grey rafted pumice clast
angular, blocky with radial cooling joints

Reverse graded, well sorted, matrix poor, angular to sub-angular pumice clasts
Contains small pieces of grey pumice

Sand

Lithic rich sand

Lithic rich sand with alternating layers of more pumiceous rich sands; very well sorted
Dune bedded
Upper part conatins grey pumice clasts

Poor to medium sorted, matrix poor, angular to sub-rounded pumice clasts

Lithic rich sand with alternating layers of more pumiceous rich sands
Planar bedded near bottom, dune bedded near the top

Lithic rich sand containing clasts, usually of lithic origin, 3 to 15cm across

Lithic rich sand with alternating layers of more pumiceous rich sands
Planar bedded

Lithic rich sand

Lithic rich sand with alternating layers of more pumiceous rich sands
Planar bedded

Lithic rich sand

Lithic rich sand with alternating layers of more pumiceous rich sands
Areas of coarser gravel and also larger pumice and lithic clasts
Sand part has planar bedding

Height above a.l.l.	Log	Section: 098 Pt 2	Logged by: Isabella J. von Lichtan
		Grainsize	Descriptions and comments

6270592.00, 2772900.14, 370.31 m, 14.46 m
[Northing, Easting, elevation, elevation above lake level]

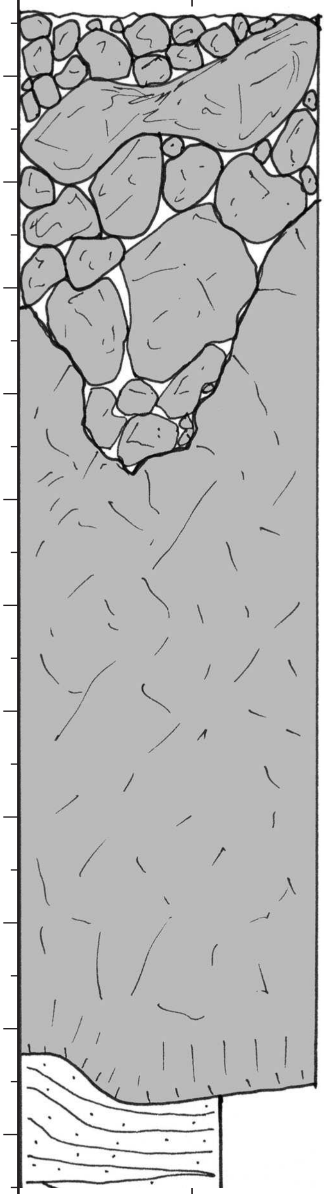

GRP24
Grey rafted pumice block with smaller clasts of grey pumice above.
Clasts are angular, blocky, clast supported, contains between the clasts. The block and larger clasts have radial cooling joints. The smaller clasts perhaps are broken pieces from the larger one.

Laminated and dune bedded pumiceous sand. Some beds have a slight lithic content.

Height above a.l.l.	Log	Section: 109	Logged by: Isabella J. von Lichtan
		Grainsize	Descriptions and comments

6268426.09, 2777254.96, 366.15 m, 10.30 m
[Northing, Easting, elevation, elevation above lake level]

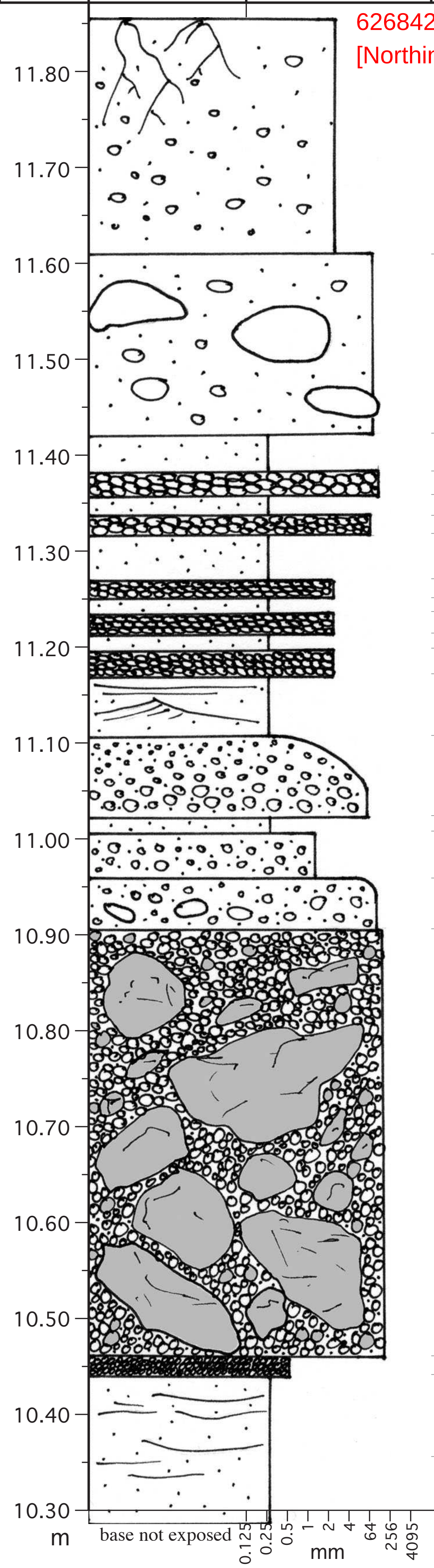

Matrix supported, very poorly sorted podsol

Matrix supported, very poorly sorted, contains very rounded clasts in a sandy matrix - ‘drop pumice’

Laminated and dune bedded
alternating layers of lithic rich and lithic poor sands

Clast supported, medium to well sorted white pumice clasts

Laminated and dune bedded
alternating layers of lithic rich and lithic poor sands

Clast supported, medium to well sorted white pumice clasts

Laminated and dune bedded
alternating layers of lithic rich and lithic poor sands

Clast supported, medium to well sorted white pumice clasts

Laminated and dune bedded
alternating layers of lithic rich and lithic poor sands

Clast supported, medium to well sorted white pumice clasts

Laminated and dune bedded
alternating layers of lithic rich and lithic poor sands

Clast supported, medium to well sorted white pumice clasts

Laminated and dune bedded
alternating layers of lithic rich and lithic poor sands

Matrix supported, medium sorted, contains pumice clasts in a sandy matrix, normally graded

Laminated and dune bedded
alternating layers of lithic rich and lithic poor sands

Matrix supported, poorly sorted, contains pumice clasts in a sandy matrix

Matrix supported, very poorly sorted, contains pumice clasts in a sandy matrix

Very poorly sorted
clast supported
contains grey pumice clasts and blocks with small white pumice
contains a fine sand sized matrix

Lithic rich sand, with small pumice clasts

Lithic rich sand, dune bedded

Lithic poor sand, dune bedded

Height above a.l.l.	Log	Section: 131	Logged by: Isabella J. von Lichtan
		Grainsize	Descriptions and comments

6268383,40, 2777267.20, 366.12 m, 10.27 m
[Northing, Easting, elevation, elevation above lake level]

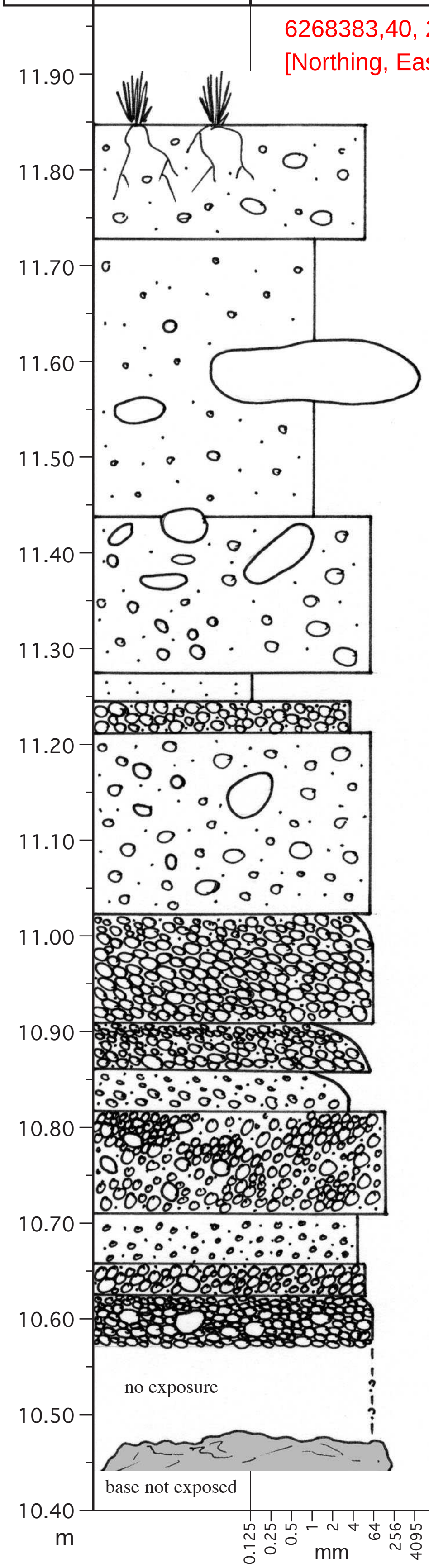

Matrix supported, very poorly sorted podsol

Matrix supported, very poorly sorted, sub-angular pumice clasts as well as rounded 'drop pumice'

Matrix supported, very poorly sorted, sub-angular pumice clasts as well as rounded 'drop pumice'

Sandy layer, well sorted

Clast supported, poorly sorted, contains matrix

Matrix supported, very poorly sorted, sub-angular pumice clasts
Contains some grey pumice clasts

Clast supported, poorly sorted, contains matrix

Clast supported, poorly sorted, contains matrix

Matrix supported, very poorly sorted, sub-angular pumice clasts

Alternates form being clast supported, to matrix supported
poorly sorted, contains sub-angular to sub-roundedwhite pumice clasts and sub-angular grey pumice clasts

matrix supported, very poorly sorted, sub-angular pumice clasts

Clast supported, poorly sorted, contains matrix

Clast supported, poorly sorted, matrix poor, rounded vesicular pumice clasts

No outcrop - talus and vegetation

Grey pumice clast
It is blocky, angular, medium vesicular

Height above a.l.l.	Log	Section: 133	Logged by: Isabella J. von Lichtan
		Grainsize	Descriptions and comments

6268369.80, 2777275.42, 366.12 m, 10.27 m
[Northing, Easting, elevation, elevation above lake level]

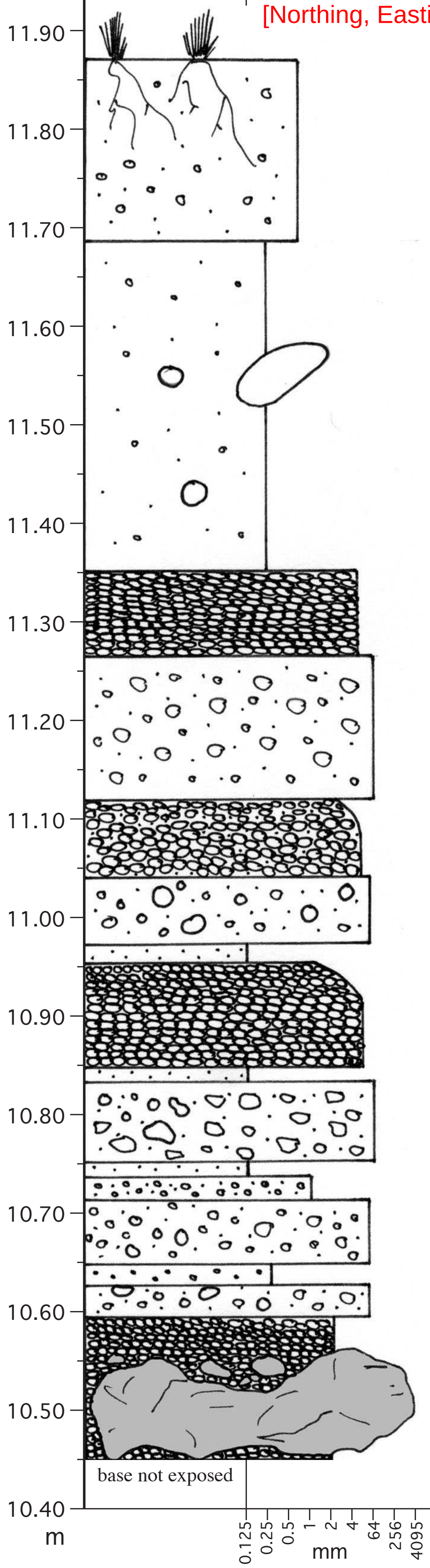

Matrix supported, very poorly sorted podsol

Very poorly sorted, matrix supported, contains sub-angular to sub-rounded pumiceContains some larger white pumice clasts - ‘drop pumice’

Sub-angular to sub-rounded pumiceous clasts, matrix poor, well sorted, normally graded

Very poorly sorted, matrix supported, contains sub-angular to sub-rounded pumice, mostly sub-angular

Sub-angular to sub-rounded pumiceous clasts, well sorted, normally graded
Contains matrix

Very poorly sorted, matrix supported, contains sub-angular to sub-rounded pumice, mostly sub-angular

Sandy layer

Sub-angular to sub-rounded pumiceous clasts, matrix poor, well sorted, normally graded

Sandy layer

Very poorly sorted, matrix supported, contains sub-angular to sub-rounded pumice, mostly sub-angular

Sandy layer

Very poorly sorted, matrix supported, contains sub-angular to sub-rounded pumice

Very poorly sorted, matrix supported, contains sub-angular to sub-rounded pumice

Sandy layer

Very poorly sorted, matrix supported, contains sub-angular to sub-rounded pumice

Poorly sorted, clasts supported, contains a fine matrix
Clasts are large and small grey pumice clasts surrounded by white pumice clasts
Graded to being well sorted above the grey pumice blocks

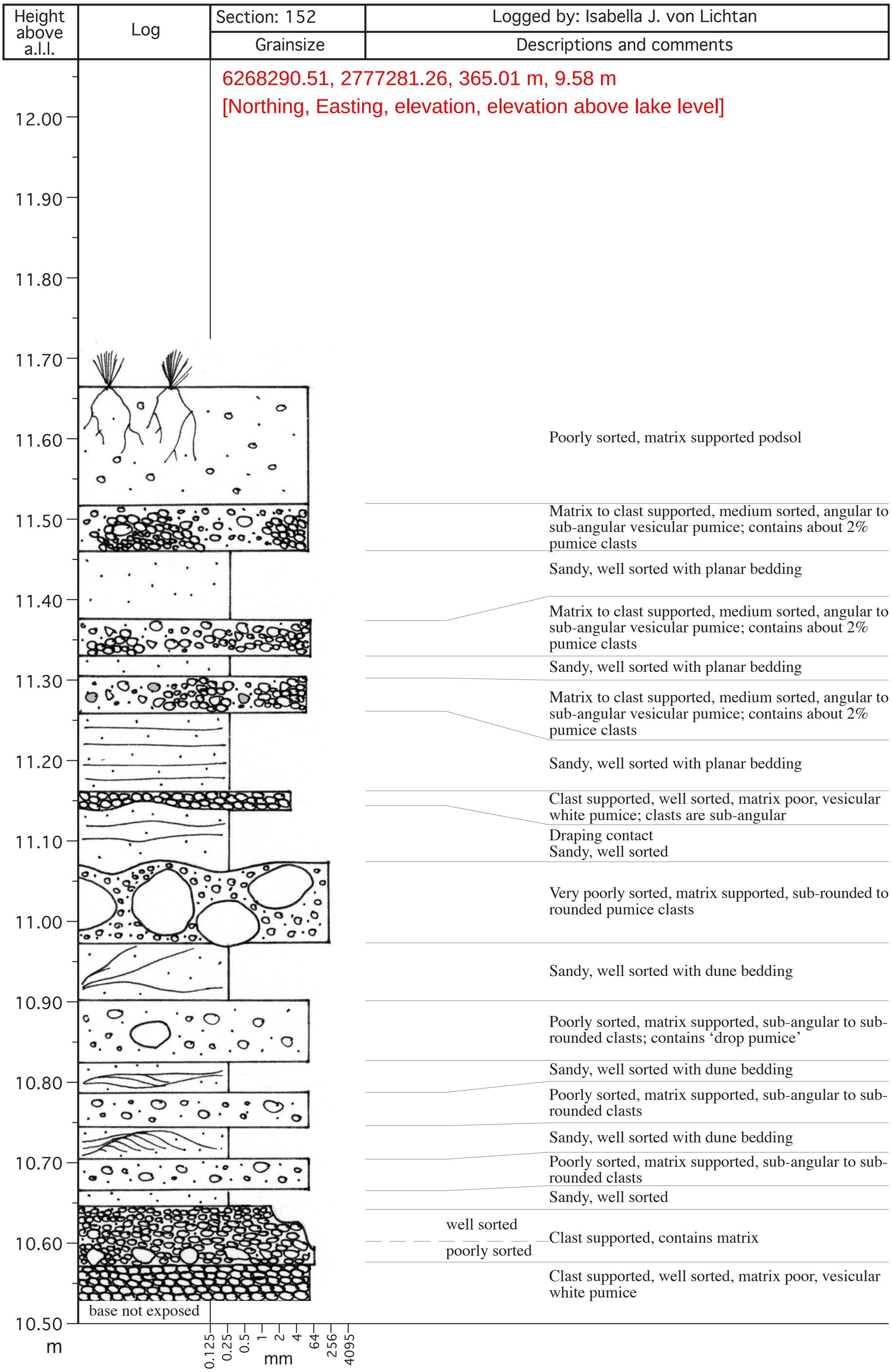
Height above a.l.l.
Log
Section: 152
Logged by: Isabella J. von Lichtan
Grainsize
Descriptions and comments
6268290.51, 2777281.26, 365.01 m, 9.58 m
[Northing, Easting, elevation, elevation above lake level]
12.00
11.90
11.80
11.70
11.60
11.50
11.40
11.30
11.20
11.10
11.00
10.90
10.80
10.70
10.60
10.50
m
Poorly sorted, matrix supported podsol
Matrix to clast supported, medium sorted, angular to sub-angular vesicular pumice; contains about 2% pumice clasts
Sandy, well sorted with planar bedding
Matrix to clast supported, medium sorted, angular to sub-angular vesicular pumice; contains about 2% pumice clasts
Sandy, well sorted with planar bedding
Matrix to clast supported, medium sorted, angular to sub-angular vesicular pumice; contains about 2% pumice clasts
Sandy, well sorted with planar bedding
Clast supported, well sorted, matrix poor, vesicular white pumice; clasts are sub-angular
Draping contact
Sandy, well sorted
Very poorly sorted, matrix supported, sub-rounded to rounded pumice clasts
Sandy, well sorted with dune bedding
Poorly sorted, matrix supported, sub-angular to sub-rounded clasts; contains 'drop pumice'
Sandy, well sorted with dune bedding
Poorly sorted, matrix supported, sub-angular to sub-rounded clasts
Sandy, well sorted with dune bedding
Poorly sorted, matrix supported, sub-angular to sub-rounded clasts
Sandy, well sorted
well sorted
Clast supported, contains matrix
poorly sorted
Clast supported, well sorted, matrix poor, vesicular white pumice
base not exposed
0.125
0.25
0.5
1
2
4
64
256
4095
mm

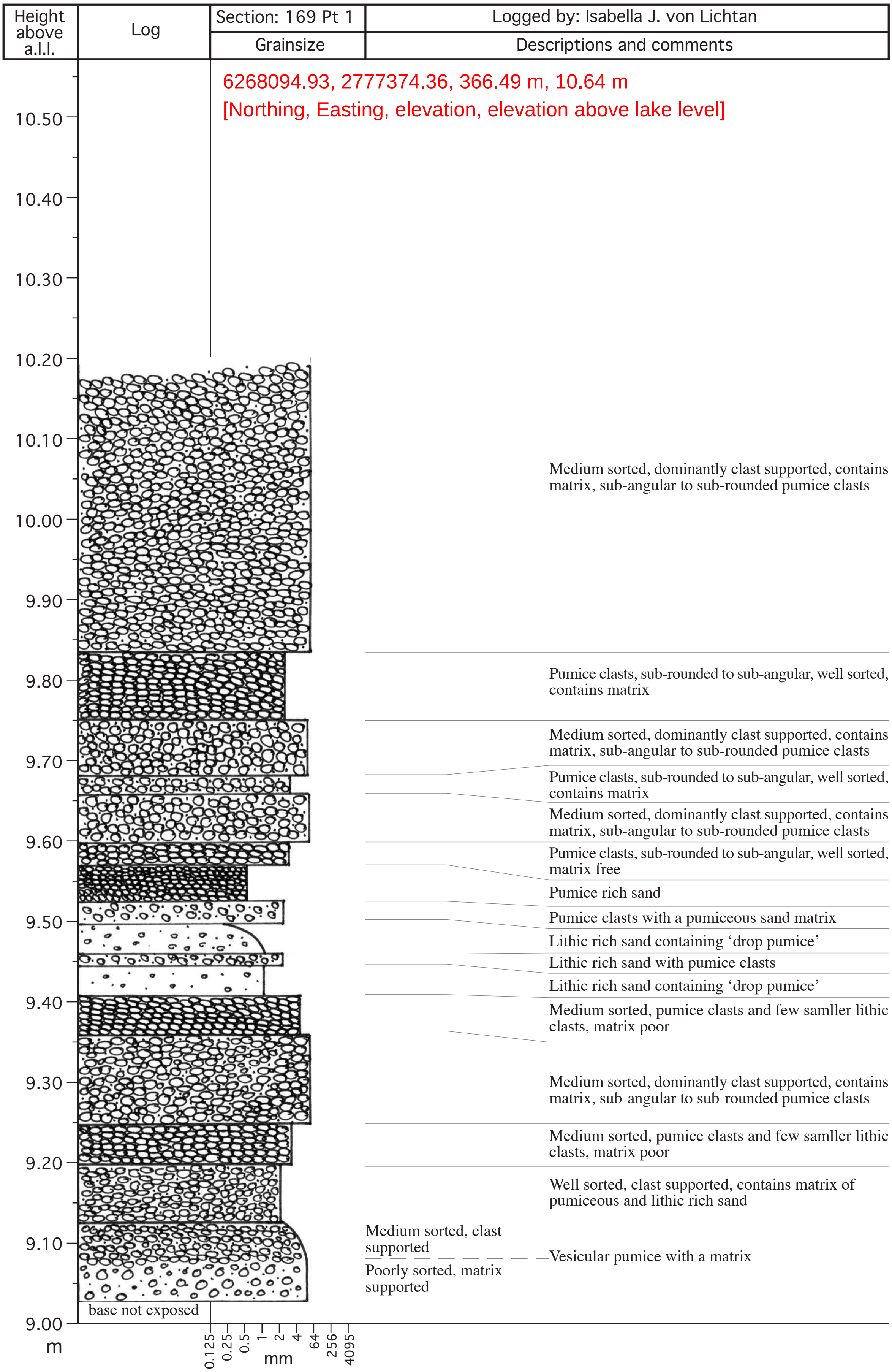
Height above a.l.l.
Log
Section: 169 Pt 1
Logged by: Isabella J. von Lichtan
Grainsize
Descriptions and comments
6268094.93, 2777374.36, 366.49 m, 10.64 m
[Northing, Easting, elevation, elevation above lake level]
10.50
10.40
10.30
10.20
10.10
10.00
9.90
9.80
9.70
9.60
9.50
9.40
9.30
9.20
9.10
9.00
m
Medium sorted, dominantly clast supported, contains matrix, sub-angular to sub-rounded pumice clasts
Pumice clasts, sub-rounded to sub-angular, well sorted, contains matrix
Medium sorted, dominantly clast supported, contains matrix, sub-angular to sub-rounded pumice clasts
Pumice clasts, sub-rounded to sub-angular, well sorted, contains matrix
Medium sorted, dominantly clast supported, contains matrix, sub-angular to sub-rounded pumice clasts
Pumice clasts, sub-rounded to sub-angular, well sorted, matrix free
Pumice rich sand
Pumice clasts with a pumiceous sand matrix
Lithic rich sand containing 'drop pumice'
Lithic rich sand with pumice clasts
Lithic rich sand containing 'drop pumice'
Medium sorted, pumice clasts and few samller lithic clasts, matrix poor
Medium sorted, dominantly clast supported, contains matrix, sub-angular to sub-rounded pumice clasts
Medium sorted, pumice clasts and few samller lithic clasts, matrix poor
Well sorted, clast supported, contains matrix of pumiceous and lithic rich sand
Medium sorted, clast supported
Poorly sorted, matrix supported
Vesicular pumice with a matrix
base not exposed
0.125
0.25
0.5
1
2
4
64
256
4095
mm

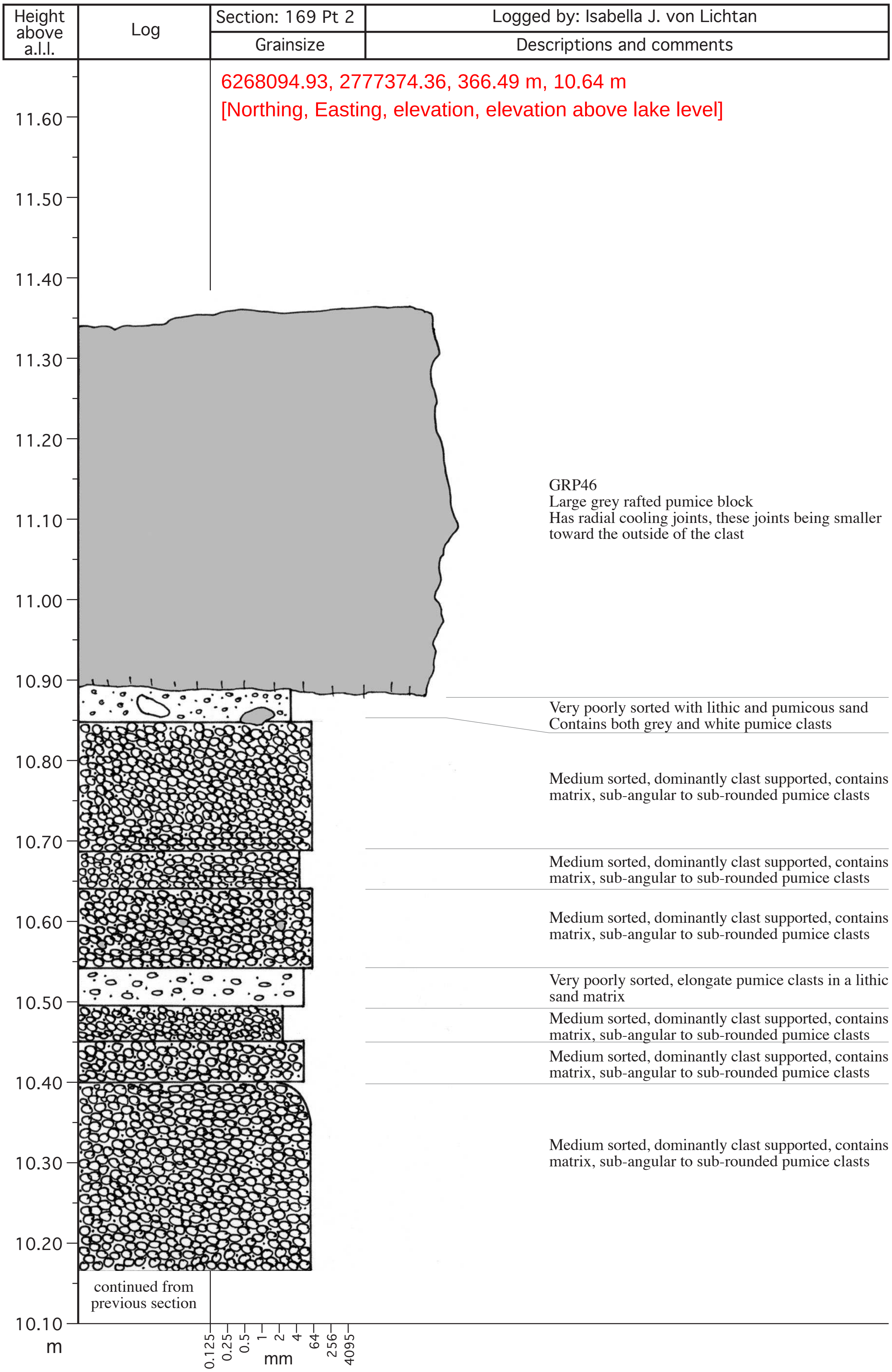
Height above a.l.l.
Log
Section: 169 Pt 2
Logged by: Isabella J. von Lichtan
Grainsize
Descriptions and comments
6268094.93, 2777374.36, 366.49 m, 10.64 m
[Northing, Easting, elevation, elevation above lake level]
11.60
11.50
11.40
11.30
11.20
11.10
11.00
10.90
10.80
10.70
10.60
10.50
10.40
10.30
10.20
10.10
m
GRP46
Large grey rafted pumice block
Has radial cooling joints, these joints being smaller toward the outside of the clast
Very poorly sorted with lithic and pumicous sand
Contains both grey and white pumice clasts
Medium sorted, dominantly clast supported, contains matrix, sub-angular to sub-rounded pumice clasts
Medium sorted, dominantly clast supported, contains matrix, sub-angular to sub-rounded pumice clasts
Medium sorted, dominantly clast supported, contains matrix, sub-angular to sub-rounded pumice clasts
Very poorly sorted, elongate pumice clasts in a lithic sand matrix
Medium sorted, dominantly clast supported, contains matrix, sub-angular to sub-rounded pumice clasts
Medium sorted, dominantly clast supported, contains matrix, sub-angular to sub-rounded pumice clasts
Medium sorted, dominantly clast supported, contains matrix, sub-angular to sub-rounded pumice clasts
continued from previous section
0.125
0.25
0.5
1
2
4
64
256
4095
mm

Height above a.l.l.	Log	Section: 171 Pt 1	Logged by: Isabella J. von Lichtan
		Grainsize	Descriptions and comments

6268062.14, 2777389.03, 367.86 m, 12.01 m
[Northing, Easting, elevation, elevation above lake level]

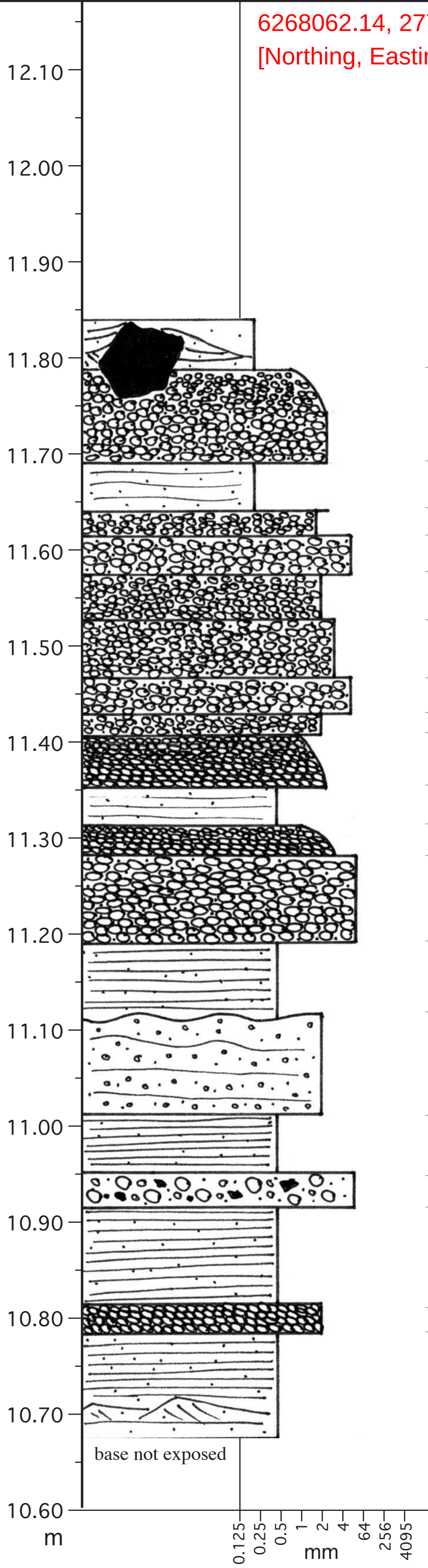

Alternating layer of lithic rich and lithic poor sand. Mostly laminated, but also dune bedded in places. Very well sorted. Contains a large lithic of bandded rhyolite

Medium sorted, dominantly clast supported, contains matrix, sub-angular to sub-rounded pumice clasts

Alternating layer of lithic rich and lithic poor sand. Mostly laminated, but also dune bedded in places. Very well sorted.

Medium sorted, dominantly clast supported, contains matrix, sub-angular to sub-rounded pumice clasts

Medium sorted, dominantly clast supported, contains matrix, sub-angular to sub-rounded pumice clasts

Medium sorted, dominantly clast supported, contains matrix, sub-angular to sub-rounded pumice clasts

Medium sorted, dominantly clast supported, contains matrix, sub-angular to sub-rounded pumice clasts

Medium sorted, dominantly clast supported, contains matrix, sub-angular to sub-rounded pumice clasts

Medium sorted, dominantly clast supported, contains matrix, sub-angular to sub-rounded pumice clasts

Well sorted, clast supported, pumacious clasts, matrix free.

Alternating layer of lithic rich and lithic poor sand. Mostly laminated, but also dune bedded in places. Very well sorted.

Well sorted, clast supported, pumacious clasts, matrix free.

Medium sorted, dominantly clast supported, contains matrix, sub-angular to sub-rounded pumice clasts

Alternating layer of lithic rich and lithic poor sand. Mostly laminated, but also dune bedded in places. Very well sorted.

Alternating layer of lithic poor andvery lithic rich sand. Mostly laminated, but also dune bedded in places. Has a wavy upper contact. Medium sorted.

Alternating layer of lithic rich and lithic poor sand. Mostly laminated, but also dune bedded in places. Very well sorted.

Poorly sorted, matrix supported, contains sub-angular pumice and lithic clasts

Alternating layer of lithic rich and lithic poor sand. Mostly laminated, but also dune bedded in places. Very well sorted.

Medium sorted, pumice clasts and few samller lithic clasts, matrix poor

Alternating layer of lithic rich and lithic poor sand. Mostly laminated, but also dune bedded. Very well sorted.

Height above a.l.l.	Log	Section: 171 Pt 2	Logged by: Isabella J. von Lichtan
		Grainsize	Descriptions and comments

6268062.14, 2777389.03, 367.86 m, 12.01 m
[Northing, Easting, elevation, elevation above lake level]

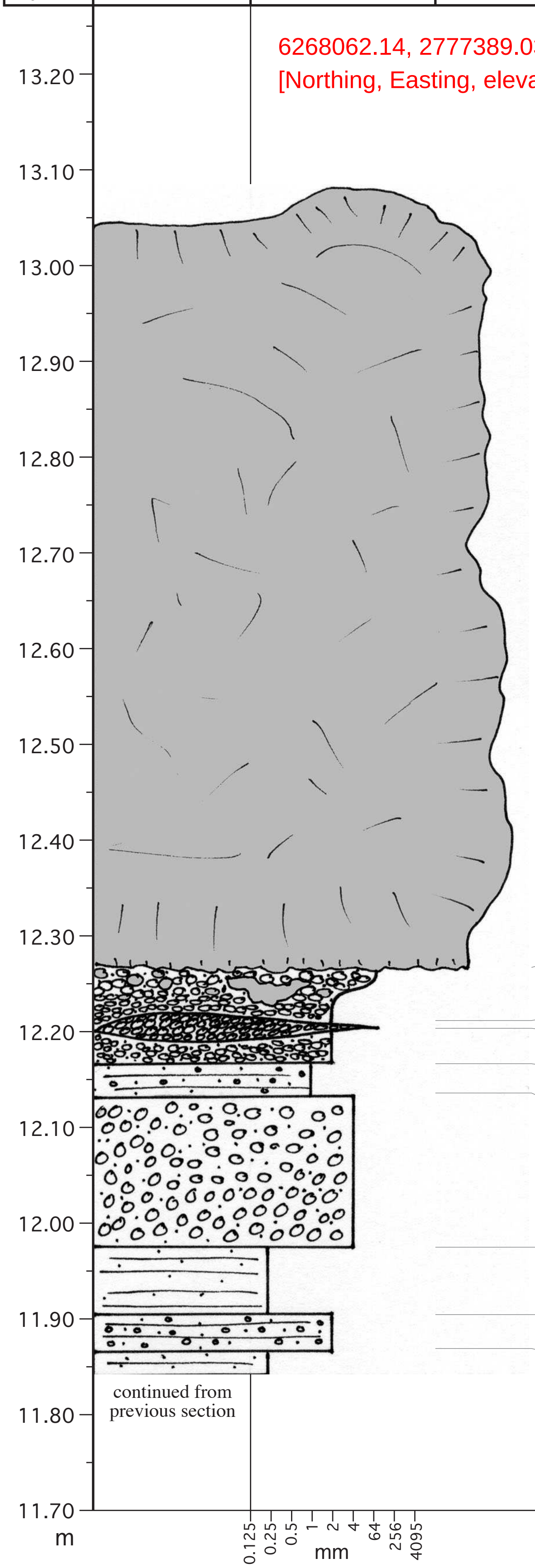

GRP47
Large grey rafted pumice block
Has radial cooling joints, these joints being smaller toward the outside of the clast

Well sorted near the bottom and poorly sorted towards the top; clast supported, contains matrix; has both grey a nd white pumice clasts; reverse graded.

Lense of lithic rich clasts, clasts supported, matrix free

Well sorted, clast supported, contains matrix. has both grey and white pumice clasts.

Alternating layer of lithic rich and lithic poor sand. Mostly laminated, but also dune bedded. Very well sorted.

Medium sorted, matrix supported, sub-angular to sub-rounded pumice clasts

Alternating layer of lithic rich and lithic poor sand. Mostly laminated, but also dune bedded. Very well sorted.

Alternating layer of lithic rich and lithic poor sand. Mostly laminated, but also dune bedded. Very well sorted.

Alternating layer of lithic rich and lithic poor sand. Mostly laminated, but also dune bedded. Very well sorted.

continued from previous section

APPENDIX II
DGPS DATA

A2.1 DATA FROM DRAUGHT LINE ESTIMATE

GRP #	Distance (m)	Height of clast above lake (m) a.l.l.	Compensation relative to 5 Mile Bay	Final height (m) a.l.l.	Height of clasts (m)	Draught	Predicted palaeowater line	Width (m)
23		10.0	1.8	11.8	1.9	1.7	13.5	7.1
24		14.46	-5.30	9.16	0.95	0.9	10.0	1.1
104			0.00	0.00	1.5	1.4	1.4	5.1
107			0.00	0.00	1.7	1.5	1.5	4.2
108			0.00	0.00	0.9	0.8	0.8	3.7
01	300.2	11.6	0.08	11.68	0.5	0.5	12.1	0.74
03	351.9	9.54	0.09	9.63	2.8	2.5	12.1	14
04	307.9	9.89	0.08	9.97	0.95	0.9	10.8	1.15
05	290.4	9.67	0.07	9.74	1.06	1.0	10.7	1.12
06	288.6	11.2	0.07	11.30	0.09	0.1	11.4	0.13
07	267.4	10.26	0.07	10.32	0.86	0.8	11.1	1.06
08	243.7	11.0	0.06	11.02	0.05	0.0	11.1	0.1
09	250.3	11.3	0.06	11.33	2.8	2.5	13.8	8
10	247.9	11.39	0.06	11.45	1.1	1.0	12.4	1.3
11	191.3	10.0	0.05	10.02	0.1	0.1	10.1	0.2
112		9.2	2.8	12.0	4.2	3.8	15.7	20
12	194.5	10.3	0.05	10.35	0.32	0.3	10.6	0.35
14	189.7	10.2	0.05	10.25	0.32	0.3	10.5	0.4
15	151.0	11.3	0.04	11.36	0.3	0.3	11.6	0.4
16	161.5	10.12	0.04	10.16	1.7	1.5	11.7	2.5
17	125.3	10.43	0.03	10.47	0.2	0.2	10.6	0.3
18	144.0	10.38	0.04	10.41	0.2	0.2	10.6	0.3
19	130.0	10.6	0.03	10.60	0.4	0.4	11.0	0.6
20	117.7	11.1	0.03	11.14	0.25	0.2	11.4	0.4
21	100.0	10.98	0.02	11.01	1.6	1.4	12.4	0.74
22	81.8	11.2	0.02	11.24	0.6	0.5	11.8	0.5
25	597.7	11.25	0.15	11.40	0.8	0.7	12.1	0.94
26	600.5	10.96	0.15	11.11	1.27	1.1	12.3	1.7
27	607.3	9.89	0.15	10.04		0.0	10.0	
28	629.9	10.19	0.16	10.35	0.8	0.7	11.1	0.75
29	666.4	8.82	0.17	8.98	4.5	4.1	13.0	16
30	649.7	10.3	0.16	10.46	0.15	0.1	10.6	0.25
31	660.7	10.64	0.17	10.81	0.6	0.5	11.3	0.6
32	660.9	10.68	0.17	10.84	0.15	0.1	11.0	0.55
35	693.4	10.3	0.17	10.44	0.1	0.1	10.5	0.25
36	709.2	10.3	0.18	10.45	0.13	0.1	10.6	0.4
37	718.6	10.3	0.18	10.45	0.4	0.4	10.8	0.63
38	782.7	9.16	0.20	9.36	4.3	3.9	13.2	16
39	946.2	8.71	0.24	8.95	2.8	2.5	11.5	9.5
40	1037.0	10.24	0.26	10.50	3	2.7	13.2	4.85
46	999.3	10.64	0.25	10.89	0.48	0.4	11.3	1.9
47	1035.2	12.01	0.26	12.26	1.24	1.1	13.4	2
53	588.5	9.66	0.15	9.81	1	0.9	10.7	

Draught = the depth of water in which an object, like a ship, will float

A2.2 RELATIVE DISTANCE ESTIMATES AT FIVE MILE BAY

GRP #	A.L.L.	Height	Easting X2	Northing Y2	Y1 =-2X+11822900	N=Y0-Y2	B=Y2-Y1	R=N/CosTheta	A=bCosTheta	Distance (m) = Length=R+A	Y0, X=0 (Y-intercept)	Theta
22	11.22	367.07	2776973.06	6268920.02	6268953.882	46	34	52	30.2870468	82	6269000	0.463647589
21	10.98	366.83	2776982.31	6268904.36	6268935.387	65	31	72	27.74990351	100		
20	11.11	366.96	2776991.03	6268888.97	6268917.949	82	29	92	25.91793616	118		
19	10.56	366.41	2776995.25	6268877.25	6268909.5	90	32	101	28.84165554	130		
17	10.43	366.28	2776992.08	6268880.91	6268915.83	84	35	94	31.23061698	125		
18	10.38	366.23	2777001.50	6268864.78	6268896.996	103	32	115	28.81666702	144		
16	10.12	365.97	2777009.23	6268849.06	6268881.547	118	32	132	29.05650798	161		
15	11.32	367.17	2777009.93	6268861.18	6268880.138	120	19	134	16.95533852	151		
14	10.20	366.05	2777025.28	6268825.52	6268849.444	151	24	168	21.39620414	190		
12	10.30	366.15	2777028.29	6268821.64	6268843.411	157	22	175	19.47736765	195		
11	9.98	365.83	2777024.87	6268823.57	6268850.258	150	27	167	23.87139881	191		
09	11.27	367.12	2777061.21	6268775.76	6268777.572	222	2	249	1.616420186	250		
08	10.96	366.81	2777056.90	6268781.03	6268786.203	214	5	239	4.62793648	244		
10	11.39	367.24	2777060.74	6268778.25	6268778.52	221	0	248	0.238562741	248		
07	10.26	366.11	2777065.80	6268758.93	6268768.405	232	9	259	8.472659197	267		
06	11.23	367.08	2777077.46	6268741.02	6268745.074	255	4	285	3.626162919	289		
05	9.67	365.52	2777076.13	6268738.42	6268747.748	252	9	282	8.342939195	290		
04	9.89	365.74	2777086.62	6268724.11	6268726.765	273	3	305	2.379305141	308		
01	11.60	367.45	2777095.25	6268736.95	6268709.497	291	-27	325	-24.55313971	300		
03	9.54	365.39	2777108.89	6268685.96	6268682.221	318	-4	355	-3.347778213	352		
53	9.66	365.51	2777231.17	6268482.61	6268437.668	562	-45	629	-40.20101814	589		
25	11.25	367.10	2777241.74	6268477.67	6268416.52	583	-61	652	-54.69359742	598		
26	10.96	366.81	2777242.23	6268474.79	6268415.543	584	-59	653	-52.99143905	600		
27	9.89	365.74	2777237.18	6268464.63	6268425.641	574	-39	642	-34.8700304	607		
28	10.19	366.04	2777248.22	6268444.91	6268403.563	596	-41	667	-36.98327901	630		
29	8.82	364.67	2777253.57	6268406.70	6268392.863	607	-14	679	-12.37731137	666		
30	10.30	366.15	2777254.96	6268426.09	6268390.089	610	-36	682	-32.20062242	650		
31	10.64	366.49	2777260.69	6268416.69	6268378.628	621	-38	695	-34.04646555	661		
32	10.68	366.53	2777260.82	6268416.52	6268378.363	622	-38	695	-34.1297203	661		
35	10.27	366.12	2777267.20	6268383.40	6268365.61	634	-18	709	-15.91152545	693		
36	10.27	366.12	2777275.42	6268369.80	6268349.158	651	-21	728	-18.46168531	709		
37	10.27	366.12	2777275.72	6268359.44	6268348.562	651	-11	728	-9.734181949	719		
38	9.16	365.01	2777281.26	6268290.51	6268337.487	663	47	741	42.01579425	783		
39	8.71	364.56	2777331.75	6268133.02	6268236.494	764	103	854	92.54793972	946		
46	10.64	366.49	2777374.36	6268094.93	6268151.273	849	56	949	50.39736922	999		
40	10.24	366.09	2777371.10	6268051.14	6268157.795	842	107	942	95.39234933	1037		
47	12.01	367.86	2777389.03	6268062.14	6268121.932	878	60	982	53.47679907	1035		

A2.3 ORIGINAL RAW DGPS DATA WITH ACTUAL LAKE LEVEL (A.L.L.) LISTED

ID #	Northing	Easting	Height	Height above a.l.l.	Location	GRP #
1	6268736.95	2777095.25	367.45	11.60	Five Mile Bay Reserve	01
2	6268737.13	2777095.46	367.34	11.49	Five Mile Bay Reserve	
3	6268737.76	2777095.66	367.39	11.54	Five Mile Bay Reserve	
4	6268738.03	2777095.59	367.47	11.62	Five Mile Bay Reserve	
5	6268738.21	2777095.55	367.44	11.59	Five Mile Bay Reserve	
6	6268738.61	2777095.68	367.42	11.57	Five Mile Bay Reserve	
7	6268738.97	2777095.63	367.44	11.59	Five Mile Bay Reserve	
8	6268739.20	2777095.66	367.41	11.56	Five Mile Bay Reserve	
9	6268739.39	2777095.73	367.46	11.61	Five Mile Bay Reserve	
10	6268739.68	2777095.81	367.45	11.60	Five Mile Bay Reserve	
11	6268739.87	2777095.98	367.46	11.61	Five Mile Bay Reserve	
12	6268740.21	2777096.05	367.49	11.64	Five Mile Bay Reserve	
13	6268740.77	2777096.02	367.57	11.72	Five Mile Bay Reserve	
14	6268740.89	2777096.22	367.56	11.71	Five Mile Bay Reserve	
15	6268741.19	2777096.18	367.67	11.82	Five Mile Bay Reserve	
16	6268742.26	2777096.58	367.85	12.00	Five Mile Bay Reserve	
17	6268742.87	2777096.95	367.88	12.03	Five Mile Bay Reserve	
18	6268744.34	2777097.10	368.04	12.19	Five Mile Bay Reserve	
19	6268735.75	2777094.83	367.25	11.40	Five Mile Bay Reserve	
20	6268735.46	2777094.84	367.19	11.34	Five Mile Bay Reserve	
21	6268735.29	2777094.77	367.19	11.34	Five Mile Bay Reserve	
22	6268735.02	2777094.77	367.16	11.31	Five Mile Bay Reserve	
23	6268734.85	2777094.64	367.13	11.28	Five Mile Bay Reserve	
24	6268734.44	2777094.55	367.07	11.22	Five Mile Bay Reserve	
25	6268734.27	2777094.54	367.03	11.18	Five Mile Bay Reserve	
26	6268733.95	2777094.44	366.94	11.09	Five Mile Bay Reserve	
27	6268733.65	2777094.27	366.91	11.06	Five Mile Bay Reserve	
28	6268733.54	2777094.29	366.94	11.09	Five Mile Bay Reserve	
29	6268733.27	2777094.11	366.90	11.05	Five Mile Bay Reserve	
30	6268733.02	2777094.11	366.89	11.04	Five Mile Bay Reserve	
31	6268732.95	2777094.07	366.93	11.08	Five Mile Bay Reserve	
32	6268732.51	2777093.99	366.89	11.04	Five Mile Bay Reserve	
33	6268732.24	2777093.96	366.86	11.01	Five Mile Bay Reserve	
34	6268732.04	2777093.87	366.86	11.01	Five Mile Bay Reserve	
35	6268731.85	2777093.80	366.87	11.02	Five Mile Bay Reserve	
36	6268731.51	2777093.57	366.82	10.97	Five Mile Bay Reserve	
37	6268730.92	2777093.65	366.68	10.83	Five Mile Bay Reserve	
38	6268730.93	2777093.68	366.76	10.91	Five Mile Bay Reserve	
39	6268730.41	2777093.63	366.63	10.78	Five Mile Bay Reserve	
40	6268730.42	2777093.69	366.69	10.84	Five Mile Bay Reserve	
41	6268730.00	2777093.31	366.66	10.81	Five Mile Bay Reserve	
42	6268730.03	2777093.47	366.72	10.87	Five Mile Bay Reserve	
43	6268728.32	2777092.65	366.63	10.78	Five Mile Bay Reserve	
44	6268728.37	2777092.63	366.45	10.60	Five Mile Bay Reserve	
45	6268727.94	2777092.64	366.48	10.63	Five Mile Bay Reserve	
46	6268727.83	2777092.67	366.40	10.55	Five Mile Bay Reserve	
47	6268727.35	2777092.51	366.34	10.49	Five Mile Bay Reserve	
48	6268726.92	2777092.33	366.38	10.53	Five Mile Bay Reserve	
49	6268726.70	2777092.09	366.28	10.43	Five Mile Bay Reserve	
50	6268726.22	2777091.86	366.34	10.49	Five Mile Bay Reserve	
51	6268726.15	2777091.80	366.41	10.56	Five Mile Bay Reserve	
52	6268725.90	2777091.79	366.48	10.63	Five Mile Bay Reserve	
53	6268725.76	2777091.57	366.28	10.43	Five Mile Bay Reserve	
54	6268725.52	2777091.48	366.35	10.50	Five Mile Bay Reserve	
55	6268724.99	2777091.19	366.26	10.41	Five Mile Bay Reserve	
56	6268724.88	2777091.17	366.25	10.40	Five Mile Bay Reserve	
57	6268724.42	2777090.87	366.27	10.42	Five Mile Bay Reserve	
58	6268723.93	2777090.38	366.30	10.45	Five Mile Bay Reserve	
59	6268723.88	2777089.58	366.32	10.47	Five Mile Bay Reserve	
60	6268682.31	2777112.04	365.76	9.91	Five Mile Bay Reserve	
61	6268681.76	2777111.69	365.31	9.46	Five Mile Bay Reserve	
62	6268684.15	2777110.36	365.29	9.44	Five Mile Bay Reserve	
63	6268683.61	2777110.58	365.71	9.86	Five Mile Bay Reserve	
64	6268684.19	2777109.90	366.17	10.32	Five Mile Bay Reserve	
65	6268684.17	2777110.07	365.88	10.03	Five Mile Bay Reserve	
66	6268685.96	2777108.89	365.39	9.54	Five Mile Bay Reserve	03
67	6268687.44	2777108.05	365.54	9.69	Five Mile Bay Reserve	
68	6268687.80	2777107.76	365.71	9.86	Five Mile Bay Reserve	
69	6268689.73	2777105.69	365.12	9.27	Five Mile Bay Reserve	
70	6268690.06	2777106.19	365.33	9.48	Five Mile Bay Reserve	
71	6268689.98	2777106.46	365.51	9.66	Five Mile Bay Reserve	
72	6268690.64	2777106.37	365.37	9.52	Five Mile Bay Reserve	
73	6268692.58	2777106.41	365.95	10.10	Five Mile Bay Reserve	
74	6268693.27	2777106.27	365.81	9.96	Five Mile Bay Reserve	
75	6268693.87	2777106.42	365.75	9.90	Five Mile Bay Reserve	

ID #	Northing	Easting	Height	Height above a.l.l.	Location	GRP #
76	6268694.24	2777105.43	365.67	9.82	Five Mile Bay Reserve	
77	6268724.11	2777086.62	365.74	9.89	Five Mile Bay Reserve	04
78	6268724.81	2777086.17	366.04	10.19	Five Mile Bay Reserve	
79	6268725.61	2777086.43	366.65	10.80	Five Mile Bay Reserve	
80	6268725.74	2777085.74	366.37	10.52	Five Mile Bay Reserve	
81	6268725.63	2777085.36	365.79	9.94	Five Mile Bay Reserve	
82	6268726.17	2777085.07	366.05	10.20	Five Mile Bay Reserve	
83	6268726.15	2777084.76	365.72	9.87	Five Mile Bay Reserve	
84	6268738.42	2777076.13	365.52	9.67	Five Mile Bay Reserve	05
85	6268738.52	2777078.32	366.98	11.13	Five Mile Bay Reserve	
86	6268741.02	2777077.46	367.08	11.23	Five Mile Bay Reserve	06
87	6268745.50	2777074.12	366.17	10.32	Five Mile Bay Reserve	
88	6268758.93	2777065.80	366.11	10.26	Five Mile Bay Reserve	07
89	6268771.67	2777059.93	366.46	10.61	Five Mile Bay Reserve	
90	6268775.76	2777061.21	367.12	11.27	Five Mile Bay Reserve	09
91	6268777.97	2777060.54	366.82	10.97	Five Mile Bay Reserve	
92	6268777.94	2777060.62	367.02	11.17	Five Mile Bay Reserve	
93	6268777.85	2777060.84	367.11	11.26	Five Mile Bay Reserve	
94	6268778.25	2777060.74	367.24	11.39	Five Mile Bay Reserve	10
95	6268781.03	2777056.90	366.81	10.96	Five Mile Bay Reserve	08
96	6268780.27	2777060.05	367.29	11.44	Five Mile Bay Reserve	
97	6268781.03	2777059.49	367.79	11.94	Five Mile Bay Reserve	
98	6268779.54	2777053.76	366.38	10.53	Five Mile Bay Reserve	
99	6268780.03	2777053.08	366.71	10.86	Five Mile Bay Reserve	
100	6268779.73	2777052.38	366.65	10.80	Five Mile Bay Reserve	
101	6268779.91	2777052.13	366.94	11.09	Five Mile Bay Reserve	
102	6268780.30	2777051.70	367.42	11.57	Five Mile Bay Reserve	
103	6268779.10	2777051.51	366.44	10.59	Five Mile Bay Reserve	
104	6268778.87	2777051.06	365.98	10.13	Five Mile Bay Reserve	
105	6268784.08	2777048.01	366.38	10.53	Five Mile Bay Reserve	
106	6268814.93	2777030.85	366.13	10.28	Five Mile Bay Reserve	
107	6268821.64	2777028.29	366.15	10.30	Five Mile Bay Reserve	
108	6268823.49	2777024.85	365.75	9.90	Five Mile Bay Reserve	
109	6268823.57	2777024.87	365.83	9.98	Five Mile Bay Reserve	12
110	6268823.81	2777024.83	365.82	9.97	Five Mile Bay Reserve	
111	6268823.82	2777024.84	365.85	10.00	Five Mile Bay Reserve	
112	6268824.38	2777025.05	365.84	9.99	Five Mile Bay Reserve	
113	6268824.58	2777025.15	365.86	10.01	Five Mile Bay Reserve	
114	6268824.77	2777025.22	365.84	9.99	Five Mile Bay Reserve	
115	6268824.84	2777025.22	365.88	10.03	Five Mile Bay Reserve	
116	6268825.07	2777025.31	366.05	10.20	Five Mile Bay Reserve	
117	6268825.17	2777025.29	366.02	10.17	Five Mile Bay Reserve	
118	6268825.25	2777025.33	365.89	10.04	Five Mile Bay Reserve	
119	6268825.49	2777025.29	366.05	10.20	Five Mile Bay Reserve	
120	6268825.52	2777025.28	366.05	10.20	Five Mile Bay Reserve	14
121	6268849.15	2777009.17	365.91	10.06	Five Mile Bay Reserve	
122	6268849.06	2777009.23	365.97	10.12	Five Mile Bay Reserve	16
123	6268849.12	2777008.96	365.98	10.13	Five Mile Bay Reserve	
124	6268849.19	2777008.88	365.86	10.01	Five Mile Bay Reserve	
125	6268849.26	2777008.82	365.96	10.11	Five Mile Bay Reserve	
126	6268849.25	2777008.74	365.89	10.04	Five Mile Bay Reserve	
127	6268849.29	2777008.76	365.85	10.00	Five Mile Bay Reserve	
128	6268852.61	2777007.43	365.73	9.88	Five Mile Bay Reserve	
129	6268853.43	2777009.25	366.20	10.35	Five Mile Bay Reserve	
130	6268853.47	2777009.24	366.19	10.34	Five Mile Bay Reserve	
131	6268853.52	2777009.25	366.25	10.40	Five Mile Bay Reserve	
132	6268853.53	2777009.36	366.39	10.54	Five Mile Bay Reserve	
133	6268853.62	2777009.37	366.53	10.68	Five Mile Bay Reserve	
134	6268853.68	2777009.45	366.66	10.81	Five Mile Bay Reserve	
135	6268853.78	2777009.50	366.66	10.81	Five Mile Bay Reserve	
136	6268853.83	2777009.48	366.45	10.60	Five Mile Bay Reserve	
137	6268853.93	2777009.50	366.57	10.72	Five Mile Bay Reserve	
138	6268853.91	2777009.63	366.48	10.63	Five Mile Bay Reserve	
139	6268854.01	2777009.84	366.40	10.55	Five Mile Bay Reserve	
140	6268854.11	2777009.76	366.36	10.51	Five Mile Bay Reserve	
141	6268854.13	2777009.83	366.59	10.74	Five Mile Bay Reserve	
142	6268854.17	2777010.10	366.56	10.71	Five Mile Bay Reserve	
143	6268854.23	2777010.14	366.70	10.85	Five Mile Bay Reserve	
144	6268854.28	2777010.10	366.69	10.84	Five Mile Bay Reserve	
145	6268854.60	2777010.37	366.79	10.94	Five Mile Bay Reserve	
146	6268856.82	2777011.53	366.73	10.88	Five Mile Bay Reserve	
147	6268856.35	2777011.38	366.74	10.89	Five Mile Bay Reserve	
148	6268856.18	2777011.25	366.75	10.90	Five Mile Bay Reserve	
149	6268856.18	2777011.15	367.01	11.16	Five Mile Bay Reserve	
150	6268856.18	2777011.16	367.14	11.29	Five Mile Bay Reserve	

ID #	Northing	Easting	Height	Height above a.l.l.	Location	GRP #
151	6268856.39	2777011.14	367.14	11.29	Five Mile Bay Reserve	
152	6268856.45	2777011.23	367.10	11.25	Five Mile Bay Reserve	
153	6268856.51	2777011.30	366.91	11.06	Five Mile Bay Reserve	
154	6268856.58	2777011.36	366.75	10.90	Five Mile Bay Reserve	
155	6268858.08	2777011.19	366.54	10.69	Five Mile Bay Reserve	
156	6268858.91	2777010.81	366.54	10.69	Five Mile Bay Reserve	
157	6268859.62	2777010.75	366.91	11.06	Five Mile Bay Reserve	
158	6268859.97	2777010.54	367.30	11.45	Five Mile Bay Reserve	
159	6268861.18	2777009.93	367.17	11.32	Five Mile Bay Reserve	15
160	6268861.39	2777009.56	366.89	11.04	Five Mile Bay Reserve	
161	6268860.72	2777004.72	366.04	10.19	Five Mile Bay Reserve	
162	6268860.62	2777004.53	366.31	10.46	Five Mile Bay Reserve	
163	6268860.72	2777004.53	366.00	10.15	Five Mile Bay Reserve	
164	6268860.67	2777003.82	365.73	9.88	Five Mile Bay Reserve	
165	6268860.75	2777003.84	366.02	10.17	Five Mile Bay Reserve	
166	6268860.68	2777003.41	365.84	9.99	Five Mile Bay Reserve	
167	6268860.85	2777003.01	366.12	10.27	Five Mile Bay Reserve	
168	6268861.11	2777002.23	365.93	10.08	Five Mile Bay Reserve	
169	6268862.91	2777000.94	365.32	9.47	Five Mile Bay Reserve	
170	6268863.16	2777001.76	366.10	10.25	Five Mile Bay Reserve	
171	6268863.14	2777001.74	366.00	10.15	Five Mile Bay Reserve	
172	6268863.36	2777001.66	366.02	10.17	Five Mile Bay Reserve	
173	6268863.86	2777001.48	366.09	10.24	Five Mile Bay Reserve	
174	6268864.78	2777001.50	366.23	10.38	Five Mile Bay Reserve	18
175	6268877.10	2776996.41	366.59	10.74	Five Mile Bay Reserve	
176	6268877.09	2776996.34	366.52	10.67	Five Mile Bay Reserve	
177	6268877.25	2776995.25	366.41	10.56	Five Mile Bay Reserve	
178	6268877.54	2776995.55	366.61	10.76	Five Mile Bay Reserve	
179	6268877.78	2776995.55	366.69	10.84	Five Mile Bay Reserve	
180	6268880.91	2776992.08	366.28	10.43	Five Mile Bay Reserve	17
181	6268879.68	2776993.11	366.49	10.64	Five Mile Bay Reserve	
182	6268882.57	2776991.40	366.32	10.47	Five Mile Bay Reserve	
183	6268886.42	2776990.01	366.13	10.28	Five Mile Bay Reserve	
184	6268886.98	2776990.10	366.18	10.33	Five Mile Bay Reserve	
185	6268885.72	2776989.77	365.63	9.78	Five Mile Bay Reserve	
186	6268885.97	2776989.74	365.67	9.82	Five Mile Bay Reserve	
187	6268886.12	2776990.78	366.13	10.28	Five Mile Bay Reserve	
188	6268887.21	2776991.15	366.40	10.55	Five Mile Bay Reserve	
189	6268887.58	2776991.26	366.56	10.71	Five Mile Bay Reserve	
190	6268887.74	2776991.51	366.76	10.91	Five Mile Bay Reserve	
191	6268887.84	2776991.37	366.86	11.01	Five Mile Bay Reserve	
192	6268887.81	2776991.22	366.95	11.10	Five Mile Bay Reserve	
193	6268887.93	2776991.15	367.20	11.35	Five Mile Bay Reserve	
194	6268887.84	2776991.00	367.12	11.27	Five Mile Bay Reserve	
195	6268887.96	2776991.37	366.83	10.98	Five Mile Bay Reserve	
196	6268888.23	2776991.35	366.89	11.04	Five Mile Bay Reserve	
197	6268888.36	2776991.26	367.00	11.15	Five Mile Bay Reserve	
198	6268888.36	2776991.34	366.95	11.10	Five Mile Bay Reserve	
199	6268888.38	2776991.31	366.92	11.07	Five Mile Bay Reserve	
200	6268888.70	2776991.17	366.91	11.06	Five Mile Bay Reserve	
201	6268888.82	2776990.92	366.99	11.14	Five Mile Bay Reserve	
202	6268888.86	2776990.89	366.97	11.12	Five Mile Bay Reserve	
203	6268888.97	2776991.03	366.96	11.11	Five Mile Bay Reserve	20
204	6268904.81	2776984.02	367.07	11.22	Five Mile Bay Reserve	
205	6268904.84	2776984.03	367.20	11.35	Five Mile Bay Reserve	
206	6268904.87	2776984.10	367.29	11.44	Five Mile Bay Reserve	
207	6268904.88	2776984.12	367.33	11.48	Five Mile Bay Reserve	
208	6268904.69	2776984.12	367.04	11.19	Five Mile Bay Reserve	
209	6268904.72	2776984.08	367.00	11.15	Five Mile Bay Reserve	
210	6268904.73	2776984.04	367.03	11.18	Five Mile Bay Reserve	
211	6268904.48	2776983.66	367.10	11.25	Five Mile Bay Reserve	
212	6268904.46	2776983.56	367.31	11.46	Five Mile Bay Reserve	
213	6268904.42	2776983.62	367.30	11.45	Five Mile Bay Reserve	
214	6268904.15	2776983.55	367.19	11.34	Five Mile Bay Reserve	
215	6268904.16	2776983.55	367.02	11.17	Five Mile Bay Reserve	
216	6268904.17	2776983.79	367.01	11.16	Five Mile Bay Reserve	
217	6268904.09	2776983.74	366.95	11.10	Five Mile Bay Reserve	
218	6268904.20	2776983.76	366.94	11.09	Five Mile Bay Reserve	
219	6268904.15	2776983.62	366.91	11.06	Five Mile Bay Reserve	
220	6268904.28	2776983.75	366.93	11.08	Five Mile Bay Reserve	
221	6268903.80	2776982.95	367.09	11.24	Five Mile Bay Reserve	
222	6268903.65	2776982.86	367.01	11.16	Five Mile Bay Reserve	
223	6268903.51	2776982.93	366.78	10.93	Five Mile Bay Reserve	
224	6268903.45	2776982.24	366.71	10.86	Five Mile Bay Reserve	
225	6268903.49	2776982.22	366.75	10.90	Five Mile Bay Reserve	

ID #	Northing	Easting	Height	Height above a.l.l.	Location	GRP #
226	6268903.54	2776982.28	366.92	11.07	Five Mile Bay Reserve	
227	6268903.56	2776982.11	366.74	10.89	Five Mile Bay Reserve	
228	6268903.62	2776982.32	367.01	11.16	Five Mile Bay Reserve	
229	6268904.19	2776982.55	367.12	11.27	Five Mile Bay Reserve	
230	6268904.27	2776982.54	366.96	11.11	Five Mile Bay Reserve	
231	6268904.30	2776982.41	367.04	11.19	Five Mile Bay Reserve	
232	6268904.35	2776982.37	366.94	11.09	Five Mile Bay Reserve	
233	6268904.34	2776982.30	366.83	10.98	Five Mile Bay Reserve	
234	6268904.36	2776982.31	366.83	10.98	Five Mile Bay Reserve	21
235	6268904.33	2776982.34	367.15	11.30	Five Mile Bay Reserve	
236	6268904.33	2776982.40	367.11	11.26	Five Mile Bay Reserve	
237	6268917.86	2776973.82	367.06	11.21	Five Mile Bay Reserve	
238	6268917.99	2776973.79	366.92	11.07	Five Mile Bay Reserve	
239	6268917.99	2776973.81	366.90	11.05	Five Mile Bay Reserve	
240	6268917.90	2776973.85	367.01	11.16	Five Mile Bay Reserve	
241	6268917.81	2776973.97	366.92	11.07	Five Mile Bay Reserve	
242	6268917.74	2776973.88	367.07	11.22	Five Mile Bay Reserve	
243	6268917.63	2776973.95	366.91	11.06	Five Mile Bay Reserve	
244	6268918.92	2776973.42	367.01	11.16	Five Mile Bay Reserve	
245	6268918.82	2776973.34	367.06	11.21	Five Mile Bay Reserve	
246	6268919.47	2776973.32	366.96	11.11	Five Mile Bay Reserve	
247	6268919.65	2776973.23	366.93	11.08	Five Mile Bay Reserve	
248	6268919.58	2776973.12	367.11	11.26	Five Mile Bay Reserve	
249	6268919.44	2776973.10	367.10	11.25	Five Mile Bay Reserve	
250	6268919.56	2776973.14	367.07	11.22	Five Mile Bay Reserve	
251	6268919.66	2776973.11	366.96	11.11	Five Mile Bay Reserve	
252	6268919.71	2776973.07	366.91	11.06	Five Mile Bay Reserve	
253	6268919.84	2776973.06	367.08	11.23	Five Mile Bay Reserve	
254	6268920.02	2776973.06	367.07	11.22	Five Mile Bay Reserve	22
255	6268920.08	2776973.05	367.00	11.15	Five Mile Bay Reserve	
256	6268920.39	2776972.75	366.90	11.05	Five Mile Bay Reserve	
257	6268920.33	2776972.69	366.86	11.01	Five Mile Bay Reserve	
258	6268920.50	2776972.74	367.00	11.15	Five Mile Bay Reserve	
259	6268920.76	2776972.76	366.97	11.12	Five Mile Bay Reserve	
260	6268920.76	2776972.79	366.95	11.10	Five Mile Bay Reserve	
261	6268920.81	2776972.83	366.94	11.09	Five Mile Bay Reserve	
262	6268920.73	2776972.69	367.02	11.17	Five Mile Bay Reserve	
263	6268920.88	2776972.62	366.90	11.05	Five Mile Bay Reserve	
264	6268920.99	2776972.31	366.93	11.08	Five Mile Bay Reserve	
265	6268921.05	2776972.29	367.06	11.21	Five Mile Bay Reserve	
266	6268922.13	2776971.79	366.96	11.11	Five Mile Bay Reserve	
267	6268922.61	2776971.61	366.95	11.10	Five Mile Bay Reserve	
268	6268922.48	2776971.61	367.13	11.28	Five Mile Bay Reserve	
269	6268927.24	2776970.41	366.96	11.11	Five Mile Bay Reserve	
270	6268927.10	2776970.38	367.00	11.15	Five Mile Bay Reserve	
271	6268927.29	2776970.25	367.01	11.16	Five Mile Bay Reserve	
272	6268927.28	2776970.24	367.04	11.19	Five Mile Bay Reserve	
273	6268927.38	2776970.19	367.21	11.36	Five Mile Bay Reserve	
274	6268927.42	2776970.20	367.17	11.32	Five Mile Bay Reserve	
275	6268927.48	2776970.19	367.15	11.30	Five Mile Bay Reserve	
276	6268927.49	2776970.09	367.07	11.22	Five Mile Bay Reserve	
277	6268927.54	2776970.12	366.97	11.12	Five Mile Bay Reserve	
278	6268927.62	2776970.08	366.99	11.14	Five Mile Bay Reserve	
279	6268927.71	2776970.04	366.98	11.13	Five Mile Bay Reserve	
280	6268927.65	2776969.87	367.12	11.27	Five Mile Bay Reserve	
281	6268927.76	2776969.84	367.00	11.15	Five Mile Bay Reserve	
282	6268928.22	2776969.49	366.96	11.11	Five Mile Bay Reserve	
283	6268928.25	2776969.48	366.95	11.10	Five Mile Bay Reserve	
284	6268928.27	2776969.59	367.01	11.16	Five Mile Bay Reserve	
285	6268928.24	2776969.59	367.07	11.22	Five Mile Bay Reserve	
286	6268928.14	2776969.58	367.12	11.27	Five Mile Bay Reserve	
287	6268939.91	2776964.81	367.39	11.54	Five Mile Bay Reserve	
288	6268940.71	2776964.95	367.51	11.66	Five Mile Bay Reserve	
289	6268940.79	2776964.90	367.61	11.76	Five Mile Bay Reserve	
290	6268940.90	2776964.99	367.52	11.67	Five Mile Bay Reserve	
291	6268941.04	2776965.05	367.55	11.70	Five Mile Bay Reserve	
292	6268941.37	2776965.06	367.54	11.69	Five Mile Bay Reserve	
293	6268941.46	2776965.08	367.58	11.73	Five Mile Bay Reserve	
294	6268935.81	2776965.86	367.14	11.29	Five Mile Bay Reserve	
295	6268935.77	2776965.72	367.14	11.29	Five Mile Bay Reserve	
296	6268483.10	2777231.62	365.69	9.84	South of Airport (Landcorp property)	
297	6268483.12	2777231.27	365.70	9.85	South of Airport (Landcorp property)	
298	6268482.75	2777231.35	365.69	9.84	South of Airport (Landcorp property)	
299	6268482.61	2777231.17	365.51	9.66	South of Airport (Landcorp property)	23
300	6268482.55	2777231.19	365.64	9.79	South of Airport (Landcorp property)	

ID #	Northing	Easting	Height	Height above a.l.l.	Location	GRP #
301	6268482.14	2777231.47	365.68	9.83	South of Airport (Landcorp property)	
302	6268479.41	2777234.97	365.83	9.98	South of Airport (Landcorp property)	
303	6268478.56	2777240.59	366.86	11.01	South of Airport (Landcorp property)	
304	6268478.34	2777240.89	367.35	11.50	South of Airport (Landcorp property)	
305	6268478.01	2777241.07	367.29	11.44	South of Airport (Landcorp property)	
306	6268477.68	2777241.69	367.19	11.34	South of Airport (Landcorp property)	
307	6268477.67	2777241.74	367.10	11.25	South of Airport (Landcorp property)	25
308	6268475.13	2777242.42	366.87	11.02	South of Airport (Landcorp property)	
309	6268475.11	2777242.37	367.00	11.15	South of Airport (Landcorp property)	
310	6268474.79	2777242.23	366.81	10.96	South of Airport (Landcorp property)	26
311	6268474.91	2777242.24	366.88	11.03	South of Airport (Landcorp property)	
312	6268470.71	2777234.72	365.06	9.21	South of Airport (Landcorp property)	
313	6268470.71	2777234.72	365.07	9.22	South of Airport (Landcorp property)	
314	6268464.63	2777237.18	365.74	9.89	South of Airport (Landcorp property)	27
315	6268464.39	2777237.82	366.14	10.29	South of Airport (Landcorp property)	
316	6268465.42	2777238.35	366.69	10.84	South of Airport (Landcorp property)	
317	6268465.53	2777238.48	366.86	11.01	South of Airport (Landcorp property)	
318	6268465.47	2777238.88	366.92	11.07	South of Airport (Landcorp property)	
319	6268465.37	2777238.97	366.84	10.99	South of Airport (Landcorp property)	
320	6268466.03	2777239.05	367.00	11.15	South of Airport (Landcorp property)	
321	6268466.05	2777238.96	366.99	11.14	South of Airport (Landcorp property)	
322	6268454.40	2777238.50	364.56	8.71	South of Airport (Landcorp property)	
323	6268454.41	2777239.24	364.55	8.70	South of Airport (Landcorp property)	
324	6268453.82	2777241.23	365.25	9.40	South of Airport (Landcorp property)	
325	6268453.53	2777241.22	365.01	9.16	South of Airport (Landcorp property)	
326	6268452.36	2777246.22	365.38	9.53	South of Airport (Landcorp property)	
327	6268444.65	2777248.32	365.92	10.07	South of Airport (Landcorp property)	
328	6268444.88	2777248.16	365.99	10.14	South of Airport (Landcorp property)	
329	6268444.91	2777248.13	366.04	10.19	South of Airport (Landcorp property)	
330	6268444.91	2777248.22	366.04	10.19	South of Airport (Landcorp property)	28
331	6268444.98	2777248.23	366.12	10.27	South of Airport (Landcorp property)	
332	6268444.96	2777248.21	366.17	10.32	South of Airport (Landcorp property)	
333	6268445.08	2777248.09	366.24	10.39	South of Airport (Landcorp property)	
334	6268445.00	2777248.01	366.23	10.38	South of Airport (Landcorp property)	
335	6268444.70	2777248.30	366.40	10.55	South of Airport (Landcorp property)	
336	6268445.02	2777248.24	366.38	10.53	South of Airport (Landcorp property)	
337	6268445.06	2777248.40	366.36	10.51	South of Airport (Landcorp property)	
338	6268445.00	2777248.25	366.37	10.52	South of Airport (Landcorp property)	
339	6268445.10	2777248.36	366.29	10.44	South of Airport (Landcorp property)	
340	6268445.21	2777248.39	366.12	10.27	South of Airport (Landcorp property)	
341	6268444.23	2777246.80	365.61	9.76	South of Airport (Landcorp property)	
342	6268444.37	2777246.44	365.72	9.87	South of Airport (Landcorp property)	
343	6268426.12	2777255.55	366.03	10.18	South of Airport (Landcorp property)	
344	6268426.28	2777255.33	366.26	10.41	South of Airport (Landcorp property)	
345	6268426.43	2777255.13	366.37	10.52	South of Airport (Landcorp property)	
346	6268426.52	2777255.26	366.19	10.34	South of Airport (Landcorp property)	
347	6268426.42	2777255.23	366.20	10.35	South of Airport (Landcorp property)	
348	6268426.09	2777254.96	366.15	10.30	South of Airport (Landcorp property)	30
349	6268424.96	2777254.07	365.93	10.08	South of Airport (Landcorp property)	
350	6268425.26	2777254.03	365.89	10.04	South of Airport (Landcorp property)	
351	6268425.37	2777253.97	365.77	9.92	South of Airport (Landcorp property)	
352	6268424.09	2777253.43	365.90	10.05	South of Airport (Landcorp property)	
353	6268424.07	2777253.37	365.98	10.13	South of Airport (Landcorp property)	
354	6268424.11	2777253.44	366.00	10.15	South of Airport (Landcorp property)	
355	6268423.64	2777255.74	366.73	10.88	South of Airport (Landcorp property)	
356	6268420.22	2777257.32	366.36	10.51	South of Airport (Landcorp property)	
357	6268420.53	2777257.00	366.54	10.69	South of Airport (Landcorp property)	
358	6268417.72	2777260.69	366.44	10.59	South of Airport (Landcorp property)	
359	6268417.24	2777260.46	366.49	10.64	South of Airport (Landcorp property)	
360	6268417.75	2777261.35	366.96	11.11	South of Airport (Landcorp property)	
361	6268417.19	2777261.12	366.89	11.04	South of Airport (Landcorp property)	
362	6268416.69	2777260.69	366.49	10.64	South of Airport (Landcorp property)	31
363	6268416.60	2777260.71	366.61	10.76	South of Airport (Landcorp property)	
364	6268416.56	2777260.78	366.71	10.86	South of Airport (Landcorp property)	
365	6268416.52	2777260.82	366.53	10.68	South of Airport (Landcorp property)	32
366	6268403.28	2777256.52	365.83	9.98	South of Airport (Landcorp property)	
367	6268402.28	2777255.86	365.88	10.03	South of Airport (Landcorp property)	
368	6268400.92	2777254.07	364.49	8.64	South of Airport (Landcorp property)	
369	6268401.58	2777253.72	364.53	8.68	South of Airport (Landcorp property)	
370	6268403.51	2777253.90	364.72	8.87	South of Airport (Landcorp property)	
371	6268405.94	2777254.22	365.14	9.29	South of Airport (Landcorp property)	
372	6268407.30	2777254.51	365.28	9.43	South of Airport (Landcorp property)	
373	6268406.70	2777253.57	364.67	8.82	South of Airport (Landcorp property)	29
374	6268395.38	2777250.54	363.73	7.88	South of Airport (Landcorp property)	
375	6268392.50	2777243.78	362.72	6.87	South of Airport (Landcorp property)	

ID #	Northing	Easting	Height	Height above a.l.l.	Location	GRP #
376	6268394.09	2777244.53	363.24	7.39	South of Airport (Landcorp property)	
377	6268394.33	2777244.85	363.21	7.36	South of Airport (Landcorp property)	34
378	6268399.63	2777256.03	364.97	9.12	South of Airport (Landcorp property)	
379	6268399.72	2777256.00	365.02	9.17	South of Airport (Landcorp property)	
380	6268399.81	2777256.15	365.11	9.26	South of Airport (Landcorp property)	
381	6268398.74	2777256.29	365.08	9.23	South of Airport (Landcorp property)	
382	6268397.39	2777257.73	365.55	9.70	South of Airport (Landcorp property)	
383	6268396.69	2777257.79	365.41	9.56	South of Airport (Landcorp property)	
384	6268396.56	2777257.71	365.39	9.54	South of Airport (Landcorp property)	
385	6268395.84	2777259.53	365.69	9.84	South of Airport (Landcorp property)	
386	6268394.61	2777260.40	365.57	9.72	South of Airport (Landcorp property)	
387	6268394.40	2777260.94	365.65	9.80	South of Airport (Landcorp property)	
388	6268393.36	2777261.23	365.61	9.76	South of Airport (Landcorp property)	
389	6268393.05	2777261.50	365.68	9.83	South of Airport (Landcorp property)	
390	6268393.39	2777262.00	366.01	10.16	South of Airport (Landcorp property)	
391	6268391.47	2777264.31	366.18	10.33	South of Airport (Landcorp property)	
392	6268391.50	2777264.42	366.22	10.37	South of Airport (Landcorp property)	
393	6268391.85	2777264.10	366.40	10.55	South of Airport (Landcorp property)	
394	6268391.74	2777264.37	366.40	10.55	South of Airport (Landcorp property)	
395	6268391.93	2777264.97	366.61	10.76	South of Airport (Landcorp property)	
396	6268383.40	2777267.20	366.12	10.27	South of Airport (Landcorp property)	35
397	6268383.38	2777266.30	365.70	9.85	South of Airport (Landcorp property)	
398	6268383.44	2777266.93	366.32	10.47	South of Airport (Landcorp property)	
399	6268383.40	2777266.92	366.36	10.51	South of Airport (Landcorp property)	
400	6268369.80	2777275.42	366.12	10.27	South of Airport (Landcorp property)	36
401	6268369.50	2777274.63	366.25	10.40	South of Airport (Landcorp property)	
402	6268360.64	2777278.12	366.06	10.21	South of Airport (Landcorp property)	
403	6268360.70	2777277.93	366.26	10.41	South of Airport (Landcorp property)	
404	6268360.59	2777278.15	366.30	10.45	South of Airport (Landcorp property)	
405	6268360.70	2777278.05	366.31	10.46	South of Airport (Landcorp property)	
406	6268360.66	2777277.97	366.36	10.51	South of Airport (Landcorp property)	
407	6268360.59	2777277.94	366.35	10.50	South of Airport (Landcorp property)	
408	6268360.54	2777277.86	366.33	10.48	South of Airport (Landcorp property)	
409	6268360.66	2777277.96	366.23	10.38	South of Airport (Landcorp property)	
410	6268360.54	2777277.95	366.18	10.33	South of Airport (Landcorp property)	
411	6268360.64	2777277.85	366.15	10.30	South of Airport (Landcorp property)	
412	6268360.61	2777277.70	366.12	10.27	South of Airport (Landcorp property)	
413	6268360.57	2777277.66	366.18	10.33	South of Airport (Landcorp property)	
414	6268360.64	2777277.62	366.17	10.32	South of Airport (Landcorp property)	
415	6268360.49	2777277.55	366.12	10.27	South of Airport (Landcorp property)	
416	6268360.45	2777277.43	366.12	10.27	South of Airport (Landcorp property)	
417	6268360.71	2777276.85	365.92	10.07	South of Airport (Landcorp property)	
418	6268360.56	2777276.65	365.89	10.04	South of Airport (Landcorp property)	
419	6268360.36	2777276.20	365.92	10.07	South of Airport (Landcorp property)	
420	6268360.23	2777276.03	365.92	10.07	South of Airport (Landcorp property)	
421	6268359.98	2777276.22	365.89	10.04	South of Airport (Landcorp property)	
422	6268359.44	2777275.72	366.12	10.27	South of Airport (Landcorp property)	37
423	6268358.65	2777274.65	365.92	10.07	South of Airport (Landcorp property)	
424	6268357.33	2777274.23	366.20	10.35	South of Airport (Landcorp property)	
425	6268356.96	2777273.04	365.61	9.76	South of Airport (Landcorp property)	
426	6268357.41	2777273.23	365.81	9.96	South of Airport (Landcorp property)	
427	6268335.99	2777280.67	366.03	10.18	South of Airport (Landcorp property)	
428	6268334.21	2777283.48	366.68	10.83	South of Airport (Landcorp property)	
429	6268328.20	2777285.38	366.12	10.27	South of Airport (Landcorp property)	
430	6268328.46	2777287.43	366.89	11.04	South of Airport (Landcorp property)	
431	6268314.63	2777300.35	366.20	10.35	South of Airport (Landcorp property)	
432	6268314.78	2777299.52	365.90	10.05	South of Airport (Landcorp property)	
433	6268311.95	2777296.58	365.88	10.03	South of Airport (Landcorp property)	
434	6268312.23	2777296.74	366.13	10.28	South of Airport (Landcorp property)	
435	6268311.59	2777296.98	366.31	10.46	South of Airport (Landcorp property)	
436	6268311.31	2777296.95	366.16	10.31	South of Airport (Landcorp property)	
437	6268310.62	2777297.74	366.64	10.79	South of Airport (Landcorp property)	
438	6268308.02	2777299.78	365.93	10.08	South of Airport (Landcorp property)	
439	6268308.01	2777299.82	366.08	10.23	South of Airport (Landcorp property)	
440	6268299.60	2777297.23	366.55	10.70	South of Airport (Landcorp property)	
441	6268301.96	2777295.12	365.96	10.11	South of Airport (Landcorp property)	
442	6268299.20	2777282.76	365.24	9.39	South of Airport (Landcorp property)	
443	6268297.79	2777282.65	365.61	9.76	South of Airport (Landcorp property)	
444	6268297.55	2777281.66	364.89	9.04	South of Airport (Landcorp property)	
445	6268290.57	2777274.65	363.08	7.23	South of Airport (Landcorp property)	
446	6268289.88	2777278.30	363.75	7.90	South of Airport (Landcorp property)	
447	6268289.57	2777280.56	364.51	8.66	South of Airport (Landcorp property)	
448	6268290.51	2777281.26	365.01	9.16	South of Airport (Landcorp property)	38
449	6268291.95	2777282.10	365.43	9.58	South of Airport (Landcorp property)	
450	6268291.15	2777282.68	365.68	9.83	South of Airport (Landcorp property)	

ID #	Northing	Easting	Height	Height above a.l.l.	Location	GRP #
451	6268285.72	2777282.66	364.49	8.64	South of Airport (Landcorp property)	
452	6268287.15	2777283.15	365.16	9.31	South of Airport (Landcorp property)	
453	6268284.58	2777284.26	364.25	8.40	South of Airport (Landcorp property)	
454	6268283.57	2777284.73	364.29	8.44	South of Airport (Landcorp property)	
455	6268282.82	2777285.06	364.28	8.43	South of Airport (Landcorp property)	
456	6268283.25	2777287.64	365.09	9.24	South of Airport (Landcorp property)	
457	6268287.54	2777285.18	366.39	10.54	South of Airport (Landcorp property)	
458	6268140.20	2777330.67	363.84	7.99	South of Airport (Landcorp property)	
459	6268140.64	2777331.12	363.60	7.75	South of Airport (Landcorp property)	
460	6268139.97	2777331.34	364.22	8.37	South of Airport (Landcorp property)	
461	6268139.55	2777332.34	364.50	8.65	South of Airport (Landcorp property)	
462	6268139.94	2777332.12	364.65	8.80	South of Airport (Landcorp property)	
463	6268139.77	2777332.44	364.76	8.91	South of Airport (Landcorp property)	
464	6268138.92	2777332.58	365.20	9.35	South of Airport (Landcorp property)	
465	6268138.11	2777333.12	365.58	9.73	South of Airport (Landcorp property)	
466	6268137.98	2777333.41	366.50	10.65	South of Airport (Landcorp property)	
467	6268139.51	2777334.46	365.38	9.53	South of Airport (Landcorp property)	
468	6268139.79	2777334.31	365.16	9.31	South of Airport (Landcorp property)	
469	6268138.39	2777332.77	365.36	9.51	South of Airport (Landcorp property)	
470	6268137.59	2777330.93	364.75	8.90	South of Airport (Landcorp property)	
471	6268137.62	2777330.60	364.66	8.81	South of Airport (Landcorp property)	
472	6268137.51	2777329.82	364.28	8.43	South of Airport (Landcorp property)	
473	6268136.51	2777329.98	364.50	8.65	South of Airport (Landcorp property)	
474	6268133.75	2777331.28	364.59	8.74	South of Airport (Landcorp property)	
475	6268133.84	2777331.26	364.79	8.94	South of Airport (Landcorp property)	
476	6268133.02	2777331.75	364.56	8.71	South of Airport (Landcorp property)	
477	6268134.57	2777334.43	365.62	9.77	South of Airport (Landcorp property)	
478	6268134.38	2777334.16	365.46	9.61	South of Airport (Landcorp property)	
479	6268131.31	2777338.58	365.38	9.53	South of Airport (Landcorp property)	
480	6268070.27	2777337.49	362.96	7.11	South of Airport (Landcorp property)	
481	6268069.80	2777336.62	362.99	7.14	South of Airport (Landcorp property)	
482	6268052.76	2777348.15	364.31	8.46	South of Airport (Landcorp property)	
483	6268061.10	2777342.57	364.19	8.34	South of Airport (Landcorp property)	
484	6268067.16	2777340.52	364.16	8.31	South of Airport (Landcorp property)	
485	6268064.54	2777337.03	364.42	8.57	South of Airport (Landcorp property)	
486	6268063.68	2777338.31	364.58	8.73	South of Airport (Landcorp property)	
487	6268063.22	2777334.73	363.68	7.83	South of Airport (Landcorp property)	41
488	6268067.85	2777330.93	362.87	7.02	South of Airport (Landcorp property)	
489	6268065.22	2777331.09	363.09	7.24	South of Airport (Landcorp property)	
490	6268039.91	2777332.75	362.56	6.71	South of Airport (Landcorp property)	
491	6268038.67	2777332.97	362.60	6.75	South of Airport (Landcorp property)	
492	6268035.19	2777334.37	362.67	6.82	South of Airport (Landcorp property)	42
493	6268051.14	2777371.10	366.09	10.24	South of Airport (Landcorp property)	40
494	6268052.62	2777374.03	365.82	9.97	South of Airport (Landcorp property)	
495	6268054.20	2777379.60	366.68	10.83	South of Airport (Landcorp property)	
496	6268059.73	2777387.11	367.80	11.95	South of Airport (Landcorp property)	
497	6268059.90	2777387.27	368.00	12.15	South of Airport (Landcorp property)	
498	6268060.02	2777387.33	368.18	12.33	South of Airport (Landcorp property)	
499	6268057.87	2777385.96	368.01	12.16	South of Airport (Landcorp property)	
500	6268057.73	2777385.87	368.01	12.16	South of Airport (Landcorp property)	
501	6268057.75	2777385.83	368.04	12.19	South of Airport (Landcorp property)	
502	6268058.43	2777386.29	367.96	12.11	South of Airport (Landcorp property)	
503	6268058.43	2777386.31	368.01	12.16	South of Airport (Landcorp property)	
504	6268058.51	2777386.26	368.06	12.21	South of Airport (Landcorp property)	
505	6268058.49	2777386.16	368.08	12.23	South of Airport (Landcorp property)	
506	6268058.86	2777386.44	367.90	12.05	South of Airport (Landcorp property)	
507	6268060.29	2777388.28	367.90	12.05	South of Airport (Landcorp property)	
508	6268060.58	2777388.16	367.91	12.06	South of Airport (Landcorp property)	
509	6268060.51	2777388.12	367.98	12.13	South of Airport (Landcorp property)	
510	6268060.76	2777388.27	368.08	12.23	South of Airport (Landcorp property)	
511	6268062.05	2777389.14	368.14	12.29	South of Airport (Landcorp property)	
512	6268062.14	2777389.03	367.86	12.01	South of Airport (Landcorp property)	47
513	6268063.53	2777390.12	368.24	12.39	South of Airport (Landcorp property)	
514	6268063.55	2777390.24	368.14	12.29	South of Airport (Landcorp property)	
515	6268063.51	2777390.29	368.06	12.21	South of Airport (Landcorp property)	
516	6268068.05	2777391.59	368.08	12.23	South of Airport (Landcorp property)	
517	6268067.93	2777391.54	368.31	12.46	South of Airport (Landcorp property)	
518	6268068.24	2777391.58	368.14	12.29	South of Airport (Landcorp property)	
519	6268072.16	2777391.91	368.12	12.27	South of Airport (Landcorp property)	
520	6268071.66	2777392.01	368.17	12.32	South of Airport (Landcorp property)	
521	6268071.66	2777391.93	368.14	12.29	South of Airport (Landcorp property)	
522	6268071.45	2777392.03	368.10	12.25	South of Airport (Landcorp property)	
523	6268071.40	2777391.83	368.21	12.36	South of Airport (Landcorp property)	
524	6268071.33	2777391.87	368.11	12.26	South of Airport (Landcorp property)	
525	6268071.27	2777391.90	368.13	12.28	South of Airport (Landcorp property)	

ID #	Northing	Easting	Height	Height above a.l.l.	Location	GRP #
526	6268071.07	2777391.80	368.20	12.35	South of Airport (Landcorp property)	
527	6268070.95	2777391.89	368.15	12.30	South of Airport (Landcorp property)	
528	6268075.95	2777386.77	367.83	11.98	South of Airport (Landcorp property)	
529	6268076.00	2777386.76	367.71	11.86	South of Airport (Landcorp property)	
530	6268075.65	2777387.22	367.52	11.67	South of Airport (Landcorp property)	
531	6268075.62	2777387.31	367.47	11.62	South of Airport (Landcorp property)	
532	6268075.47	2777387.14	367.62	11.77	South of Airport (Landcorp property)	
533	6268075.12	2777385.34	367.42	11.57	South of Airport (Landcorp property)	
534	6268075.01	2777385.43	367.28	11.43	South of Airport (Landcorp property)	
535	6268074.93	2777385.05	367.18	11.33	South of Airport (Landcorp property)	
536	6268075.02	2777384.99	367.20	11.35	South of Airport (Landcorp property)	
537	6268074.71	2777384.23	367.11	11.26	South of Airport (Landcorp property)	
538	6268074.76	2777384.29	366.95	11.10	South of Airport (Landcorp property)	
539	6268074.75	2777383.73	366.72	10.87	South of Airport (Landcorp property)	
540	6268075.31	2777383.73	366.96	11.11	South of Airport (Landcorp property)	
541	6268075.36	2777383.02	366.77	10.92	South of Airport (Landcorp property)	
542	6268075.50	2777382.86	366.85	11.00	South of Airport (Landcorp property)	
543	6268075.28	2777382.80	366.64	10.79	South of Airport (Landcorp property)	
544	6268075.32	2777381.75	366.66	10.81	South of Airport (Landcorp property)	
545	6268075.28	2777381.36	366.45	10.60	South of Airport (Landcorp property)	
546	6268075.35	2777381.37	366.26	10.41	South of Airport (Landcorp property)	
547	6268079.29	2777383.60	367.63	11.78	South of Airport (Landcorp property)	
548	6268080.39	2777383.49	366.93	11.08	South of Airport (Landcorp property)	
549	6268083.66	2777383.90	367.49	11.64	South of Airport (Landcorp property)	
550	6268083.20	2777382.99	366.86	11.01	South of Airport (Landcorp property)	
551	6268083.22	2777383.09	366.91	11.06	South of Airport (Landcorp property)	
552	6268082.90	2777383.21	366.84	10.99	South of Airport (Landcorp property)	
553	6268082.88	2777383.22	366.54	10.69	South of Airport (Landcorp property)	
554	6268093.78	2777375.82	366.42	10.57	South of Airport (Landcorp property)	
555	6268093.74	2777375.87	366.65	10.80	South of Airport (Landcorp property)	
556	6268094.93	2777374.36	366.49	10.64	South of Airport (Landcorp property)	46
557	6268078.71	2777395.75	369.58	13.73	South of Airport (Landcorp property)	
558	6268078.82	2777395.63	369.62	13.77	South of Airport (Landcorp property)	
559	6268079.14	2777395.85	369.55	13.70	South of Airport (Landcorp property)	
560	6268078.81	2777395.51	369.57	13.72	South of Airport (Landcorp property)	
561	6268043.85	2777398.05	370.86	15.01	South of Airport (Landcorp property)	
562	6268043.20	2777398.56	370.96	15.11	South of Airport (Landcorp property)	
563	6268043.20	2777399.28	371.00	15.15	South of Airport (Landcorp property)	
564	6268043.58	2777399.35	371.00	15.15	South of Airport (Landcorp property)	
565	6268043.67	2777399.28	370.95	15.10	South of Airport (Landcorp property)	
566	6268043.03	2777397.33	370.71	14.86	South of Airport (Landcorp property)	
567	6268039.58	2777395.53	370.67	14.82	South of Airport (Landcorp property)	
568	6268039.33	2777394.60	370.60	14.75	South of Airport (Landcorp property)	
569	6268038.91	2777394.69	370.63	14.78	South of Airport (Landcorp property)	
570	6268039.14	2777393.98	370.44	14.59	South of Airport (Landcorp property)	
571	6268030.95	2777394.71	370.44	14.59	South of Airport (Landcorp property)	
572	6268029.31	2777394.81	370.23	14.38	South of Airport (Landcorp property)	
573	6268026.36	2777393.22	370.34	14.49	South of Airport (Landcorp property)	
574	6268026.67	2777393.25	370.31	14.46	South of Airport (Landcorp property)	
575	6268026.61	2777393.58	370.33	14.48	South of Airport (Landcorp property)	
576	6267990.91	2777340.14	362.97	7.12	South of Airport (Landcorp property)	
577	6267887.22	2777349.23	365.48	9.63	South of Airport (Landcorp property)	
578	6267872.96	2777334.66	361.16	5.31	Fletcher Challenge Road	
579	6267865.32	2777356.50	365.00	9.15	Fletcher Challenge Road	
580	6267865.57	2777356.42	365.21	9.36	Fletcher Challenge Road	
581	6267865.44	2777356.60	365.28	9.43	Fletcher Challenge Road	
582	6267865.39	2777356.73	365.31	9.46	Fletcher Challenge Road	
583	6267865.37	2777356.73	365.08	9.23	Fletcher Challenge Road	
584	6267865.30	2777357.27	365.72	9.87	Fletcher Challenge Road	
585	6267865.28	2777357.14	365.69	9.84	Fletcher Challenge Road	
586	6267864.65	2777357.22	365.11	9.26	Fletcher Challenge Road	
587	6267864.70	2777357.19	365.11	9.26	Fletcher Challenge Road	
588	6267864.46	2777357.61	365.03	9.18	Fletcher Challenge Road	
589	6267864.56	2777357.54	364.95	9.10	Fletcher Challenge Road	
590	6267864.62	2777357.69	364.92	9.07	Fletcher Challenge Road	
591	6267864.52	2777357.59	364.87	9.02	Fletcher Challenge Road	
592	6267864.37	2777357.64	364.95	9.10	Fletcher Challenge Road	
593	6267864.07	2777358.13	365.03	9.18	Fletcher Challenge Road	
594	6267864.57	2777358.98	365.13	9.28	Fletcher Challenge Road	
595	6267864.59	2777358.69	365.01	9.16	Fletcher Challenge Road	
596	6267864.63	2777358.70	365.17	9.32	Fletcher Challenge Road	
597	6267864.67	2777358.60	365.27	9.42	Fletcher Challenge Road	
600	6270592.00	2772900.14	370.31	14.46	Te Kumi Bay	24
601	6270591.99	2772900.16	370.30	14.45	Te Kumi Bay	

ID #	Northing	Easting	Height	Height above a.l.l.	Location	GRP #
602	6270591.99	2772900.17	370.30	14.45	Te Kumi Bay	
603	6270592.02	2772900.28	370.20	14.35	Te Kumi Bay	
604	6270091.14	2776169.78	363.87	8.02	Wharewaka Point	Base station